DOT/FAA/AR-95/47

Office of Aviation Research
Washington D C 20591

Investigation of Fuselage Structure Subject to Widespread Fatigue Damage

February 1996

Final Report

U S Department of Transportation
Federal Aviation Administration

ACKNOWLEDGEMENTS

The authors would like to thank Glenn Laroya who conducted much of the pressure panel data reduction and developed many of the data plots in this report. Further, Glenn oversaw the assembly of this report. Also, special thanks are due to the test facility personnel who constructed and tested the flat panels and the two wide-body pressure test panels.

Dr. D. S. Dawicke, a contractor to NASA Langley, performed the crack tip opening angle measurements on the flat panel tests. The measuring equipment was provided by NASA Langley.

The work documented in this report was contracted by the Federal Aviation Administration (FAA). Dr. Paul Tan was the technical monitor.

Technical Report Documentation Page

1. Report No.	2. Government Accession No.	3. Recipient's Catalog No.
DOT/FAA/AR-95/47		

4. Title and Subtitle	5. Report Date
INVESTIGATION OF FUSELAGE STRUCTURE SUBJECT TO WIDESPREAD FATIGUE DAMAGE	February 1996
	6. Performing Organization Code

7. Author(s)	8. Performing Organization Report No.
M.L. Gruber, C.J. Mazur, K.E. Wilkins, R.E. Worden	D6-81738

9. Performing Organization Name and Address	10. Work Unit No. (TRAIS)
Structural Damage Technology Boeing Commercial Airplane Group P.O. Box 3707 Seattle, WA 98124	11. Contract or Grant No. DTFA03-94C-00065

12. Sponsoring Agency Name and Address	13. Type of Report and Period Covered
U.S. Department of Transportation Federal Aviation Administration Office of Aviation Research Washington, DC 20491	Final Report October 1994-October 1995
	14. Sponsoring Agency Code AAR-430

15. Supplementary Notes

FAA COTR: Dr. Paul Tan

16. Abstract

This report documents the results of the "Investigation Of Fuselage Structure Subject To Widespread Fatigue Damage" contract. The primary program objective was to obtain data on airplane fuselage structures subject to multiple site damage (MSD) in an environment that reflects typical commercial jetliner manufacturing and operating conditions. The program involves three technical tasks which include flat panel material characterization testing (Task I), Full-scale fuselage pressure panel testing (Task II) and predictions of pressure panel behavior through finite element modeling (Task III).

In Task I, six specimens were tested to characterize the lot of 2024-T3 clad material used to fabricate the skins for the Task II pressure test panels. Material static, crack growth, and toughness (K_{app} and R-curves) data were generated.

In Task II, two generic wide-body curved fuselage panels were fabricated and pressure tested. Frame centered cracks in the lap joint outer skin upper fastener row were grown by pressure cycling to two frame bays. A panel residual strength test was then conducted with the skin crack centered on a broken frame. Panel lap joints were fabricated with and without MSD sawcuts in the fasteners ahead of the lead crack to develop the head-to-head comparison.

In Task III, a detailed finite element model was constructed to analyze the pressure test panels. Predictions were made of the pressure test panel strain gage stresses, crack growth life, and residual strength.

General conclusions from the testing and analysis were drawn.

17. Key Words	18. Distribution Statement
Multiple Site Damage, Widespread Fatigue Damage, Fuselage Structure, Lap Joint, Finite Element Analysis, 2024-T3 Aluminum, Fatigue Crack Growth, and Residual Strength	This document is available to the public through the National Technical Information Service, Springfield, Virginia 22161

19. Security Classif. (of this report)	20. Security Classif. (of this page)	21. No. of Pages	22. Price
Unclassified	Unclassified	243	N/A

Form DOT F1700.7 (8-72) Reproduction of completed page authorized

EXECUTIVE SUMMARY

This document is the final report covering the results of a one-year program entitled "Investigation of Fuselage Structure Subject to Widespread Fatigue Damage." The program focused on developing representative data on the effects of widespread fatigue damage on fuselage lap joints using unique Boeing testing capabilities and expertise in airplane analysis and design. Widespread fatigue damage (WFD) is defined as the simultaneous presence of cracks at multiple structural details that are of sufficient size and density whereby the structure will no longer meet its damage tolerance requirements. Multiple site damage (MSD) is a subset of WFD which was the focus of this program. MSD involves the simultaneous presence of fatigue cracks in the same structural element. The most notable example of an area with potential for having MSD is airplane fuselage structure. The understanding of MSD and the development of analytical prediction capability would be a major step forward in developing an understanding of its effects on all structure susceptible to WFD.

The need exists for data on MSD in structure representing actual airplane geometry and fabrication processes, and which is tested in a realistic operating environment. The primary objective of this program was to fabricate test panels representative of actual airplane structure and conduct residual strength tests in a fixture which can realistically simulate airplane pressure loading. This program was divided into three technical tasks which are documented in this report.

Task I consisted of six tests conducted to characterize the 2024-T3 sheet material that was used for the skins of the two curved fuselage pressure test panels fabricated for Task II. Static, crack growth rate, and fracture toughness data were generated.

Task II involved curved pressure panel tests conducted in the Boeing 127-inch-radius pressure test fixture. Two panels representative of typical wide-body crown fuselage construction were fabricated and tested. The testing focused on the outer skin lap joint upper fastener row with and without simulated MSD. Lead cracks were grown in the lap joints by pressure cycling from an initial 5-inch sawcut to two frame bays (40 inches). Test results indicated that the crack growth rate was faster in the presence of MSD. The frame spanning the 40-inch crack was then cut and residual strength tests conducted by gradually increasing the pressure until dynamic panel failure occurred. Test results indicated that panel residual strength was reduced 20 percent in the presence of MSD for the panel geometry tested.

Task III consisted of performing analyses to predict the crack growth and residual strength of the pressure test panels. Stress intensity factors were obtained from a material and geometric nonlinear finite element model developed using standard Boeing practices. Crack growth rate and residual strength predictions were made and correlated with test results from the pressure tests. The crack growth predictions correlated very well with test results for small and no MSD cases. The analysis and residual strength prediction focused on the instability of the lead crack as the cause of the final panel failure. For the no MSD case, the test results were over predicted. From further analysis and examination of the test results a theory was developed that the panel failure was perpetuated by the static failures of the panel tear straps, rather than the instability of the lead crack.

1. INTRODUCTION

This document is the final report covering the results of a one year program entitled "Investigation of Fuselage Structure Subject to Widespread Fatigue Damage". The program was funded through the FAA Technical Center in Atlantic City under FAA contract number DTFA03-94-C-00065. The program focused on developing representative data on the effects of widespread fatigue damage on fuselage structure using unique Boeing testing capabilities and expertise in airplane analysis and design.

Widespread fatigue damage (WFD) is defined as the simultaneous presence of cracks at multiple structural details that are of sufficient size and density whereby the structure will no longer meet its damage tolerance requirements. Subsets of WFD are multiple element damage (MED) and multiple site damage (MSD). MED involves the simultaneous presence of fatigue cracking in adjacent structural elements while MSD is characterized by the simultaneous presence of fatigue cracks in the same structural element. WFD behavior occurs in structure with similar details under similar loading conditions, with the most notable area being fuselage structure. Although it is understood that WFD can occur in many areas of an airframe and considerable effort is underway within the air transport industry to identify potential WFD locations, the scope of this discussion and the "Investigation of Fuselage Structure Subject to Widespread Fatigue Damage" program (known as the program from here on) will focus on MSD of fuselage skins, in particular lap joints. The understanding of WFD and the development of analytical prediction capability on a lap joint would be a major step forward in developing an understanding of its effects on all structure susceptible to WFD.

1.1 Background

Most airplane primary structure is designed to sustain regulatory loads in the presence of damage (fatigue cracking, corrosion or accidental damage) until the damage is detected by planned inspections and repaired. Damage tolerance is mandated by the current amendments to FAR 25.571 and JAR 25.571. The damage tolerance process consists of three distinct elements: crack (damage) growth (rate of damage propagation in the structure), residual strength (the maximum damage that the structure can sustain without catastrophic failure under regulatory load conditions) and damage detection (opportunities to locate the damage through planned inspection). Boeing has developed standard analysis methods for predicting the damage tolerance of airplane structure based on these three elements. The 757 and 767 were designed with these methods and their service history demonstrates the effectiveness of the Boeing approach.

High replacement costs and competition in the commercial airline industry have led today's operators to use their airplanes beyond the originally expected design service objective. The result is an aging fleet with a higher probability of fatigue-initiated cracking. Since most of the older airplanes were designed prior to implementation of the damage tolerance regulations, the principles are applied as supplemental structural inspection programs in accordance with FAA Advisory Circular 91-56.

Damage tolerance methods that primarily focus on local damage may not be sufficient to maintain the structural airworthiness of aging airplanes. WFD is a structural ailment which if undetected or unrepaired could result in a rapid fracture and loss of structural integrity. Small undetected MSD cracks in several adjacent fastener holes can link together and reach a critical size in relatively few flights. This might reduce the opportunities to find damage prior to catastrophic failure. Further, the residual strength or final critical damage size in the structure in the presence of MSD may be smaller. Also crack arrest devices such as tear straps designed for containing damage may not function as planned. For example, narrow body fuselage structure may not vent as designed.

An increased understanding of MSD behavior and its implications on fuselage structure would allow the existing damage tolerance processes to better account for the presence of MSD. The susceptibility of the aging fleet to MSD must be evaluated on a model-by-model basis once proven analytical methods are available. Modifications to susceptible structure can then be carried out to maintain flight safety. An understanding of the fundamental behavior of MSD would also allow engineers to develop structural designs capable of containing the effects of MSD.

1.2 Program Objectives

The need exists for data on MSD in structure representing actual airplane geometry and fabrication processes, and which is tested in a realistic operating environment. The primary objective of this program was to fabricate test panels representative of actual airplane structure and conduct residual strength tests in a fixture which can realistically simulate airplane pressure loading.

Much of the experimental data available on MSD was developed using flat panel tests. The ability of this type of data to represent actual airplane structure is questionable. Test results indicate up to a 30% reduction in residual strength of a flat panel with a primary crack in the presence of MSD (References 1 and 2). Limited Boeing (Reference 2) and FAA sponsored tests (Reference 3) indicated that representative curved fuselage structure may experience only a 10% reduction in residual strength. This suggests that flat panel data cannot be applied directly to fuselage structure. Clarification of this issue was a second objective of this program.

A third objective of the program was to evaluate existing analytical capability for predicting the crack growth and residual strength behavior of fuselage structure containing MSD.

1.3 Program Overview

The program was divided into the following three technical tasks which are documented in this report:

- Task I Flat Panel Testing
- Task II Curved Pressure Panel Testing
- Task III Analysis

Task I consisted of six tests to characterize the material that was used for the skins of the two curved fuselage pressure test panels fabricated for Task II. Four center-cracked tension panels were tested to determine crack growth rates and material fracture toughness. Two tensile specimens were also fabricated and tested to determine the static properties of the material.

Task II curved pressure panel tests were conducted in the Boeing 127-inch-radius pressure test fixture. Two panels representative of typical wide body fuselage construction were fabricated and tested. Original test plans called for two crack growth and residual strength tests on each panel allowing for a total of four tests. However, circumstances encountered during the initial testing made it impractical to attempt two residual strength tests on the same panel. Thus the program scope was revised to conduct a total of two residual strength tests, one on each panel. The two tests focused on comparing residual strength of the lap joints with and without MSD.

Task III consisted of performing analyses to predict the crack growth and residual strength of fuselage structure. Stress intensity factors were obtained from a material and geometric nonlinear finite element model developed using standard Boeing practices. Crack growth rate and residual strength predictions were made and correlated with test results from the pressure tests. The MSD cracks were not modeled in the finite element analyses.

2. TASK I: FLAT PANEL TESTING

2.1 Test Objective

The following sections describe the design, fabrication and testing of tensile and center-cracked tension specimens. These tests were performed in order to develop stress-strain, crack growth, and the toughness (R-curve) properties for the skin material used to fabricate the large curved pressure panels in Task II (0.063-inch-thick 2024-T3 clad aluminum sheet). Four center-cracked tension, M(t), specimens were used to generate the material's crack growth and R-curve properties, while two tensile coupons were tested to develop the material's stress-strain relationship.

2.2 Material and Specimen Details

The tensile specimen geometry and dimensions are shown in Figure 1. Note that the material grain direction ("L") is perpendicular to the loading direction. Figure 2 shows the geometry and dimensions of the M(t) specimens. Each M(t) panel was 48.0 inches wide ("L" or grain direction) by 80 inches long ("T" direction). The crack was oriented in the "L" direction, which corresponds to the orientation of a typical airplane lap joint crack. The initial crack was installed in each M(t) panel with a series of sawcuts. The geometry of the initial crack is also shown in figure 2.

The flat panel specimens and large curved pressure panel skins were all fabricated from 2024-T3 clad aluminum sheet obtained from the same heat lot. The certification report provided by ALCOA for this material is shown in figure 3.

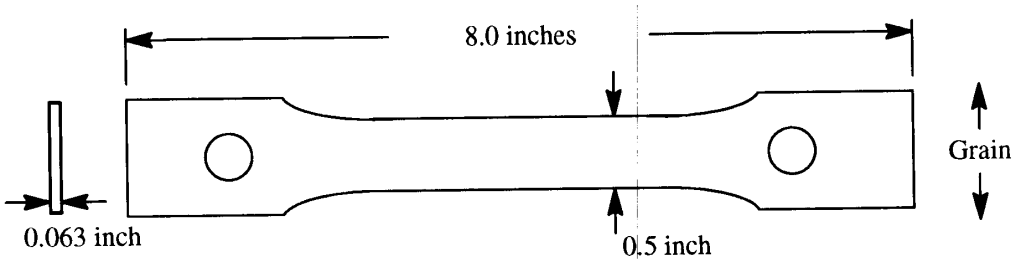

Fig 1 Tensile Specimen Geometry

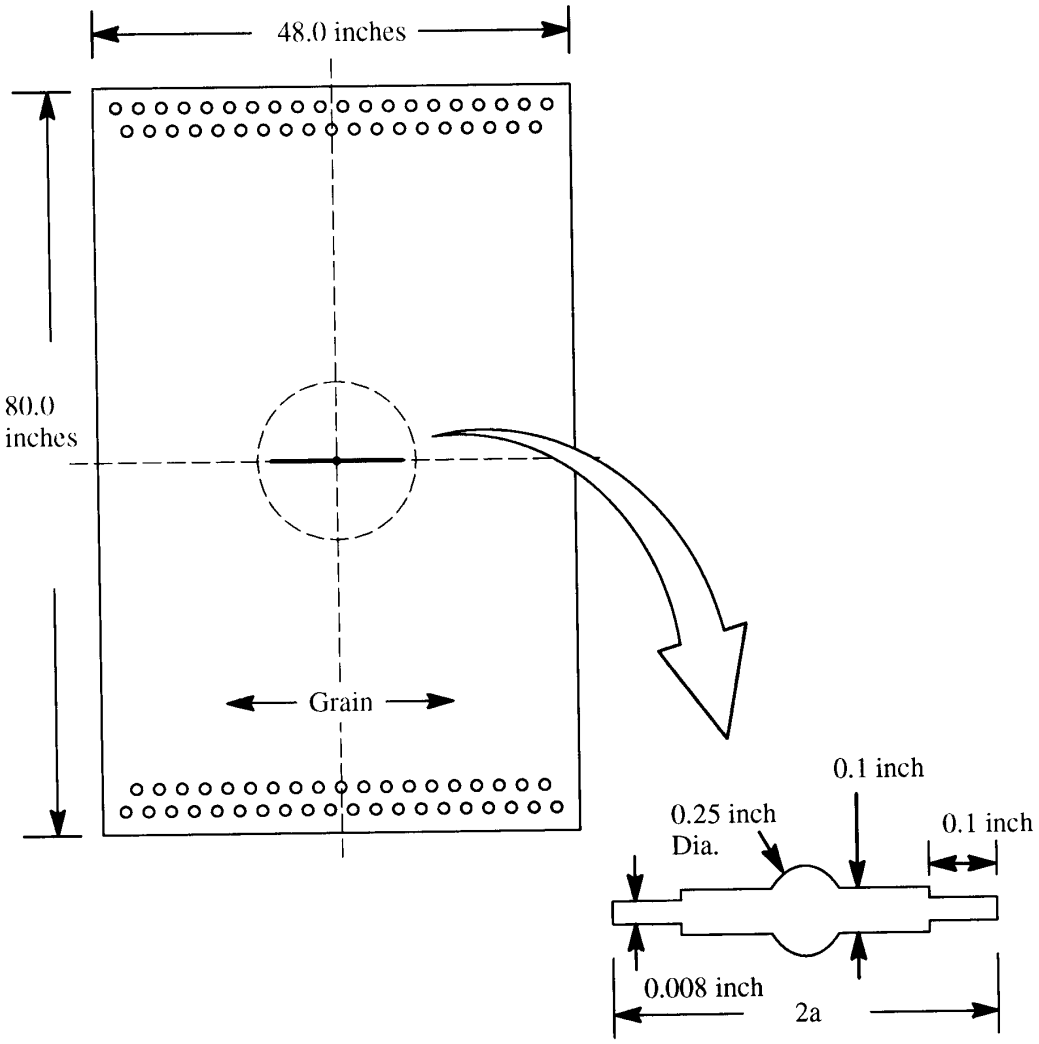

Figure 2. Flat M(t) Panel Geometry

CERTIFIED INSPECTION REPORT

ALCOA ALUMINUM COMPANY OF AMERICA PITTSBURGH, PA.

SHIPPED FROM: DAVENPORT, IOWA

CUSTOMER P.O. NO./GOVT. CONTRACT NO. PA6244

PAGE 001

We hereby certify that the material covered by this report has been inspected in accordance with, and has been found to meet, the applicable requirements described herein, including any specifications forming a part of the description and that samples representative of the material meeting these requirements and the mechanical properties shown on the face of this sheet. Per

INVOICE NO. 22540780 | INVOICE DATE 95/01/24 | CODE 540 120423

SAM L SHELBY — QUALITY ASSURANCE MANAGER

ALCOA NO. BE 50216 | SHIP DATE 95/01/24 | VIA MERCER

PRODUCT DESCRIPTION SHEET | BA NO. | GROSS WEIGHT

ALLOY-TEMPER ALCLAD 2024 T3

A57

BOEING DEFENSE & SPACE GROUP
MAIL STOP 6H-AA
P.O. BOX 3707
SEATTLE, WA 98124-2207

BOEING DEFENSE & SPACE GROUP
ELECTRONIC DATA INTERCHANGE
MAIL STOP 6H-AA
800-643RD STREET SW
RENTON, WA 98055

ITEM	ITEM DESCRIPTION	QUANTITY SHIPPED PCS, FT., ETC.	QUANTITY SHIPPED POUNDS	NO. OF TESTS & DWG#		@ TEST	@ TEST	@ TEST	@ TEST	@ TEST	@ TEST
1		6PC	390			UTS1	TYS1	EL4D			
	.063 IN TK X 85 IN W X 120 IN LN (N) A/T ALCLAD 2024-T3 FLAT	LOT-502421	T3	2 L.T	MAX	64.3	43.2	19.5			
		6PC			MIN	63.7	43.1	19.0			
	SPECIL-AIR POLISHED SKIN SHEET, MINIMUM LUEDERING PER D37200 REV A AND PER QQ-A-250/5 REV F NT 2 ((MARKED)) INTERLEAVED	SI FE CU MN MG CR ZN TI .06 .20 4.58 .63 1.51 .01 .13 .03									
	MAX GROSS SKID WGT: 2400 LB	Cast analysis from a representative sample during the casting process									
	QUAN TOL +/-0 PC										
	CQR 00062587 REV 01										
	CUST REQ 95-01-14										
	PACKAGE TICKETS ,015604										

THIS SHIPMENT ACCEPTED BY
BOEING SUPPLIER QUALITY CONTROL
SQAL# N/A
NAME Richard Thomas Stamp

	SI	FE	CU	MN	MG	CR	ZN	TI	OTHER	OTHER	ALUMINUM
Chemical Composition ALCLAD 2024	Max. .50	.50	4.9	.9	1.8	.10	.25	.15	.05	.15	REMAINDER
	Min.		3.8	.30	1.2				EACH	TOTAL	
Alloy Chemical Composition 1230 LINER	SI+FE		CU	MN	MG	V	ZN	TI	OTHER	ALUMINUM	
	Max. .70	.10	.05	.05	.05	.10	.03	.03	REMAINDER		
	Min.								EACH	99.30	

Figure 3. Certification Inspection Report for 2024–T3 Aluminum Panels

2.3 Instrumentation

On one side of each M(t) panel, a 200 mm electronic crack measurement gage, Fractomat gage, was mounted just beyond each crack tip in order to measure crack growth during constant amplitude cycling. To cure the adhesive used to attach the Fractomat gages to the panels, the panels were put in an autoclave for three hours at a temperature of 225^{o}F. The cure time and temperature were selected to limit the temperature effects on the material and to make sure the gages would adhere to the panels. For the R-curve tests, an MTS model 632.03 extensometer was mounted across the crack during each test to monitor crack opening displacements, while an MTS 632.25 extensometer was used to measure material strain on the tensile specimens.

2.4 Test Procedures

To determine the stress-strain curve for 2024-T3 aluminum, the tensile coupons identified in table 1 were tested per ASTM E8 in a 50 kip MTS tensile test machine and at room temperature.

Table 1. Test Matrix for Tensile Specimens

Specimen ID	Material Orientation	Thickness (inch)	Width (Inch
2024_faa_t11	Long Transverse	0.0612	0.4973
2024_faa_t12	Long Transverse	0.0615	0.5006

Each of the four M(t) specimens were cycled per ASTM E647 in a 200 kip MTS fatigue test machine under the loading given in table 2 to generate material crack growth rate data. During cycling, crack growth measurements were taken on one side using the Fractomat gages, and visual measurements were taken on the other side of the panel (at intervals of approximately 0.5 inch of total crack growth) to verify the Fractomat readings. After cycling, each panel was pulled to failure per ASTM E561 to develop the material's R-curve. Visual crack extension and crack opening displacement measurements were taken during each R-curve test.

Buckling restraints were used to prevent out of plane displacements on all four panels during crack growth rate testing and on three of the four panels during the R-curve tests. Buckling restraints were not used during the R-curve test on panel tl6 because there was interest in determining the effect of the buckling restraints on the test results, and that for future analyses, the panel would be easier to model without the added complexity of the buckling restraints.

Table 2. Test Matrix for M(t) Specimens

Specimen ID	a_i (inch)	a_f (inch)	σ_{max} (ksi)	R
2024_faa_tl3	2.0	8.0	8.0	0.1
2024_faa_tl4	2.0 5.5	5.5 8.0	16.0 8.0	0.1
2024_faa_tl5	5.0	12.0	12.0	0.1
2024_faa_tl6	2.0	8.0	7.0	0.5

2.5 Test Results

2.5.1 Tensile Specimens

The stress–strain results obtained from the two tensile specimens are plotted in figure 4. As shown in the plot, similar results were obtained from the two different specimens. The stress–strain curve used for the finite element analyses in Task III consists of the points on the curve in figure 4 that are denoted by the solid circles. The numerical values associated with these discrete points are given in table 3. Table 4 gives the corresponding elastic modulus, 0.2 percent tensile yield stress, and the ultimate tensile stress obtained from the two tensile tests. The ultimate and tensile yield stresses obtained from the certification report, figure 3, are also given in table 4 for comparison.

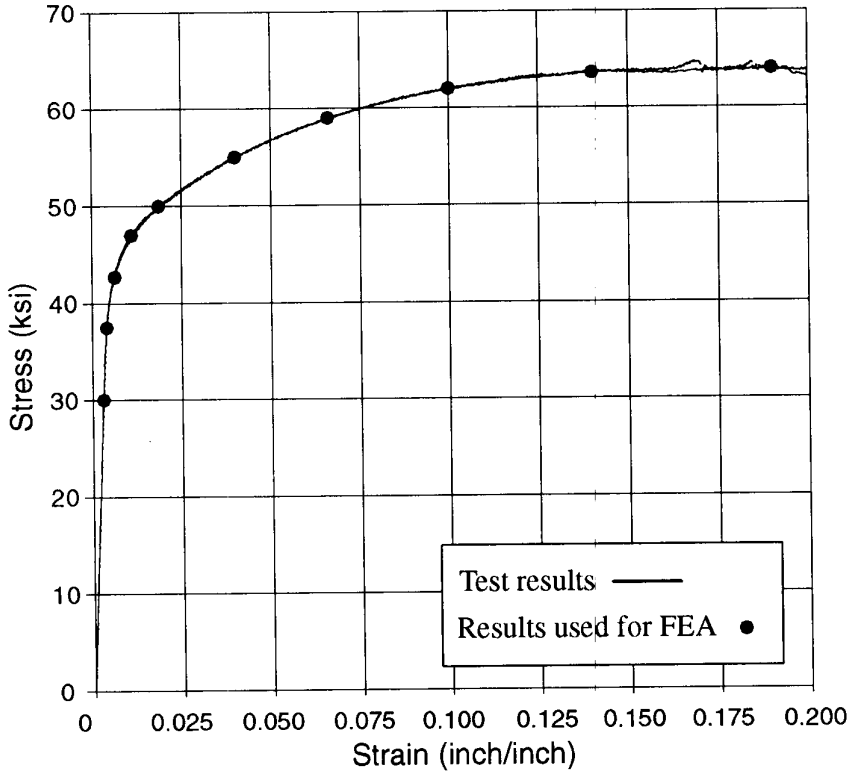

Figure 4. Engineering Stress-Strain Curve for 0.063-Inch-Thick 2024-T3 L-T Aluminum

Table 3. Stress-Strain Curve

Stress (ksi)	30.0	37.5	42.7	47.0	50.0	55.0	59.0	62.0	63.6	64.0
Strain (in/in)	0.00304	0.00400	0.00633	0.0110	0.0186	0.0399	0.0660	0.100	0.140	0.190

Table 4. Material Properties

Specimen ID	Tensile Modulu(Msi)	Tensile Yield 0.2 (ksi)	Tensile Ultimate (ksi)	%Elongation
2024_faa_t11	10.11	42.8	64.0	20
2024_faa_t12	9.61	42.7	64.6	20
certification report	N/A	42.2 43.1	64.3 63.7	19.5 19.0

2.5.2 M(t) Specimens

Crack growth testing of the four M(t) specimens was performed as outlined in previous sections. The crack growth curves comparing visual and Fractomat measurements are given in appendix A, while the crack growth rate data, da/dN versus ΔK, calculated from both the Fractomat and visual measurements for all specimens is given in Figure 5. As shown in the plot, there is very good agreement between the crack growth rate data from the visual measurements and the Fractomat gage readings for each specimen.A change was made to the test plan while testing specimen tl4, which was the first panel tested. For this panel, the final total crack length for gathering crack growth rate data was reduced from 16 inches to approximately 11 inches. This change was made because the crack was growing very fast and there was concern that the panel might fracture before the crack reached a total length of 16 inches. The data missed by not continuing the crack growth testing on this panel was expected to be obtained from one of the other panels, so no gaps in the crack growth rate curve occurred because of this change. After cycling was stopped on specimen tl4 at a total crack length of 11 inches, the maximum applied stress was reduced from 16 to 8 ksi, and the crack was cycled out to a total length of 16 inches.The da/dN versus ΔK crack growth data calculated from the Fractomat gage readings that is plotted in Figure 5 was reduced to da/dN versus ΔK_{eff} data using Newman's crack opening stress equations with α= 1.2, reference 4. The ΔK_{eff} data was then modified back to da/dN versus ΔK data for a stress ratio, R, equal to zero using the same crack opening stress equations. A stress ratio equal to zero was chosen because it corresponds to the stress ratio applied in the large curved panel tests. The resulting crack growth data is given in Figure 6. Examining the reduced crack growth data shows that the data for stress ratios equal to 0.1 and 0.5 have collapsed onto the same curve. Also shown in Figure 6 is the corresponding Boeing crack growth data, which is conservative relative to the test data for the lower range of ΔK's where most of the crack growth life occurs. An equation was fit to the test data using least squares and is shown along with the corresponding data in Figure 6.

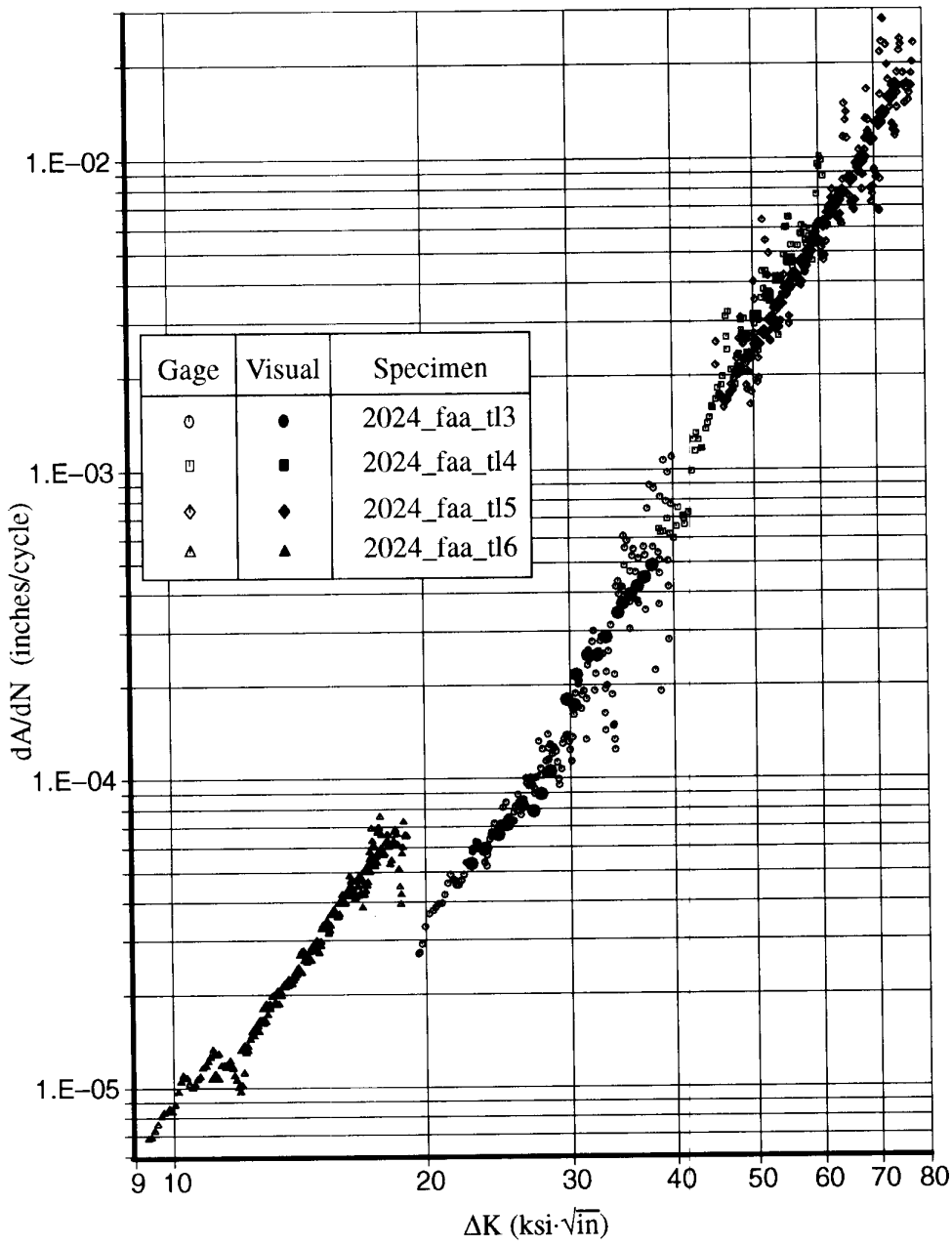

Figure 5. Crack Growth Rate Data Calculated From Fractomat and Visual Crack Length Measurements

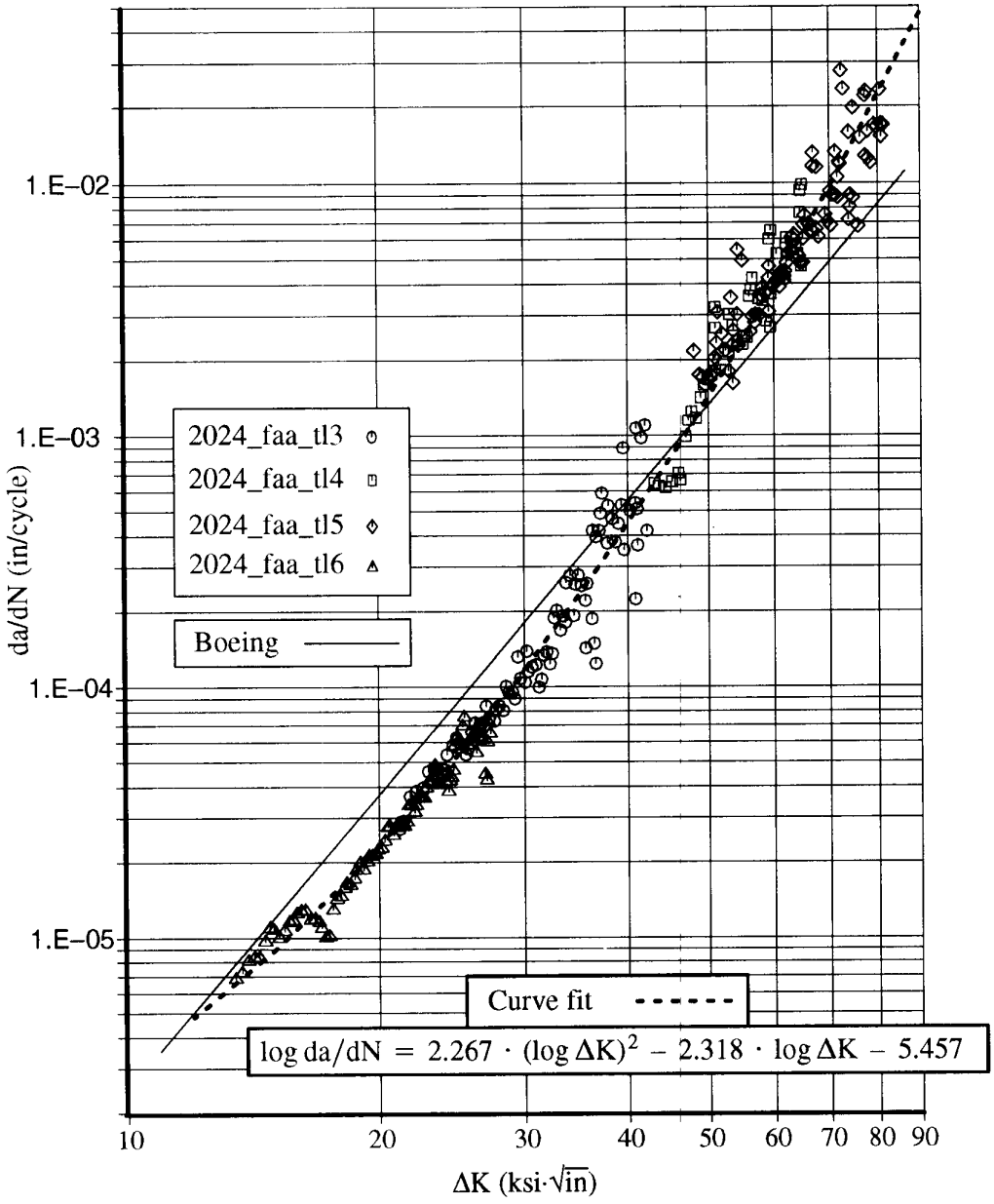

Figure 6. Crack Growth Rate Data Reduced to R = 0.0

After crack growth rate testing, each panel was pulled monotonically to obtain the material's toughness value and R–curve. As noted before, buckling restraints were used to limit out of plane deflections during loading, except on specimen tl6. The load versus crack opening displacement plots and visual crack extension versus load tables are given in appendix B.

The toughness values, K_{app} obtained from the four panels are given along with the corresponding Boeing allowable in table 5. Comparing the results from the four test panels shows good agreement for those panels tested with buckling restraints. Results for the panel tested without buckling restraints are 30 percent less than the results for panels tested with buckling restraints, which shows the importance of reducing out of plane deformations. The toughness values obtained from the four M(t) specimens are slightly lower than the Boeing value since the Boeing value was developed from M(t) panels wider than 48 inches.

Table 5. Toughness Results for 2024–T3 T–L Aluminum

Specimen	Width (inch)	Thickness (inch)	Initial half crack length (inch)	Maximum load (kips)	K_{app} (ksi·$\sqrt{in}$)
2024_faa_tl3	48.0	0.0615	7.98	71.1	130.
2024_faa_tl4	48.0	0.0613	7.98	70.1	128.
2024_faa_tl5	48.0	0.0613	12.3	51.8	131.
2024_faa_tl6	48.0	0.0608	8.11	52.6	98.0
Boeing					137

The resulting R–curves, Kr_{eff} versus Δa_{eff}, for each panel are plotted in figure 7, which shows that the results for the three panels tested with buckling restraints compare well with each other. Again, the results for tl6 are lower than the those of the other three panels. An equation was fit to the data for tl3, tl4, and tl5 using least squares, and is given along with the corresponding curve in figure 7.

The equation used to calculate the stress intensity factor, K, for a M(t) specimen is given below:

$$K = \frac{P_{max}}{tW} F \sqrt{\pi a},$$

where P_{max} = maximum load, t = thickness, W = specimen width, a = half crack length, and $F = \sqrt{\sec \frac{\pi a}{W}}$.

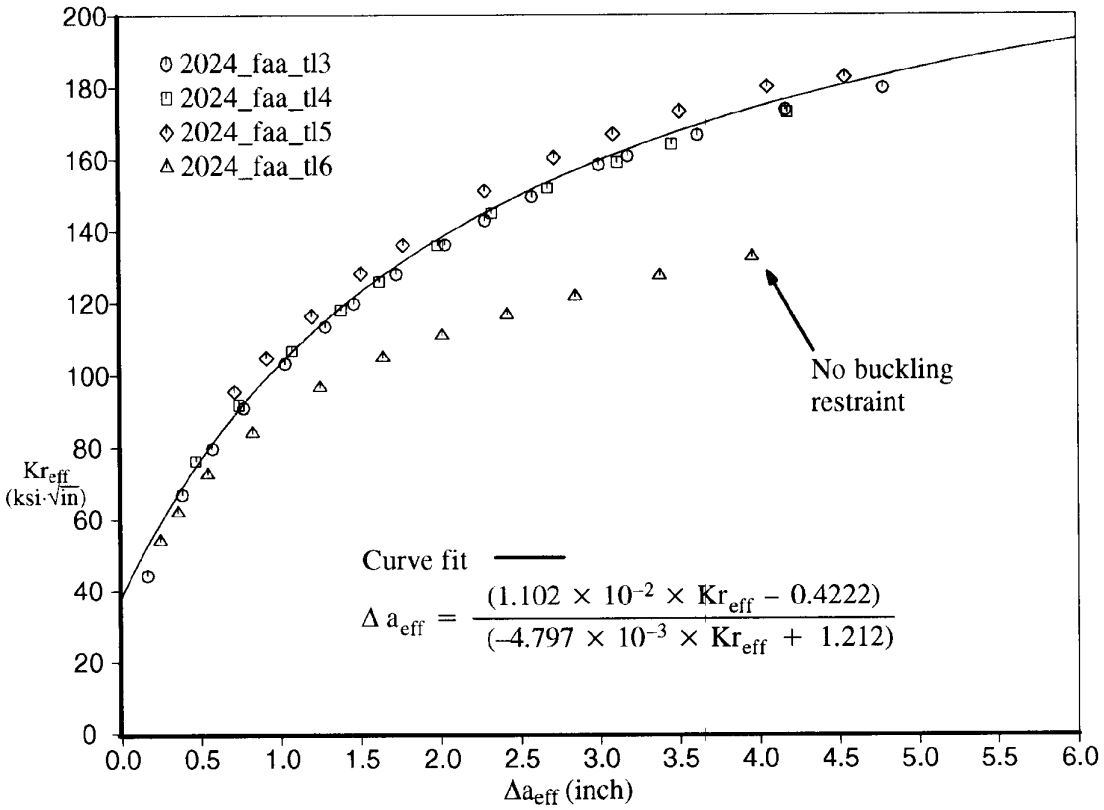

Figure 7. R-Curve Test Results

To calculate the effective crack length, Irwin's plastic zone correction, $r_y = \frac{1}{2\pi}\left(\frac{K}{\sigma_y}\right)^2$, was added to the physical crack length. The effective crack length was then used to calculate the effective stress intensity factor, Kr_{eff}.

During the R–curve test on panel tl3, an optical microscope was used to measure the critical crack tip opening angle (CTOA) at one crack tip. The results of these measurements are presented in figure 8. Averaging all of the measured angles shown in figure 8 gives a critical angle equal to 5.5°.

3. TASK II: CURVED PRESSURE PANEL TESTING

The two full-scale pressure panels with simulated multiple site damage (MSD) were tested in the wide-body pressure test fixture located in Tulalip, Washington. Each panel had two tests planned as shown in Figure 9. In general, the test procedure consisted of inserting a five inch longitudinal sawcut in the skin at the selected test location and pressure cycling until either test termination or the crack reached a length at which a residual strength test was conducted. The crack was then repaired before proceeding to the next test location.

3.1 Pressure Test Facility

The wide-body pressure test fixture used in testing of the panels has a 127 inch radius and a 20 foot length as shown in Figure 10. The overall geometry of the fixture is consistent with typical fuselage design having frames at a 20 inch pitch and stringers at a 9.25 inch pitch. The frames are attached to the stringers by means of stringer clips, but are otherwise not connected directly to the skin. The 2024-T3 clad skin, 7075-T6 frame and 2024-T3 clad stringer gages are thicker than typical minimum gage fuselage structure but have been selected to maintain realistic fixture stiffness and provide adequate longevity. External 2.8 inch wide circumferential tear straps made of 2024-T3 clad sheet are riveted to the skin at a 20 inch spacing. The end bulkheads are steel, one of which is fixed and the other on rollers to permit axial expansion during pressurization.

The wide-body fixture has a single rectangular cutout approximately 10 x 10 feet designed to accept the test panels. The test panels are attached to the fixture at the skin, frames, and stringers by a fusing arrangement that allows the panel to fail at loads below the elastic limit of the fixture components. The stringer and frame splices are designed to allow attachment fasteners to shear during a dynamic panel failure. The test panel skin is allowed to tear circumferentially along the perimeter fasteners with the help of a sharp notch introduced into the panel prior to its installation in the fixture. These features make it possible to conduct residual strength tests which result in test panel failure without extensive damage to the test fixture.

Compressed air is used as the pressurizing medium. The flow of air is regulated into the fixture by means of a digitally controlled valve. Cyclic rates were approximately two minutes per cycle. Polystyrene blocks are placed within the fixture to reduce the required air volume. To reduce air leakage through the sawcut and thus improve cyclic rates, an internal rubber dam was installed after the sawcuts were made. The dam consisted of rubber sheet that was laid up against the skin.

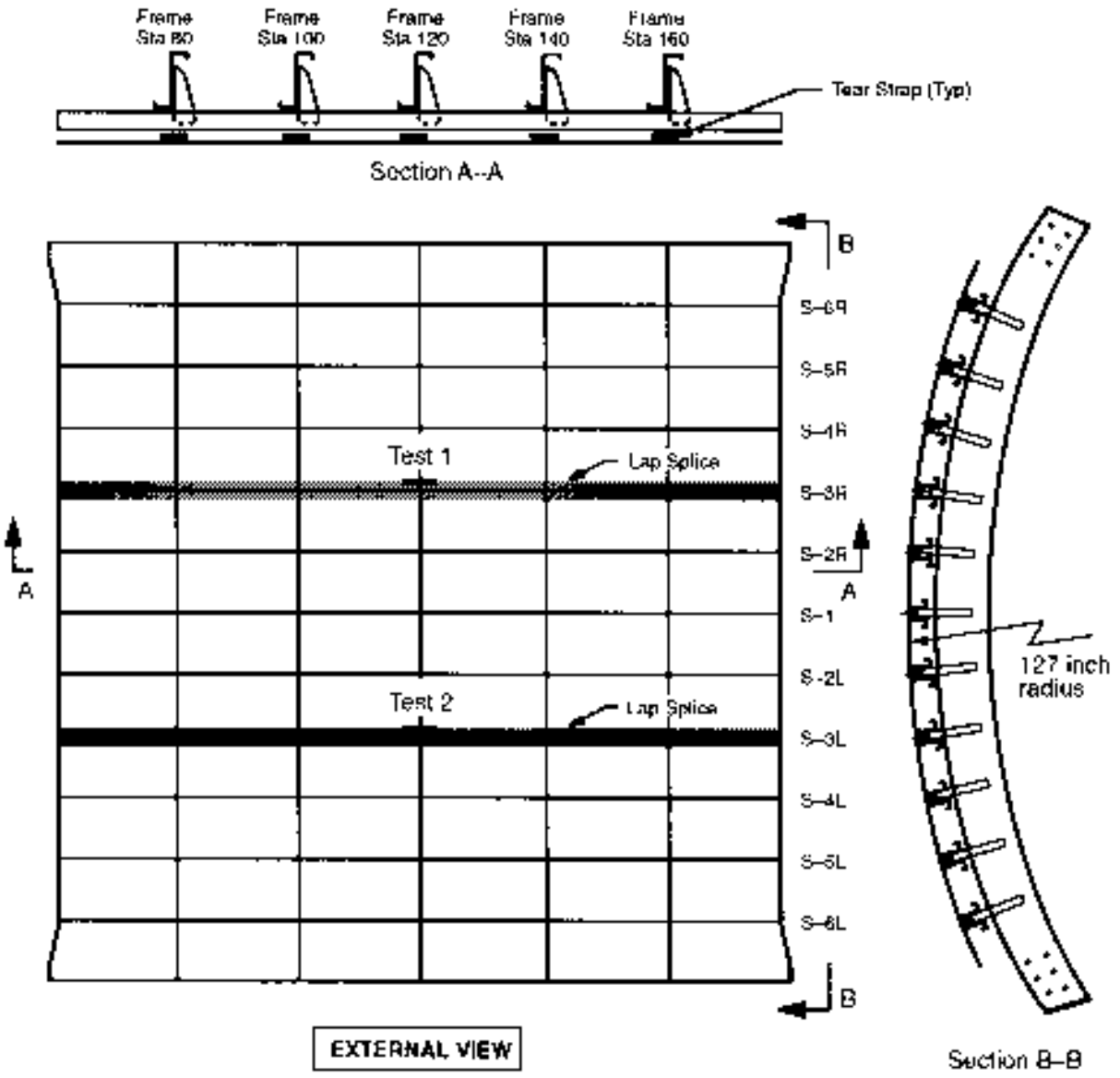

Figure 9. Structural Configuration and Test Locations of Panel FAA 1 and FAA 2

3.2 Pressure Panel Design and Drawing Preparation

Two identical curved wide-body generic panels (FAA 1 and FAA 2) were designed using standard Boeing practices. The panel design was similar to typical wide-body fuselage crown structure consisting of bonded tear straps and floating frames connected to hat section stringers via stringer clips. This is illustrated in Figure 11. The skin is divided into three sections, upper, middle and lower. These sections are joined together along the longitudinal splices (lap joints) located at stringer 3 left and right.

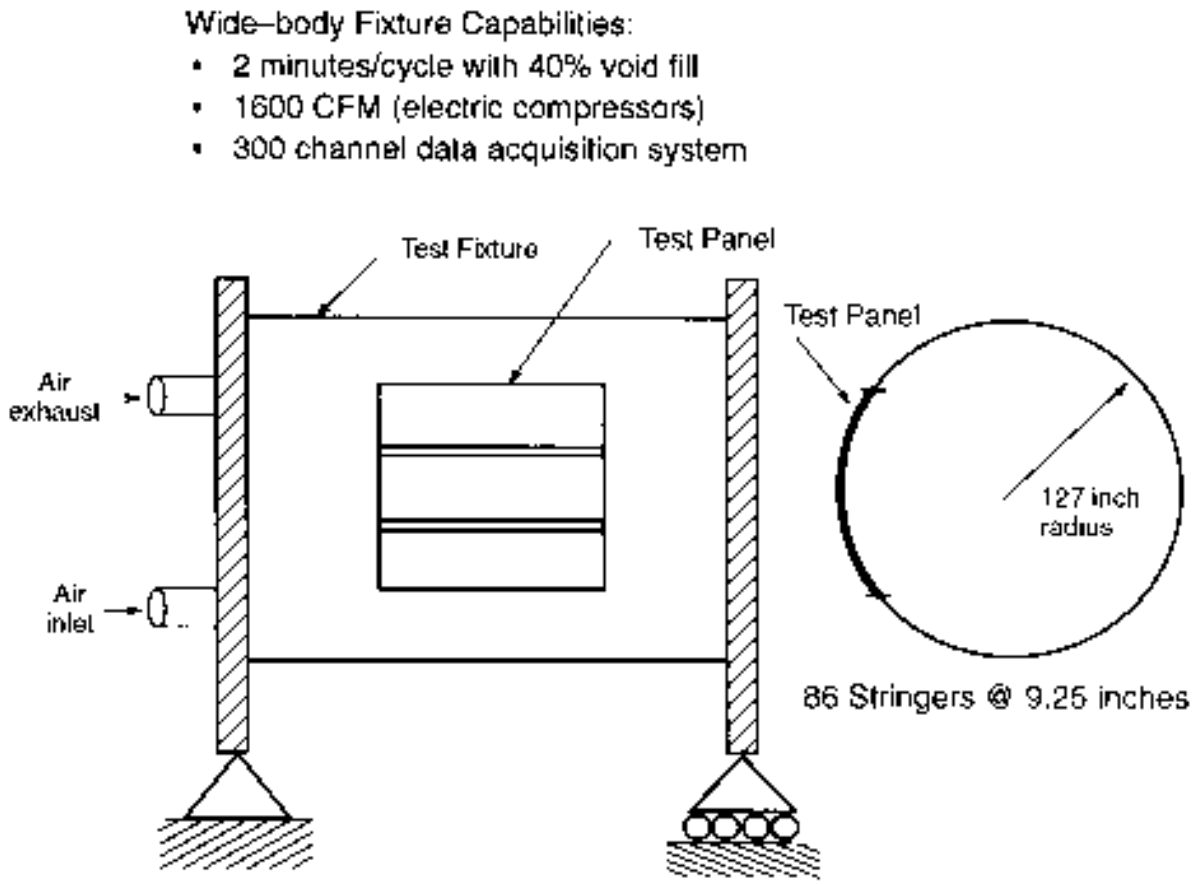

Figure 10. Wide-body Pressure Test Fixture

The lap joints are a typical three row configuration assembled using standard 3/16 inch diameter 100° countersunk head rivets and faying surface sealant. Circumferential tear straps are hot bonded to the skin at each frame station every 20 inches. The grain in the skin is oriented longitudinally unlike the hot bonded tear straps which have their grain oriented circumferentially. The typical panel details such as fastener spacing, lap joint details, tear strap, frame and stringer dimensions are found in Figures 12 through 14.
The tear strap dimensions are defined in terms of strap stiffening ratio: $R_S = A_{strap} / (B \times t_{skin})$. The frame cross sectional area is not included in this area. The stiffening ratio for both test panels was: R_S=0.12.

The drawings were produced using the CAD system CATIA and the current Boeing drafting standards. A paper and an electronic copy (IGES file) of the drawings were delivered to the FAA after drawing release by Boeing.

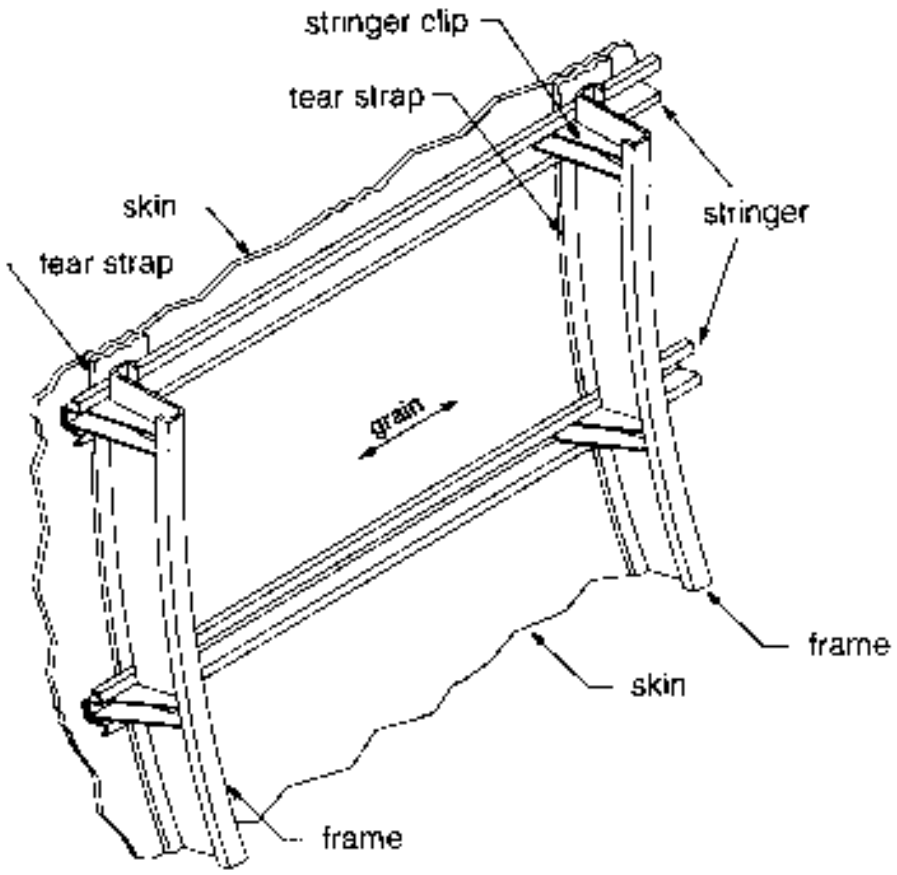

Structural Dimensions	
radius	127 inches
stringer spacing	9.25 inches
frame spacing	20.0 inches
skin thickness	0 063 inch
tear strap thickness	0.063 inch
tear strap width	2 4 inches

$R_s = A_{strap} / (B \times t_{skin})$
$= 0.12$

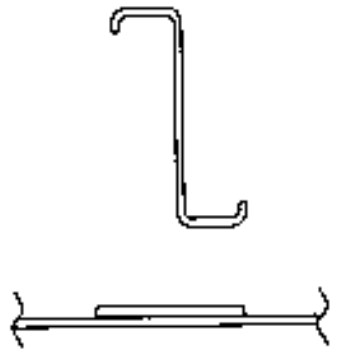

Typical
Skin / Tear strap / Floating Frame

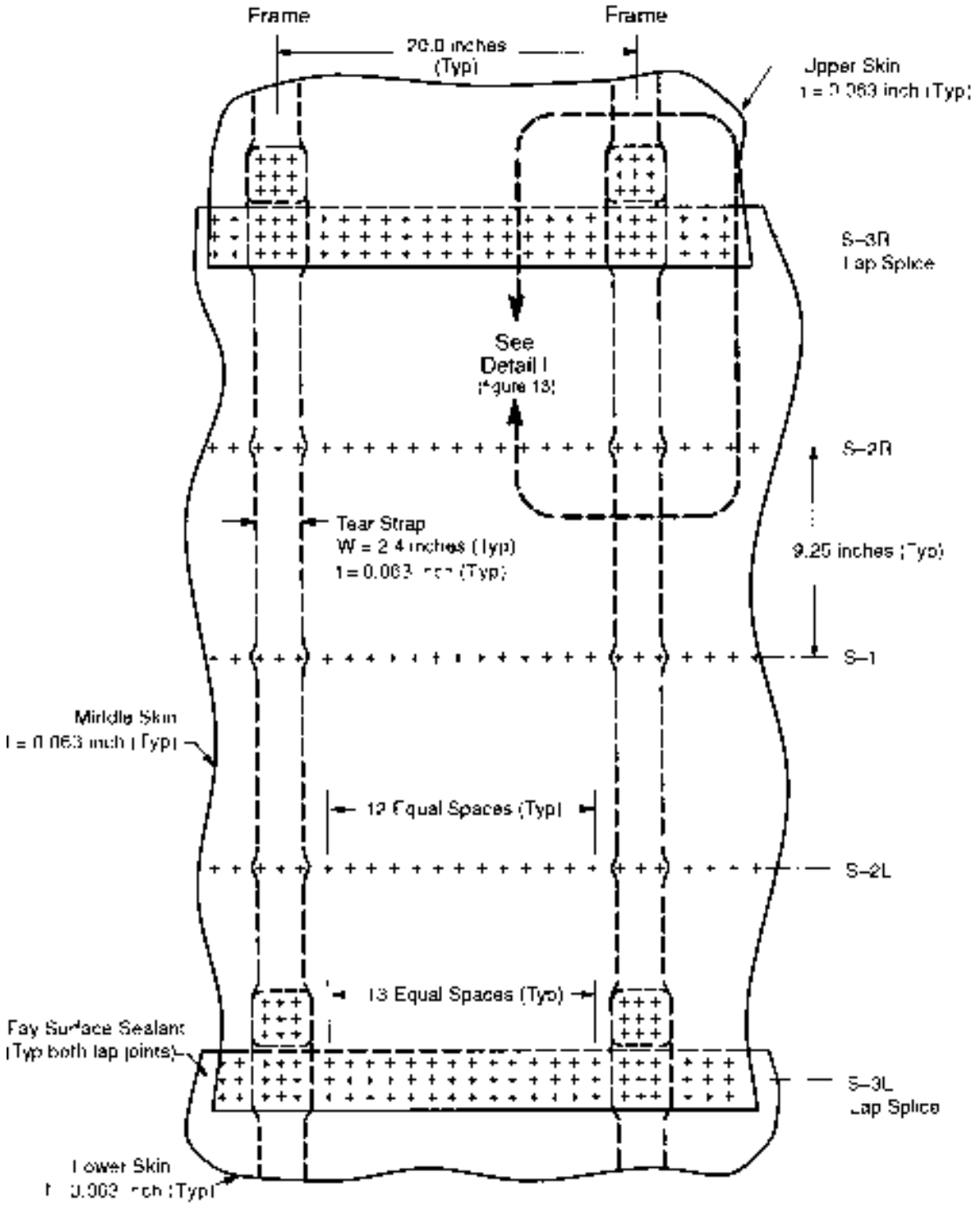

Fig 12 Structural Dimensions of Panel FAA 1 and FAA 2 With Bonded Tear Straps

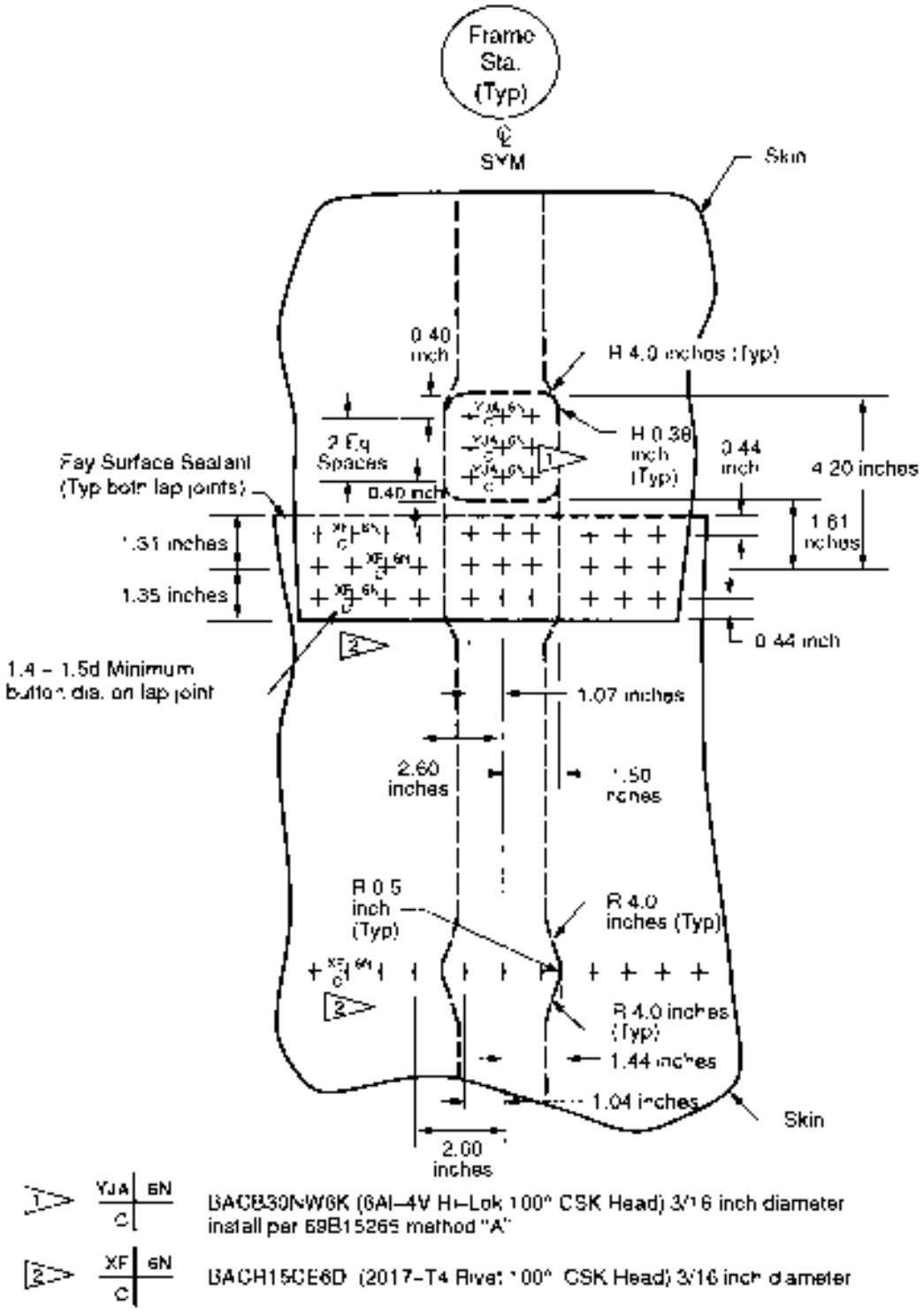

Figure 13. Structural Dimensions (Detail I) of Panel FAA 1 and FAA 2

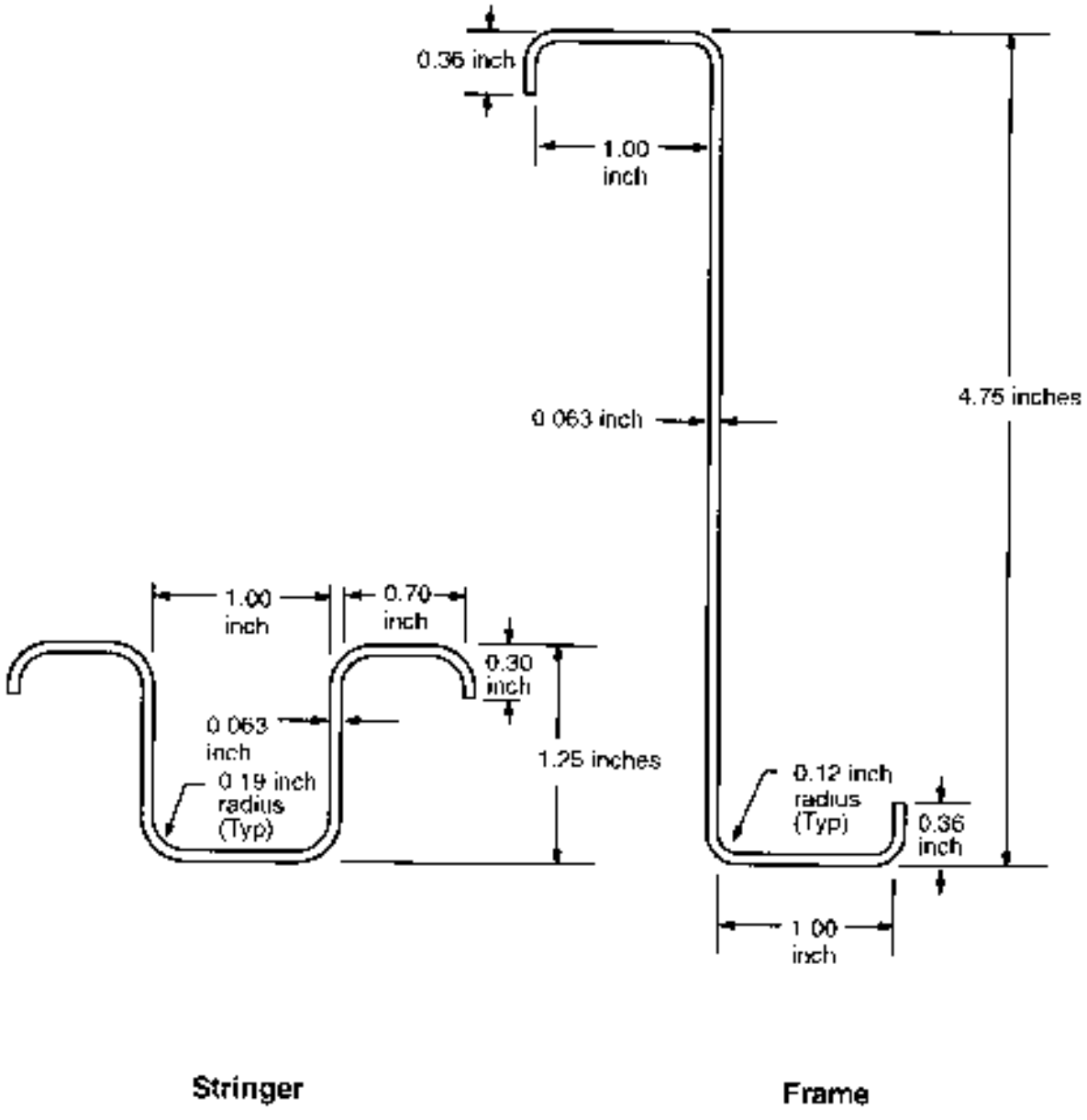

Figure 14. Frame and Stringer Dimensions of Panel FAA 1 and FAA 2

3.3 Material and Fabrication

The skin material used to fabricate the Task II wide-body pressure panels is typical of that used in current production airplanes, as well as from the same lot of material as the Task I flat panel testing program. The test panel skins were typical wide-body crown gage (0.063 inch) with (0.063 inch) circumferential tear straps hot bonded to the skin every 20 inches. This hot bonding process required specific surface treatments, namely phosphoric acid etching prior to bonding and custom autoclave fixturing. The skins and tear straps were shipped to Boeing Wichita in order to meet the hot bonding requirements.

The skin and tear straps were sheared from the same piece of 2024-T3 clad aluminum sheet received from ALCOA. The material was received in three pieces; each were 85 inches wide x 278 inches long. Figure 15 illustrates how the three pieces were divided between Task I and II. Stringers and frames were made from 7075 aluminum clad. The stringers are roll formed and the frames stretch formed into the appropriate radius then both are heat treated to the -T6 condition. The stringer clips are made from 7075-T6511 extrusion.

The detailed parts fabrication and the final assembly of both curved panels were completed at Boeing using standard production procedures and processes.

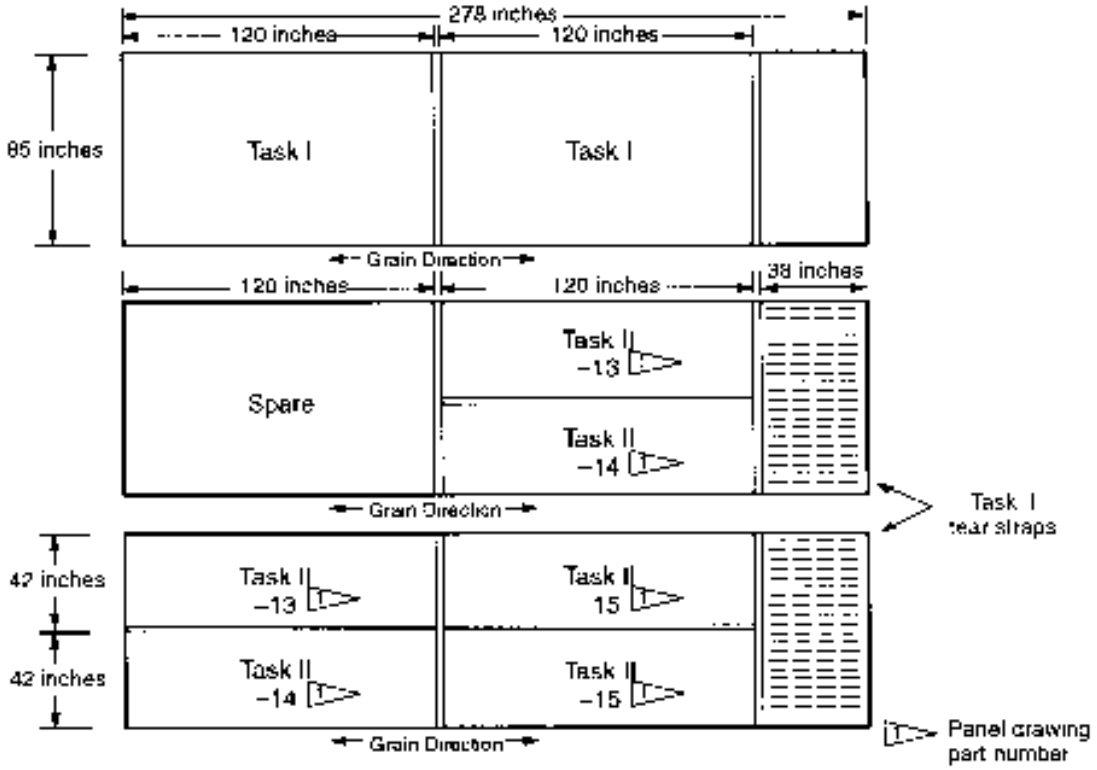

Figure 15. Skin Material Cutting Diagram

Simulated multiple site damage (MSD) was introduced in the upper row of three out of the four lap joints. Saw cuts were made in the outer skin of the lap joints along the upper row of rivets. The sawcuts were oriented out of the fastener holes longitudinally in the 3 and 9 o'clock positions by the use of a modified handsaw producing a 0.006 to 0.008-inch-wide cut. These sawcuts were introduced in the upper skin after the fastener holes had been drilled and countersunk to size, but prior to the application of the fay sealant and rivet installation. Figure 16 shows the 4 bay region (80-inch section) where the simulated MSD sawcuts were installed in both panels with figures 17 and 18 showing further detail.

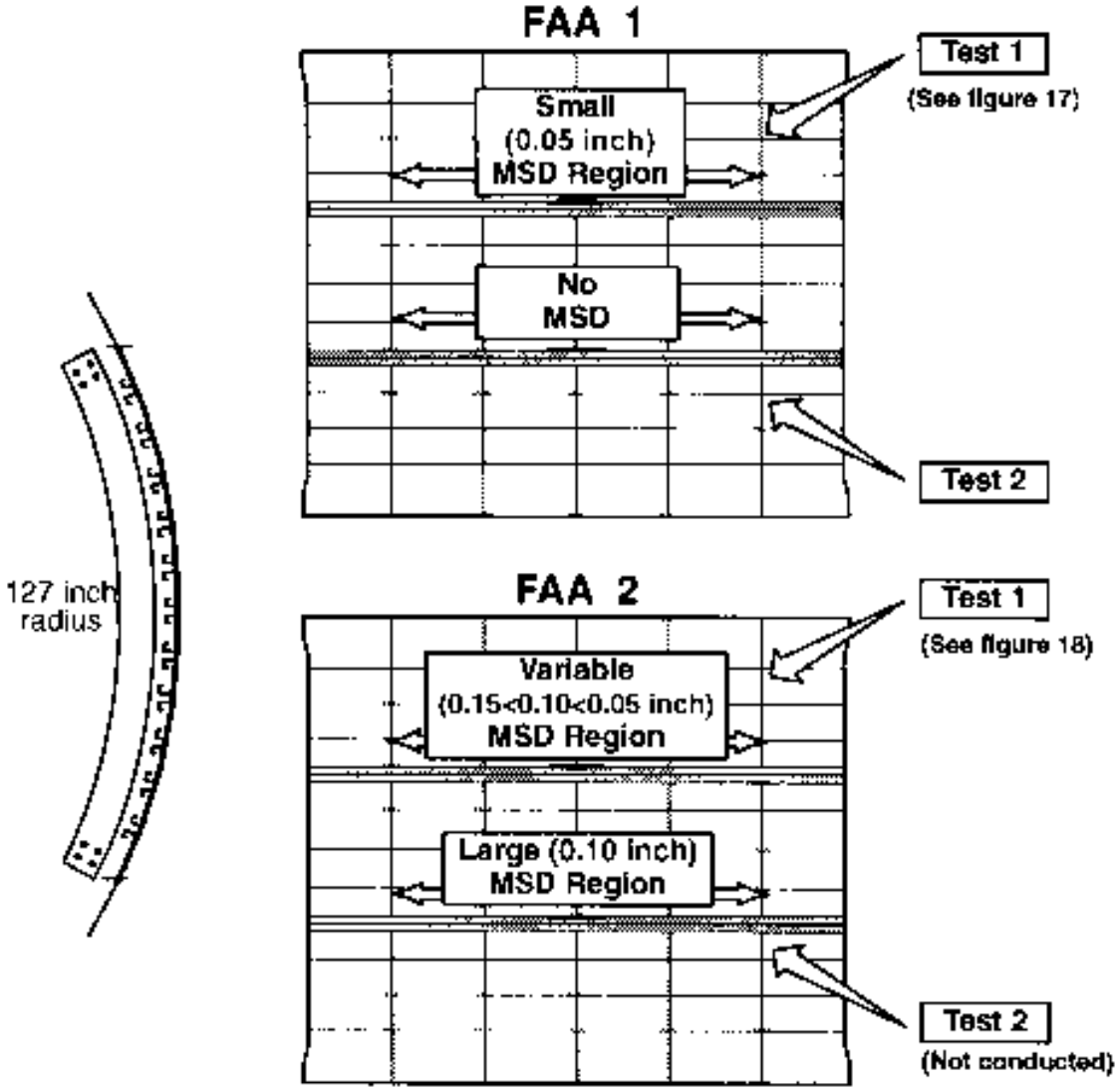

Figure 16. MSD Overview of Panels FAA 1 and FAA 2

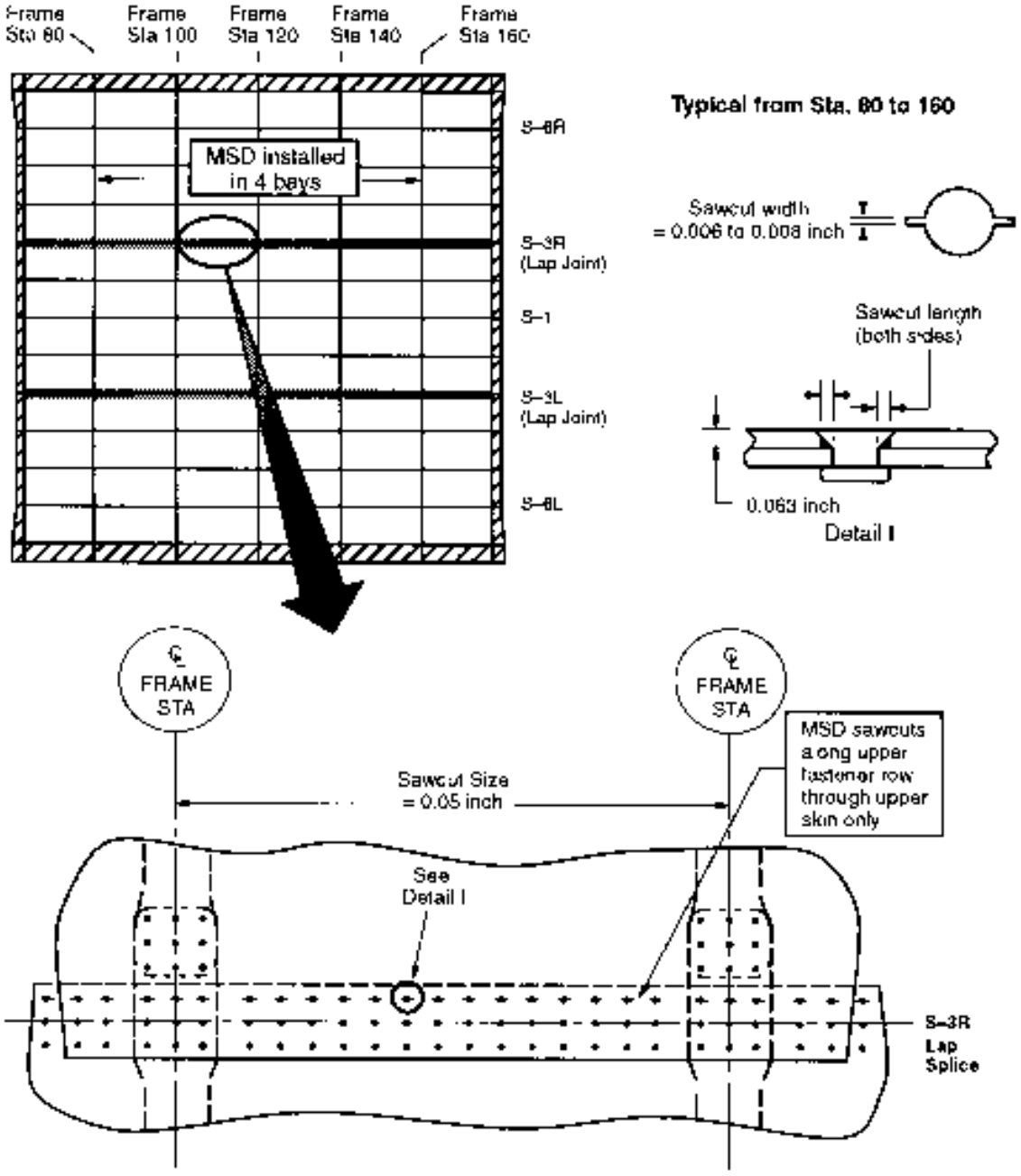

Figure 17. MSD Sawcut Details for Panel FAA 1, Test 1

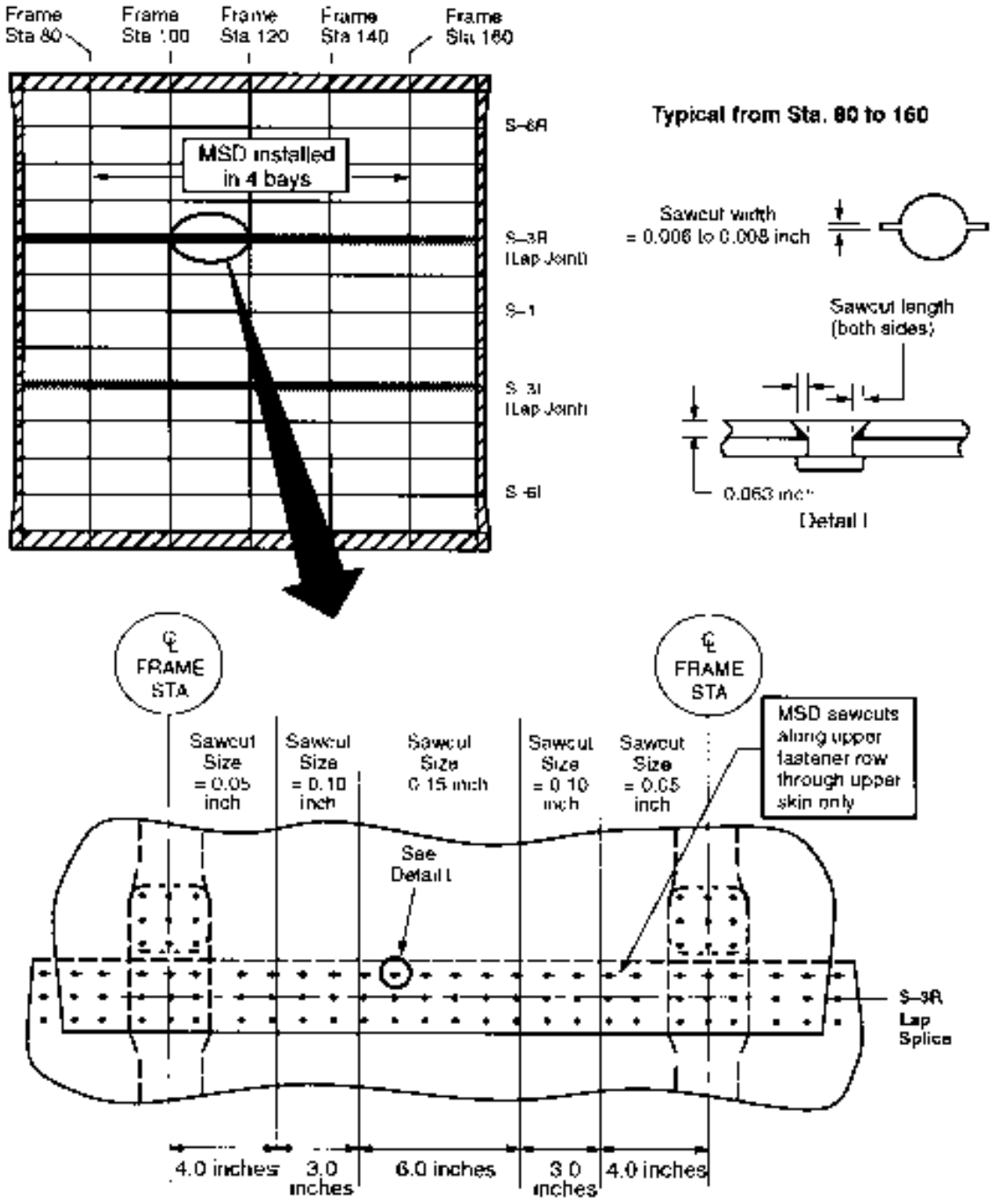

Figure 18. MSD Sawcut Details for Panel FAA 2, Test 1

3.4 Test Results

The results for the three tests conducted are divided into the following sections:

- 3.4.1 Panel FAA 1 - Test 1
  - 3.4.1.1 Crack Growth Results
  - 3.4.1.2 Residual Strength and Panel Repair
- 3.4.2 Panel FAA 1 - Test 2
  - 3.4.2.1 Crack Growth Results
  - 3.4.2.2 Residual Strength and Panel Repair
- 3.4.3 Panel FAA 2 - Test 1
  - 3.4.3.1 Crack Growth Results
  - 3.4.3.2 Residual Strength and Panel Repair

The instrumentation details and strain gage readings for all three tests are found in appendix C. All sawcuts to the skins and frames were installed by the use of an air driven hand held abrasive rotary wheel which creates a 0.1-inch-wide sawcut.

3.4.1 Panel FAA 1 - Test 1

This test was conducted on the upper row of the lap joint located at stringer S-3R centered in the 4 bay region of 0.05-inch simulated MSD shown in Figure 17. Prior to beginning the test, ten pressure cycles were applied in order to "seat" the panel in the test fixture. This allows for any permanent settling to occur prior to conducting the initial strain survey.

The 5-inch sawcut was installed in the upper skin centered on frame station 120 as shown in Figure 19. The panel was pressure cycled at 8.6 psi. No residual strength test was conducted at this location and the crack was repaired. The instrumentation details and strain gage readings are found in appendix C.

3.4.1.1 Crack Growth Results (FAA 1 - Test 1)

The initial 5-inch sawcut was made in the outer skin only. No crack initiations were visible after 281 pressure cycles. At that point the tear strap bridging the sawcut was cut and 88 cycles later 0.63 inch of total crack extension (0.3 and 0.33 inch at the individual tip) was measured. As cycling continued, the main crack steadily grew to approximately 6.5 inches. At this point, the MSD cracks near the tips of the main crack had grown from under the rivets and became visible. The crack trajectory, showing active MSD growth is illustrated pictorially in Figures 20 and 21.

The main crack ran dynamically at 1233 cycles after reaching a length of 17.2 inches and arrested at a length of 37.4 inches. The tear straps contained the dynamic crack, but as a result, created visible MSD in the fasteners common to the tear straps at frame station 100 and 140 as shown in Figure 22.The crack length versus pressure cycles plot is provided in Figure 23 showing the growth from the initial 5-inch sawcut to the final length of 37.44 inches. Table 6 contains the crack growth data for the main crack in conjunction with the visually measured MSD sizes.

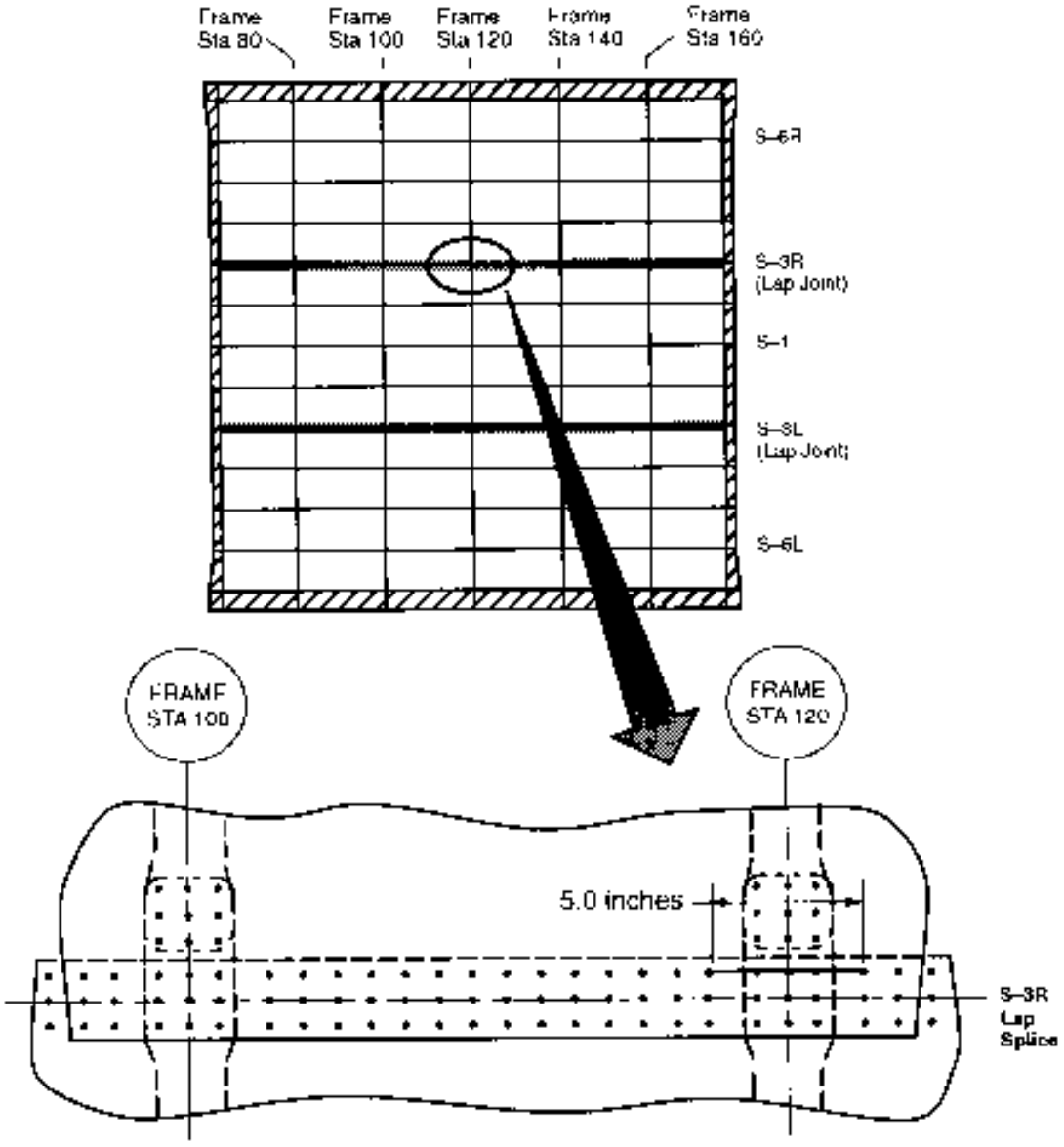

Notes:

– 5–inch sawcut centered at Sta. 120 and along upper fastener row of S–3R lap joint. Skin only at cycle 0.

– Sta 120 tear strap was cut at cycle 281.

Figure 19. Initial Sawcut Details for Panel FAA 1, Test 1

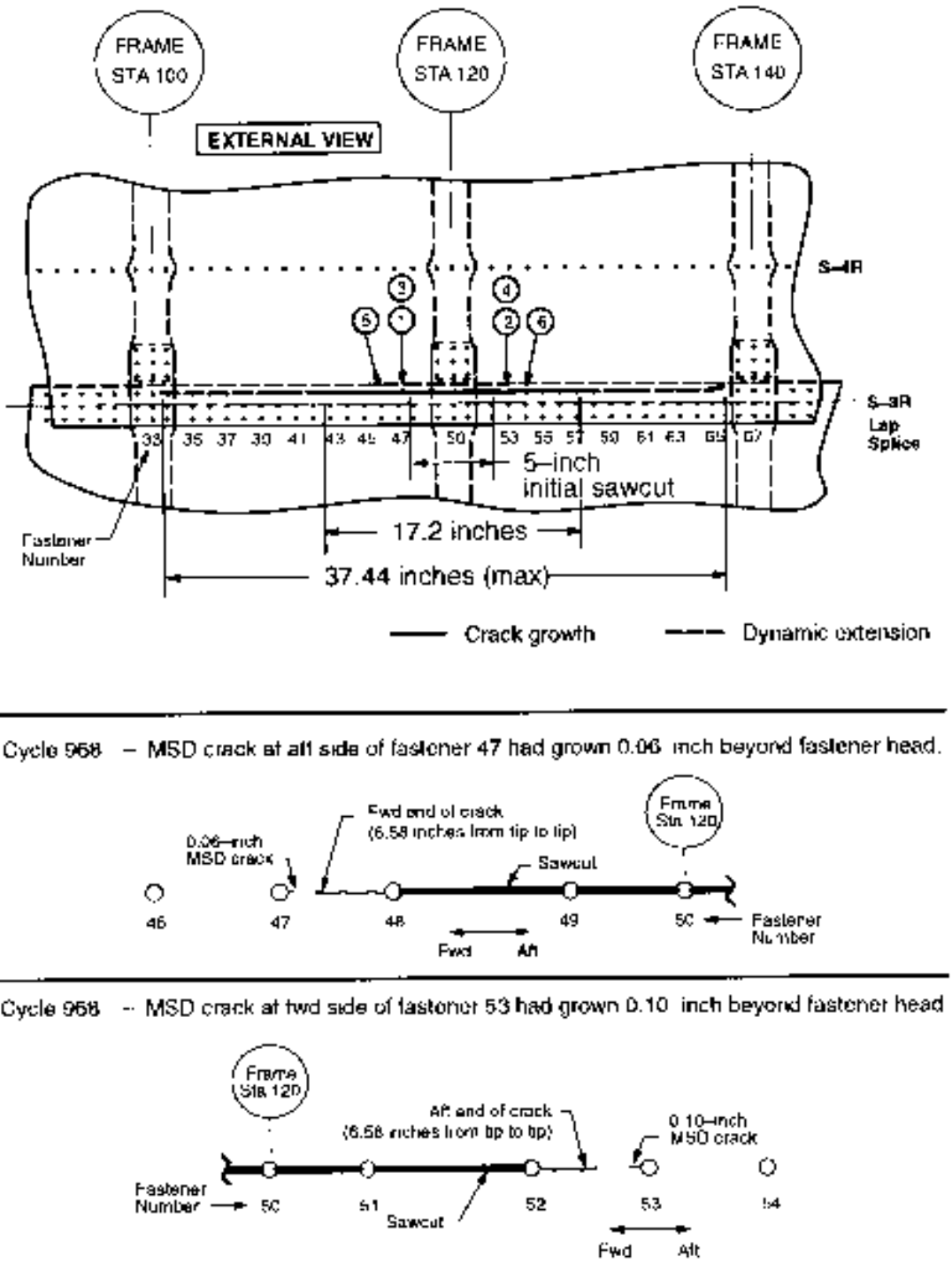

Figure 20. Crack Trajectory of Panel FAA 1, Test 1

③ Cycle 1111 – Fwd end of crack had grown through fastener 47.

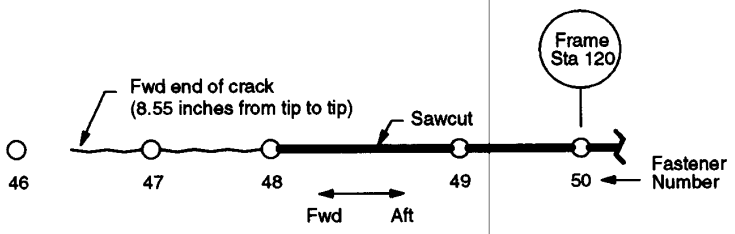

④ Cycle 1111 – Aft end of crack had grown through fastener 53.

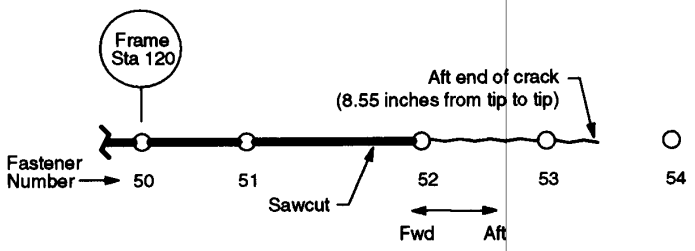

⑤ Cycle 1190 – MSD crack at aft side of fastener 45 had grown 0.11 inch beyond fastener head.

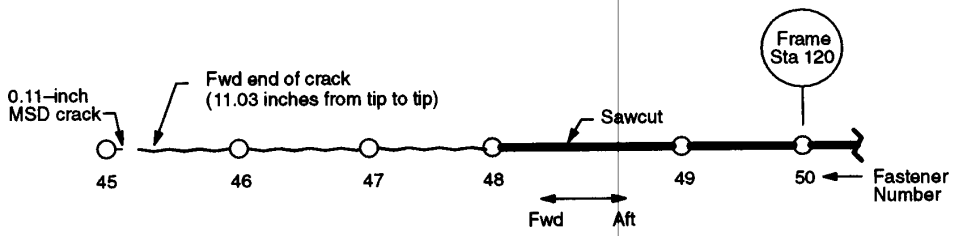

⑥ Cycle 1190 – MSD crack at fwd side of fastener 55 had grown 0.11 inch beyond fastener head.

Figure 21. Crack Trajectory of Panel FAA 1, Test 1

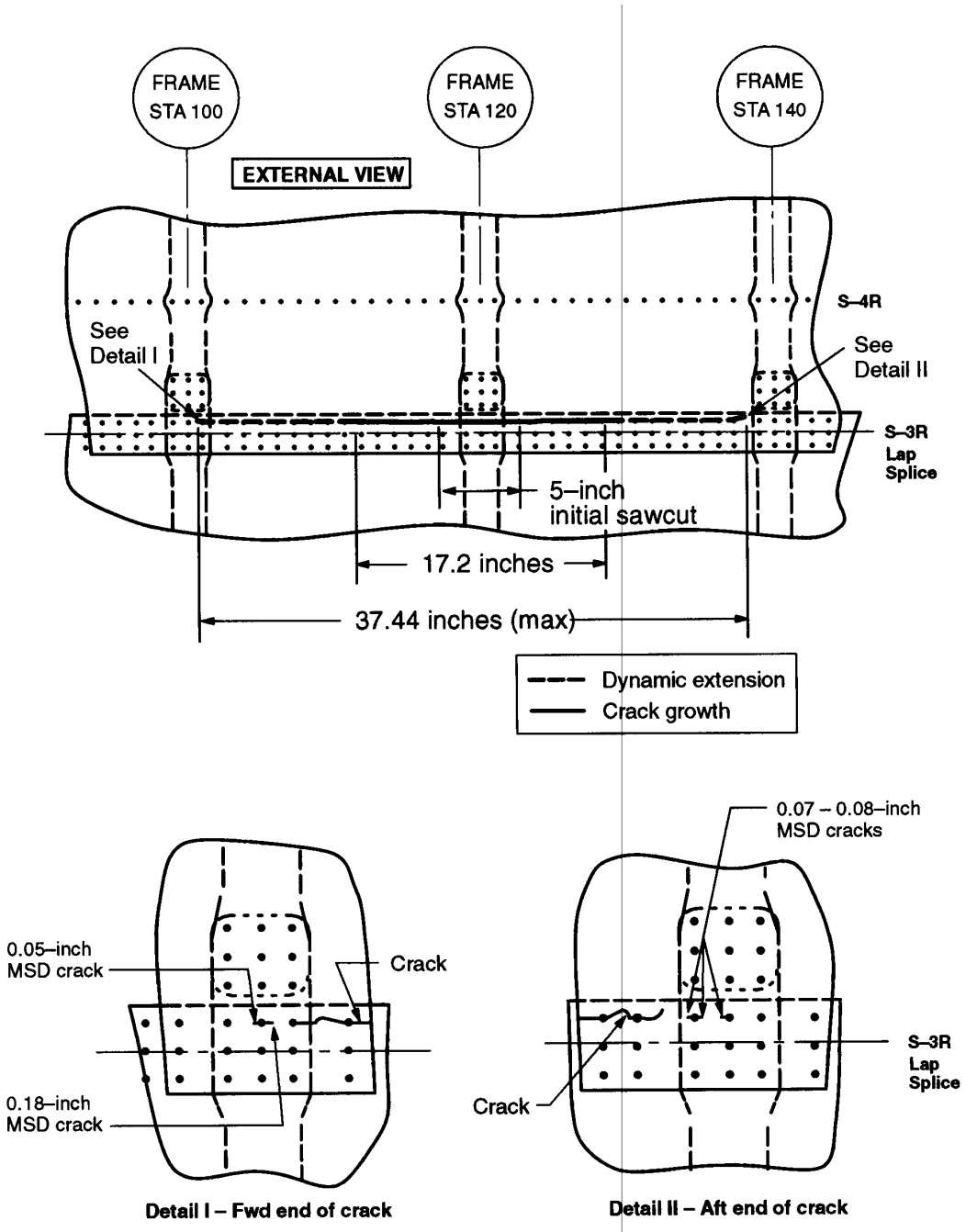

Figure 22. Crack Trajectory of Panel FAA 1, Test 1

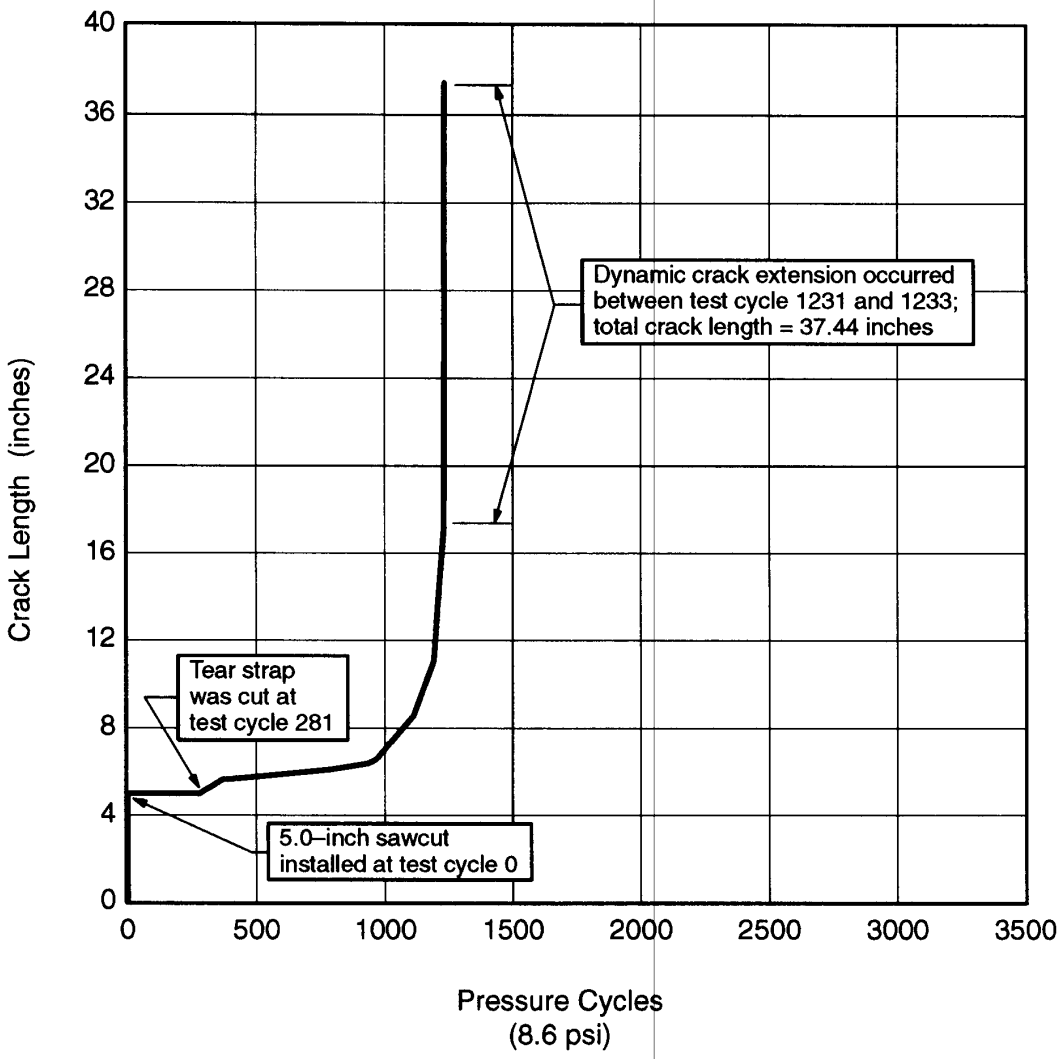

Figure 23. Crack Growth History of Panel FAA 1, Test 1

Cycle Number	Length of New Growth (inch)	Total (X) Dimension (inch)		Total (Y) Dimension (inch)		Total Crack Length (inch)
		Fwd Tip	Aft Tip	Fwd Tip	Aft Tip	
–	Intact	0	0	0	0	0
0	Sawcut installed (skin only)	–	–	–	–	5.0
281	Tear strap cut	–	–	–	–	5.0
369	0.63	0.30	0.33	0	0	5.63
569	0.22	0.44	0.41	0	0	5.85
789	0.25	0.58	0.52	0	0	6.10
937	0.28	0.70	0.68	0	0	6.38
968	0.20 MSD cracks: 0.06 at fastener 47 aft 0.10 at fastener 53 fwd	0.80	0.78	0.04	–0.04	6.58
1111	1.97 Crack grew through fasteners 47 and 53	1.77	1.78	0	0.06	8.55
1190	2.49 MSD cracks: 0.11 at fastener 45 aft 0.11 at fastener 55 fwd	3.01	3.02	0	0.04	11.03
1231	6.18	6.1	6.1	0.05	0.05	17.20
1233	20.24	16.87	15.57	0.12	0.30	37.44 Dynamic Extension

Table 6. Test Record of Crack Length Measurements From Panel FAA 1, Test 1

3.4.1.2 Residual Strength and Panel Repair (FAA 1 - Test 1)

No residual strength test was conducted at this test location as a result of the damage caused by the crack running from 17 to 37 inches in one cycle. It was agreed upon by the FAA that the Test 1 location would be repaired prior to running the residual strength test and at location 2 in order to guarantee the completion of the only non-MSD test. The risk of conducting the residual strength test at location 1 in this condition was that the panel would be destroyed if the crack dynamically ran unexpectedly.

The test 1 location was repaired by applying an external doubler as shown in Figure 24. The circumferential size of the repair was minimized in order to reduce any influence on the test 2 location.

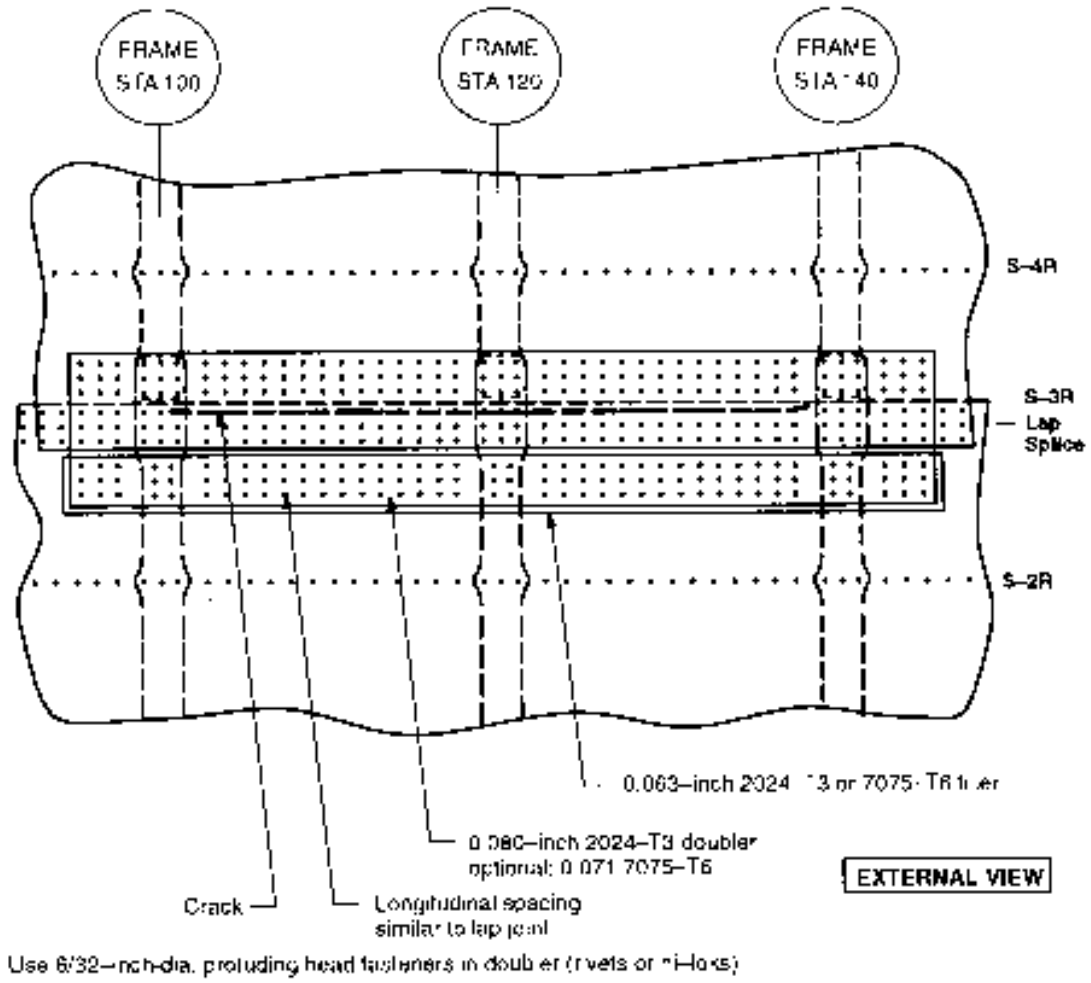

Figure 24. Panel Repair of FAA 1, Test 1

3.4.2 Panel FAA 1 - Test 2

This test was conducted on the upper row of the lap joint located at stringer S-3L with no MSD as shown in Figure 16. The initial strain survey was recorded after the repair was completed at test 1 location.

The 5-inch sawcut was installed in the upper skin and tear strap centered on frame station 120 as shown in Figure 25. The panel was pressure cycled at 8.6 psi.

The residual strength test was conducted once the crack length reached 36.91 inches with a severed central frame. Panel failure occurred at 9.4 psi.

The instrumentation details and strain gage readings are found in appendix C.

3.4.2.1 Crack Growth Results (FAA 1 - Test 2)

The initial 5-inch sawcut was made in the outer skin and tear strap. After 1172 pressure cycles, no crack growth had been detected from the sawcut, and therefore the sawcut was extended to 5.72 inches, approximately 0.25 inch beyond the fastener holes at each end of the sawcut as shown in Figure 25. After 274 additional pressure cycles, a crack extension of 0.26 inch (0.14 and 0.12 inch on the individual tips) was measured. As cycling continued the main crack steadily grew to a length of 36.91 inches, as illustrated pictorially in Figures 26 through 30.

The crack length versus pressure cycles plot is provided in Figure 31 showing the growth from the initial 5-inch sawcut to the final length of 36.91 inches. Table 7 contains the crack growth data for the main crack.

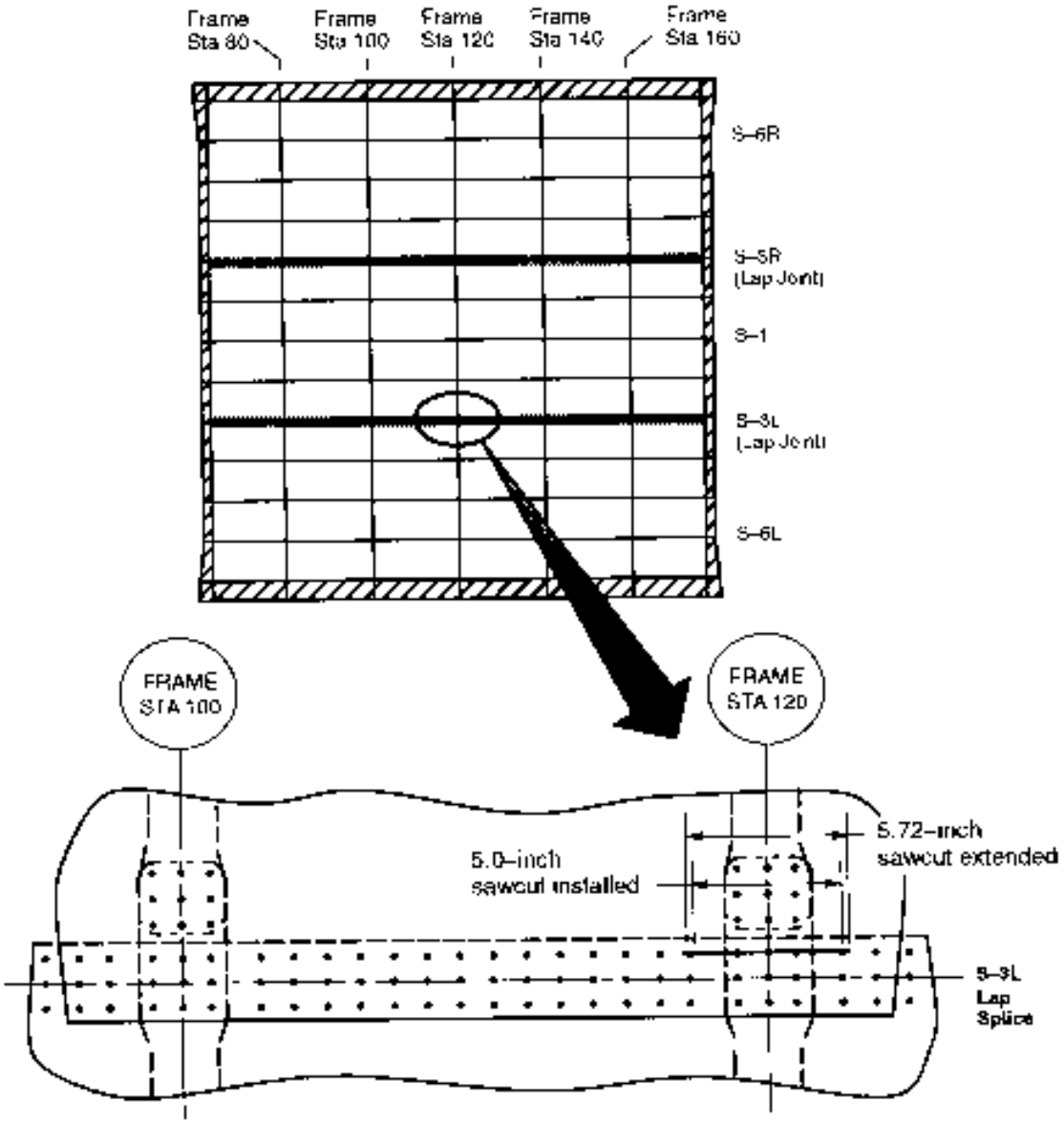

Notes:

- 5–inch sawcut centered at Sta. 120 and along upper fastener row of S–3L lap joint. Upper skin and tear strap was cut at test cycle 6 (panel cycle 1260).
- Sawcut was extended to 5.72 inches at test cycle 1172 (panel cycle 2426).

Figure 25

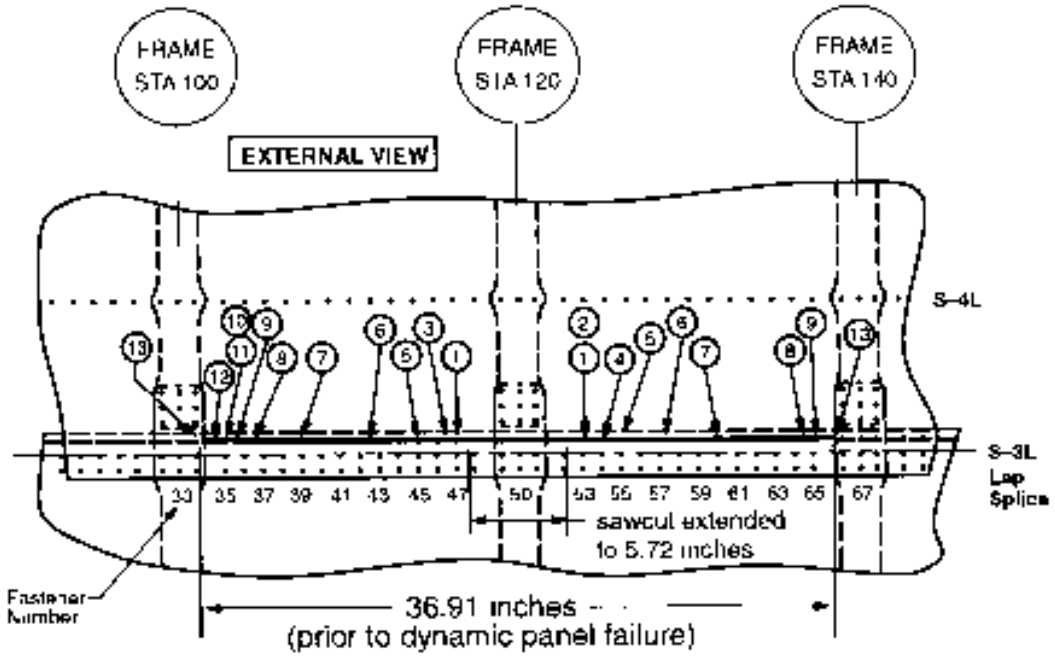

① Cycle 2056 – Fwd end of crack grew into fastener 47. Aft end of crack grew into fastener 53.

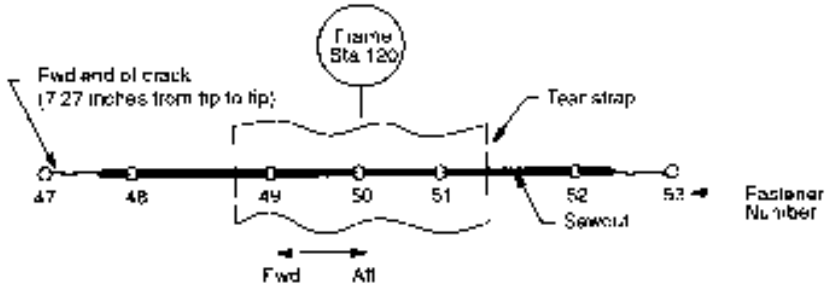

② Cycle 2162 – Aft end of crack grew thru fastener 53

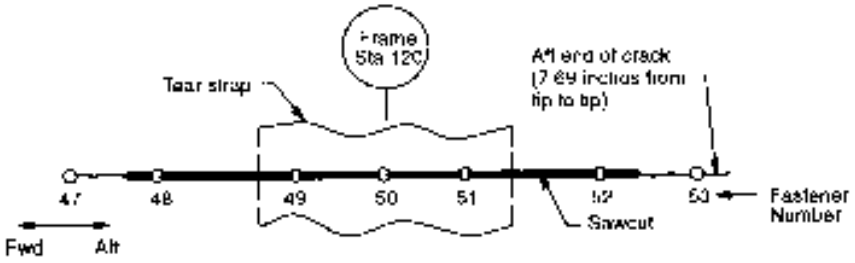

Figure 26

③ Cycle 2309 – Fwd end of crack grew thru fastener 47. Aft end of crack grew 0.23 inch.

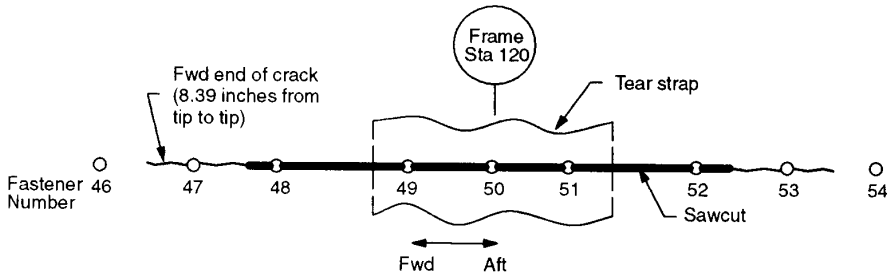

④ Cycle 2484 – Aft end of crack grew into fastener 54. Fwd end of crack grew 0.46 inch.

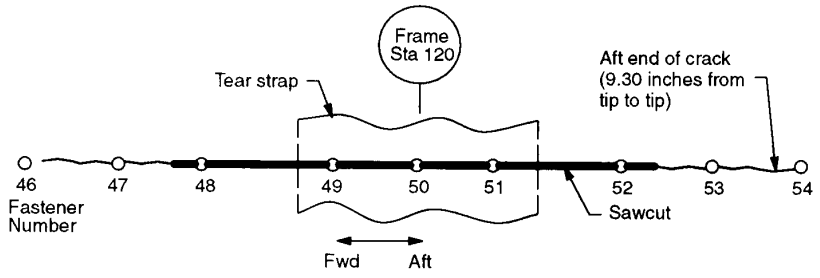

⑤ Cycle 2680 – Aft end of crack grew into fastener 55. Fwd end of crack grew into fastener 45.

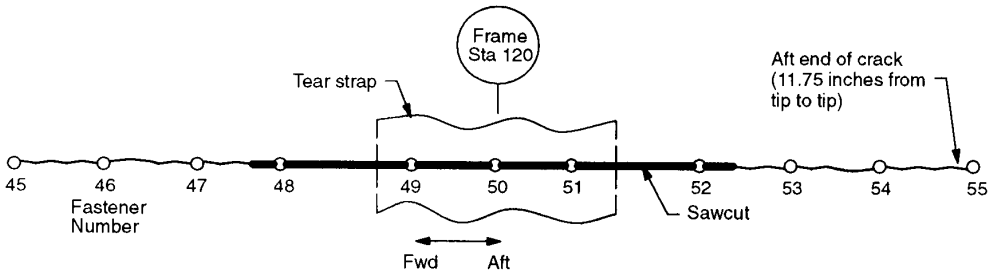

Figure 27. Crack Trajectory of Panel FAA 1, Test 2

⑥ Cycle 2859 – Fwd end of crack grew thru fastener 43. Aft end of crack grew thru fastener 57.

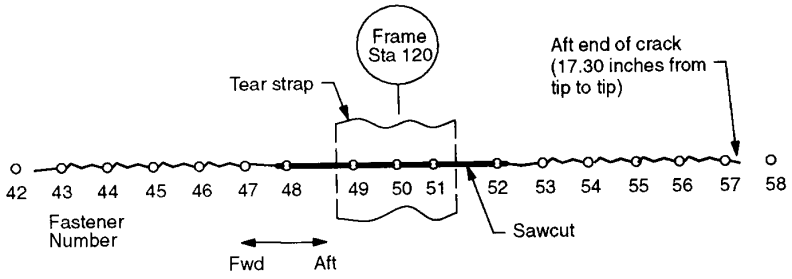

⑦ Cycle 2974 – Aft end of crack grew into fastener 60. Fwd end of crack grew into fastener 39.

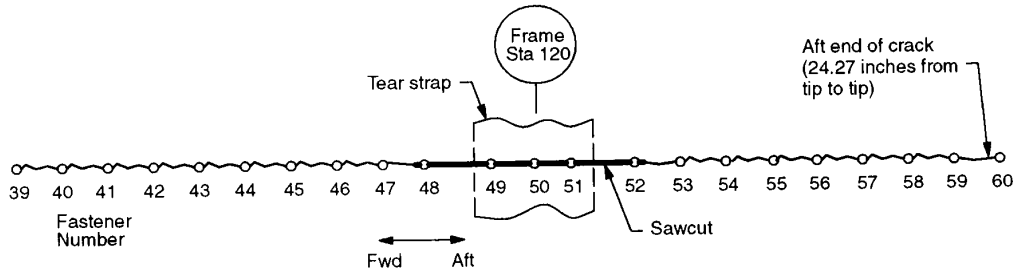

⑧ Cycle 3025 – Fwd end of crack grew thru fastener 37. Aft end of crack grew thru fastener 64.

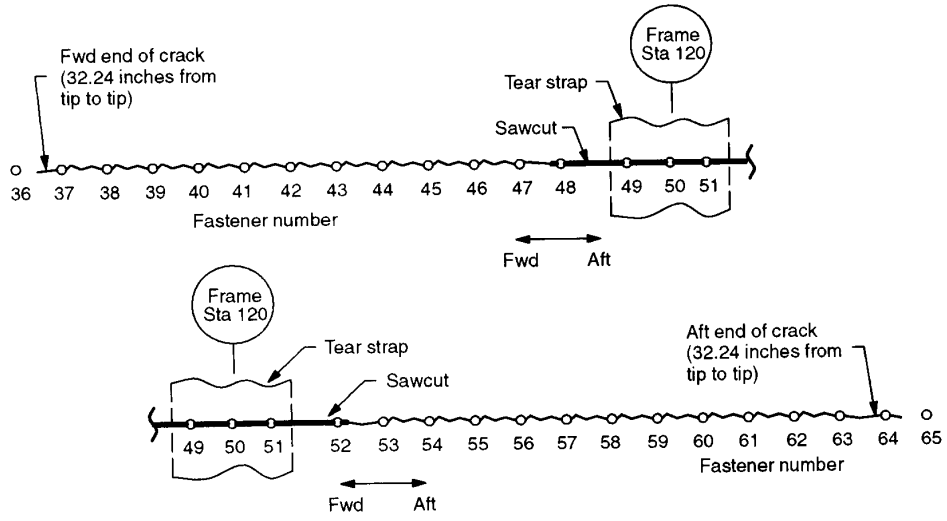

Figure 28. Crack Trajectory of Panel FAA 1, Test 2

⑨ Cycle 3035 – Fwd end of crack grew thru fastener 36. Aft end of crack grew to fastener 65.

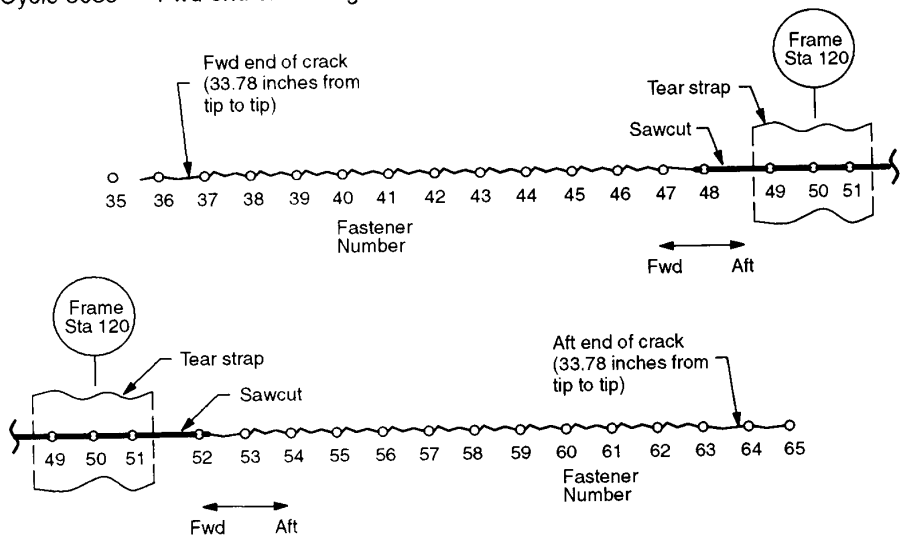

⑩ Cycle 3045 – Fwd end of crack grew 0.53 inch. No new growth at aft end of crack.

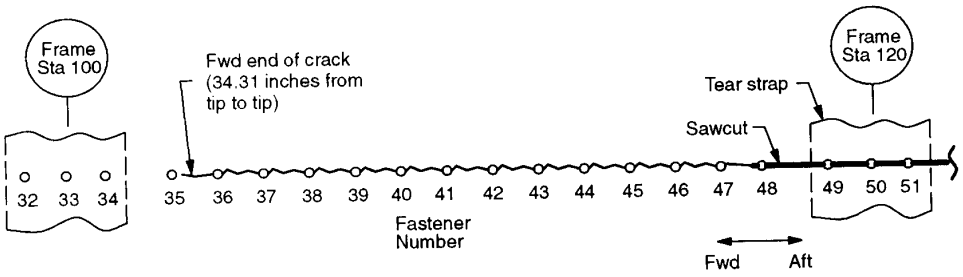

⑪ Cycle 3055 – Fwd end of crack grew into fastener 35. No new growth at aft end of crack.

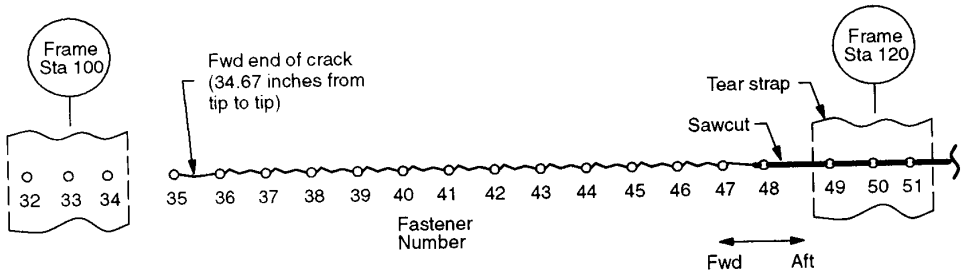

Figure 29. Crack Trajectory of Panel FAA 1, Test 2

⑫ Cycle 3065 - Fwd end of crack grew thru fastener 35. Second crack grew 0.20 inch on aft side of fastener 35. No new growth at aft end of crack.

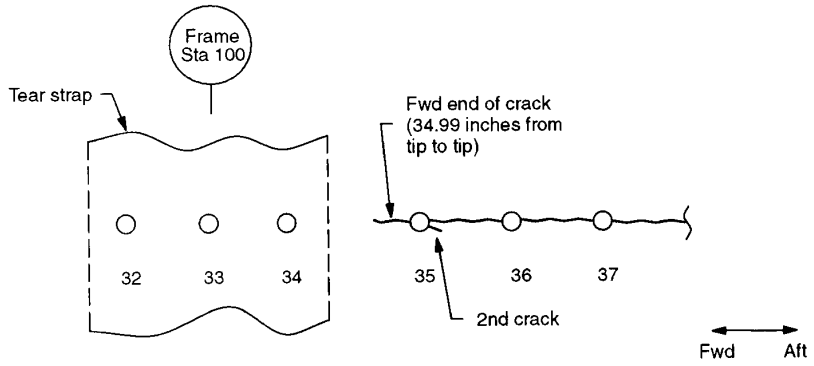

⑬ Cycle 3101 – Both ends of crack is at leading edge of tear straps. Prior to dynamic panel failure at cycle 3102.

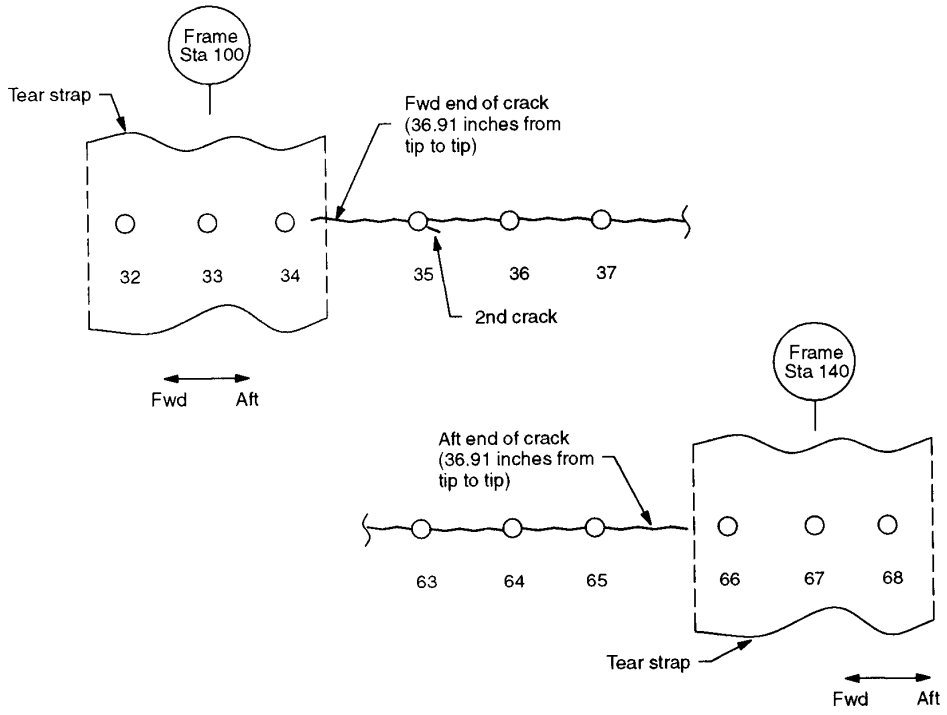

Figure 30. Crack Trajectory of Panel FAA 1, Test 2

Table 7. Test Record of Crack Length Measurements From Panel FAA 1, Test 2

Test Cycle Number	Panel Cycle Number	Length of New Growth (inch)	Total (X) Dimension (inch)		Total (Y) Dimension (inch)		Total Crack Length (inch)
			Fwd Tip	Aft Tip	Fwd Tip	Aft Tip	
–	1254	Intact	0	0	0	0	0
6	After 1260	Sawcut installed	–	–	–	–	5.00
1172	2426	Sawcut extended	–	–	–	–	5.72
1446	2700	0.26	0.14	0.12	0	0	5.98
1614	2868	0.14	0.20	0.20	0	0	6.12
1791	3045	0.22	0.32	0.30	0	0	6.34
1961	3215	0.36	0.50	0.48	0	0	6.70
2056	3310	0.57	0.77	0.78	0	0	7.27
2162	3416	0.42	0.77	1.20	0	0	7.69
2309	3563	0.70	1.24	1.43	0	0	8.39
2484	3738	0.91	1.70	1.88	0	0.04	9.30
2680	3934	2.45	3.05	2.98	0	0	11.75
2859	4113	5.55	5.86	5.72	0	0	17.30
2974	4228	6.97	9.87	8.68	0	0	24.27
3025	4279	7.97	12.75	13.77	0	0	32.24
3035	4289	1.54	13.67	14.39	0	0	33.78
3045	4299	0.53	14.20	14.39	0.12	0	34.31
3056	4310	0.36	14.56	14.39	0.08	0	34.67
3075	4329	0.32	14.88	14.39	0	0	34.99
3099	4353	1.72	15.51	15.48	0.07	0.08	36.71
3101	4355	0.20	15.64	15.55	0.06	0.08	36.91

3.4.2.2 Residual Strength (FAA 1 - Test 2)

The residual strength test consisted of increasing the internal pressure in small intervals until dynamic panel failure occurred. Prior to running the residual strength test the central frame at station 120 was severed.

The crack configuration prior to start was a 2 bay skin crack centered on a severed central frame. The tips of the 36.91-inch crack were adjacent to the edges of the tear straps as shown in Figure 30. The pressure was increased at a rate of approximately 0.2 psi. per minute. As the pressure was increased above 8.3 psi. the forward tip grew into fastener hole 34 (refer to Figure 32 below for fastener numbering) then as the pressure was increased from 9.2 to 9.3 psi. the crack stably grew to within approximately 0.1 inch of fastener 33. The aft tip showed no growth as the pressure was increased to 9.3 psi. As the pressure was further increased above 9.3 to 9.4 psi. the crack ran dynamically from approximately 38.2 inches to the ends of the panel resulting in catastrophic failure. Figures 33 and 34 illustrate the dynamic crack trajectory.

The strain gage stresses are provided at 8.6 psi. with the central frame intact and then severed for review in appendix C Figures C-35 through C-38 (intact) and C-39 through C-42 (severed) respectively.

The stresses recorded at the highest pressure (9.4 psi.) prior to failure are provided in appendix C Figures C-43 through C-46.

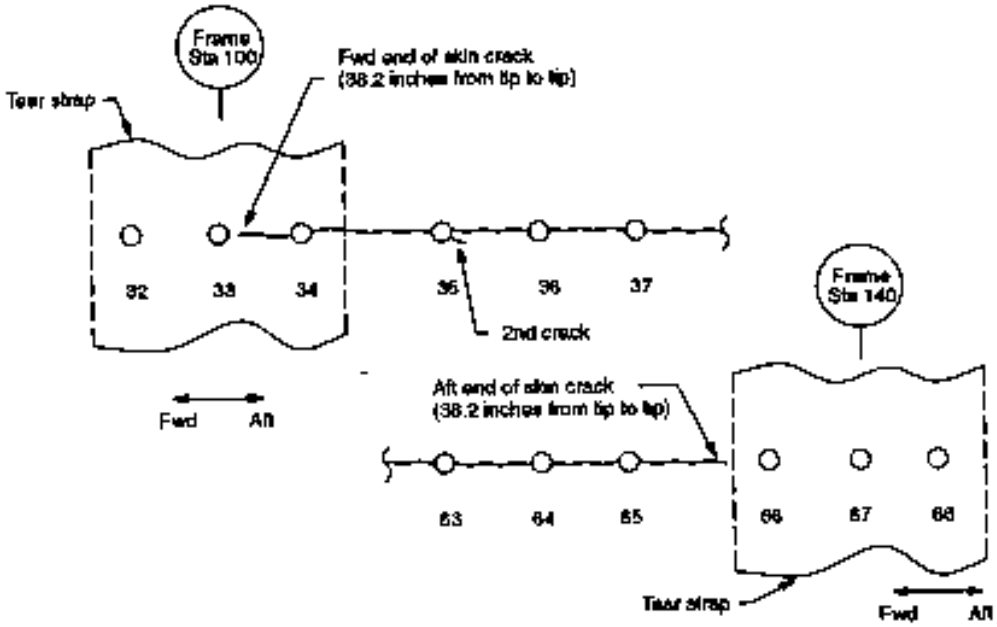

Figure 32. Crack Configuration Prior to Panel Failure

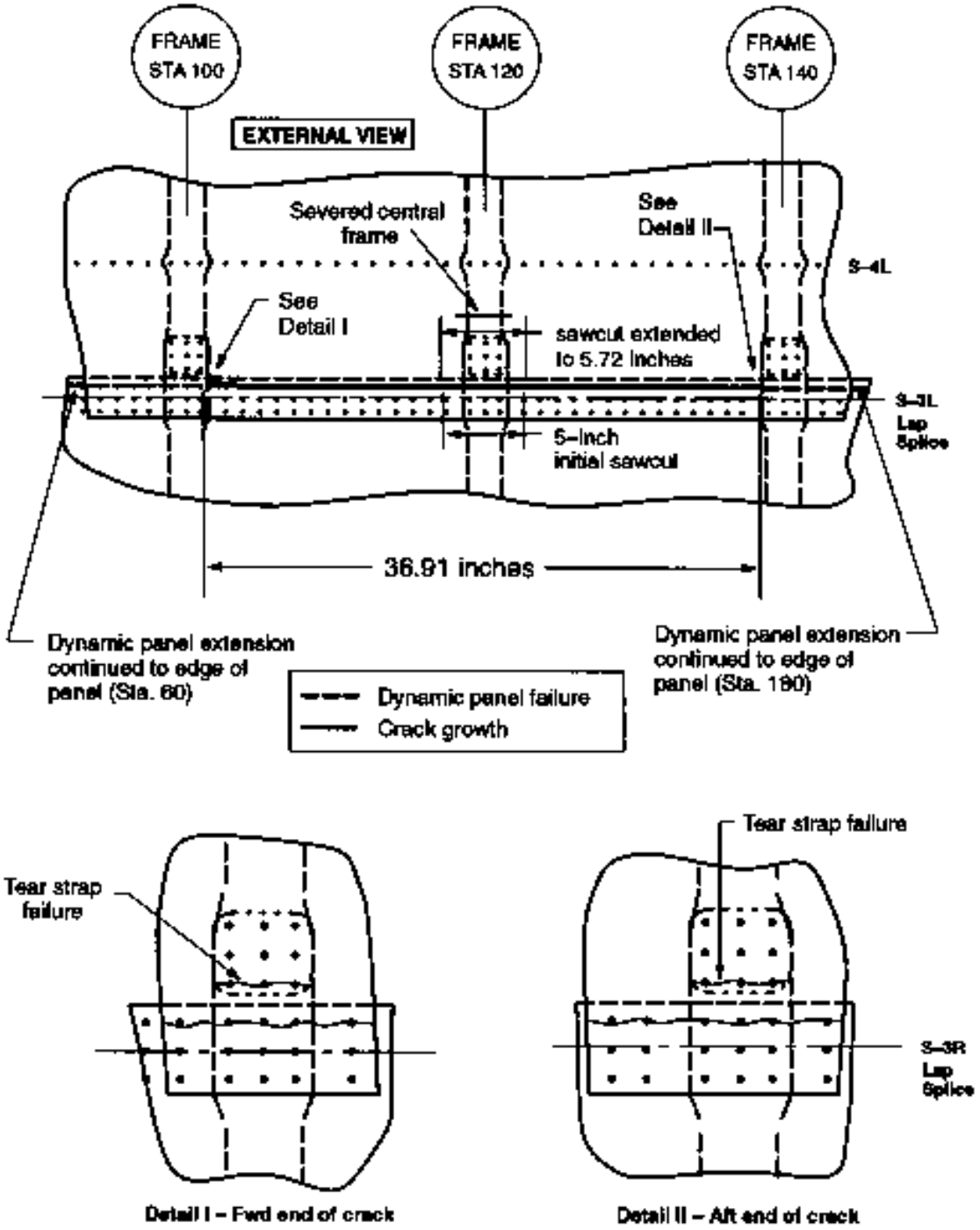

Figure 33. Crack Trajectory of Panel FAA 1, Test 2

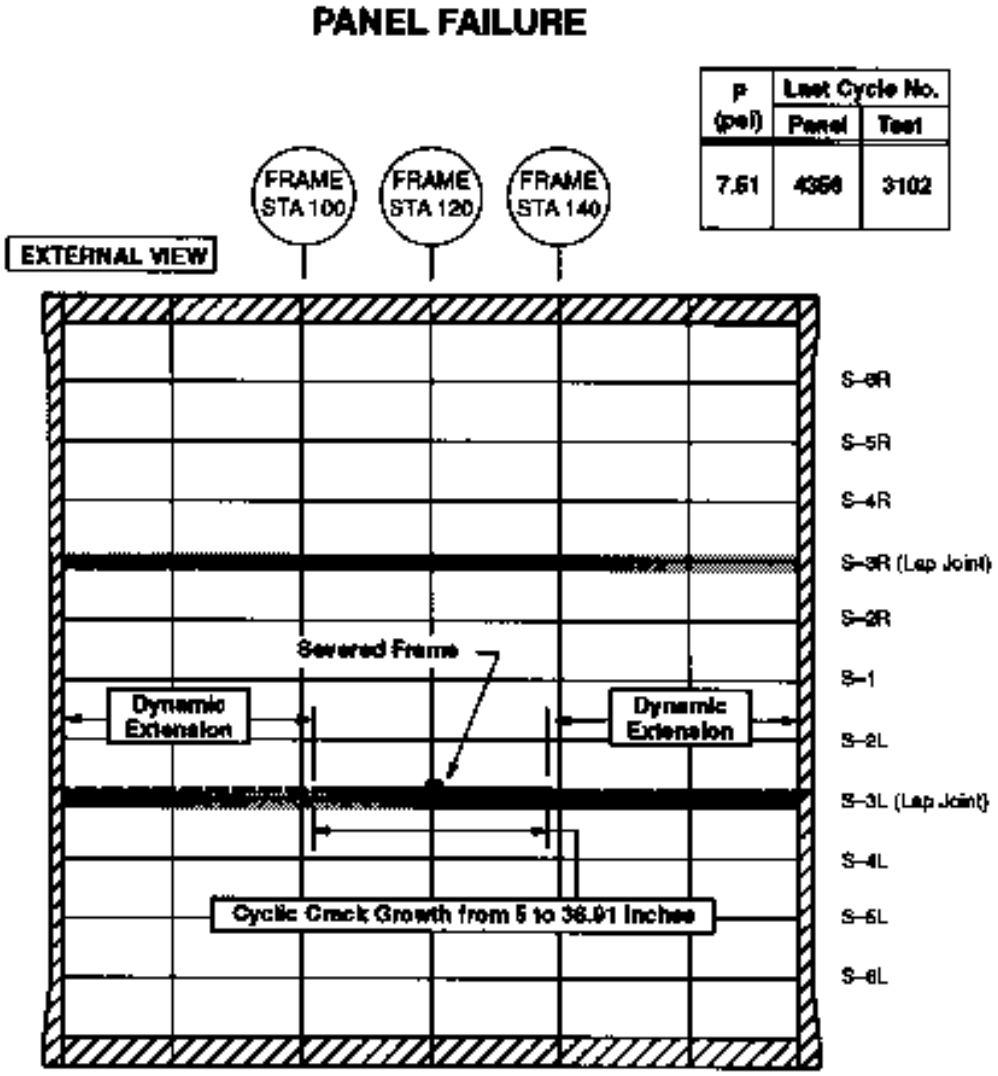

Figure 34. Dynamic Panel Failure, FAA 1, Test 2

3.4.3 Panel FAA 2 - Test 1

This test was conducted on the upper row of the lap joint located at stringer S-3R centered in the 4 bay region of variable size (0.05, 0.10 and 0.15 inch) simulated MSD shown in Figure 18. Prior to beginning the test, ten pressure cycles were applied in order to seat" the panel in the

test fixture. This allows any permanent settling to occur prior to conducting the initial strain survey.

The 5-inch sawcut was then installed in the upper skin and tear strap centered on frame station 120 as shown in Figure 35. The panel was pressure cycled initially at 8.6 psi.

The residual strength test was conducted once the crack length reached 38.50 inches with a severed central frame. Panel failure occurred at 7.51 psi.

The instrumentation details and strain gage readings are found in appendix C.

3.4.3.1 Crack Growth Results (FAA 2 - Test 1)

The initial 4.9-inch sawcut was made in the outer skin and tear strap. After 489 pressure cycles, 1.0 inch of visible crack extension (0.55 and 0.45 inch each tip) was measured. As cycling continued the main crack steadily grew to 11.84 inches where the first MSD crack became visible near the aft tip of the main crack. The crack trajectory, showing active MSD growth is illustrated pictorially in Figures 36 through 40.

At a crack length of 11.84 inches the cyclic pressure was decreased from 8.6 to 6.0 psi in an attempt to reduce the risk of the crack dynamically running as demonstrated in FAA 1, Test 1 at 17 inches. This reduced pressure significantly slowed the crack growth rate to the point where the testing schedule would be impacted. In an attempt to meet the planned testing schedule the cyclic pressure was increased from 6.0 to 7.0 psi.

As cycling continued the main crack ran dynamically at a length of 15.29 inches and arrested after reaching a length of 35.72 inches. The tips of the crack stopped 0.6 and 0.8 inch short of the tear straps. The forward tip developed a sharp 0.2 inch upward turn after running through the fastener hole adjacent to the tear strap. Conversely, the aft tip remained in the horizontal orientation. These details are illustrated in Figure 38.

Next, the crack was sawcut horizontally as shown in Figure 39 in order to develop the similar crack trajectory as in FAA 1, Test 2. One more cycle was applied in order to sharpen the new sawcut resulting in 1.88 inches of crack extension occurring at 8.0 psi. This made the tip to tip crack length 38.50 inches which is 1.6 inches longer that the final crack length on the non-MSD test performed on FAA 1, Test 2. The crack extended under the tear strap region as illustrated in Figure 40.

The crack length versus pressure cycles plot is provided in Figure 41 showing the growth from the initial 4.9-inch sawcut to the final length of 38.50 inches. Table 8 contains the crack growth data for the main crack in conjunction with the visually measured MSD sizes.

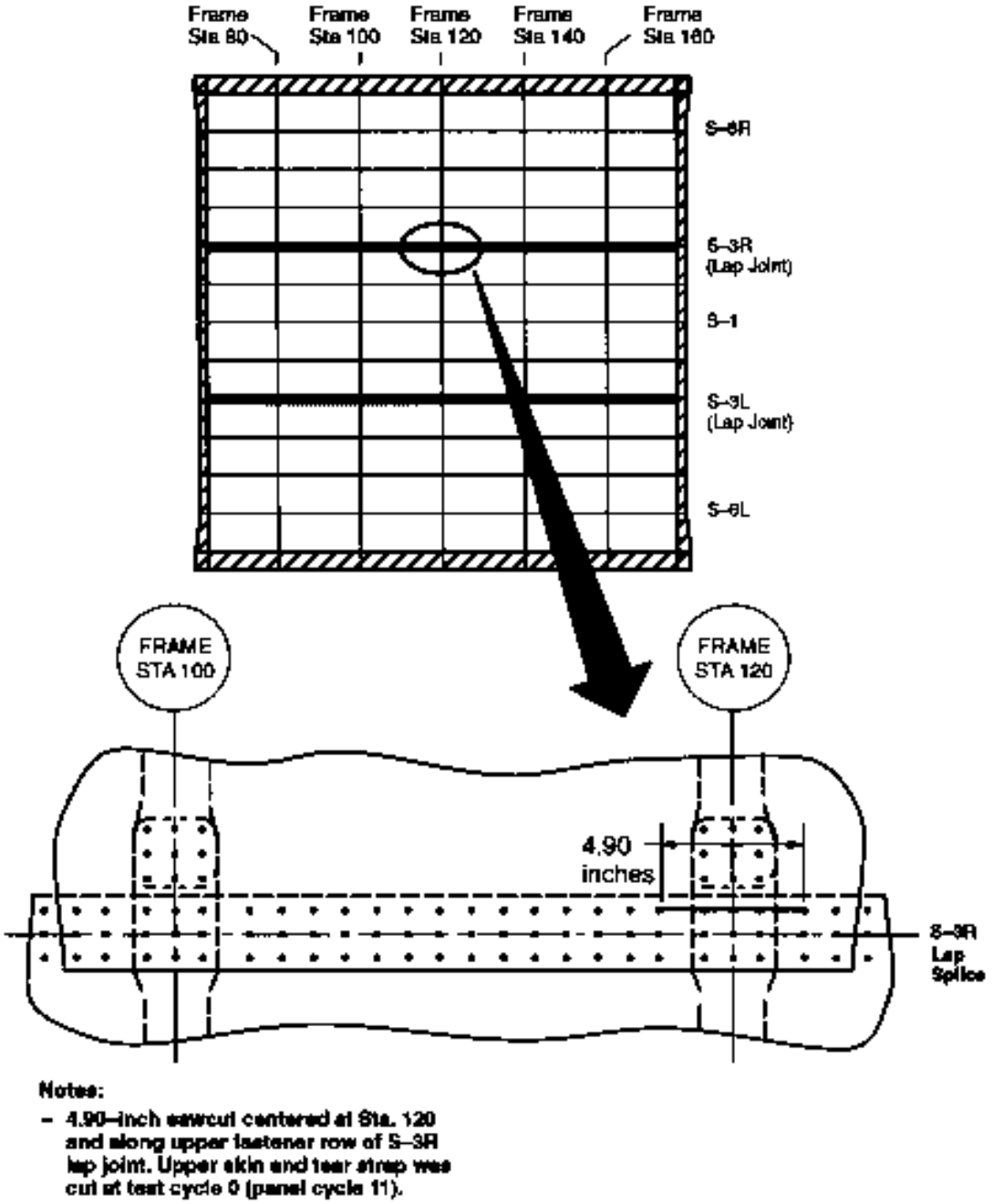

Figure 35. Initial Sawcut Details for Panel FAA 2, Test 1

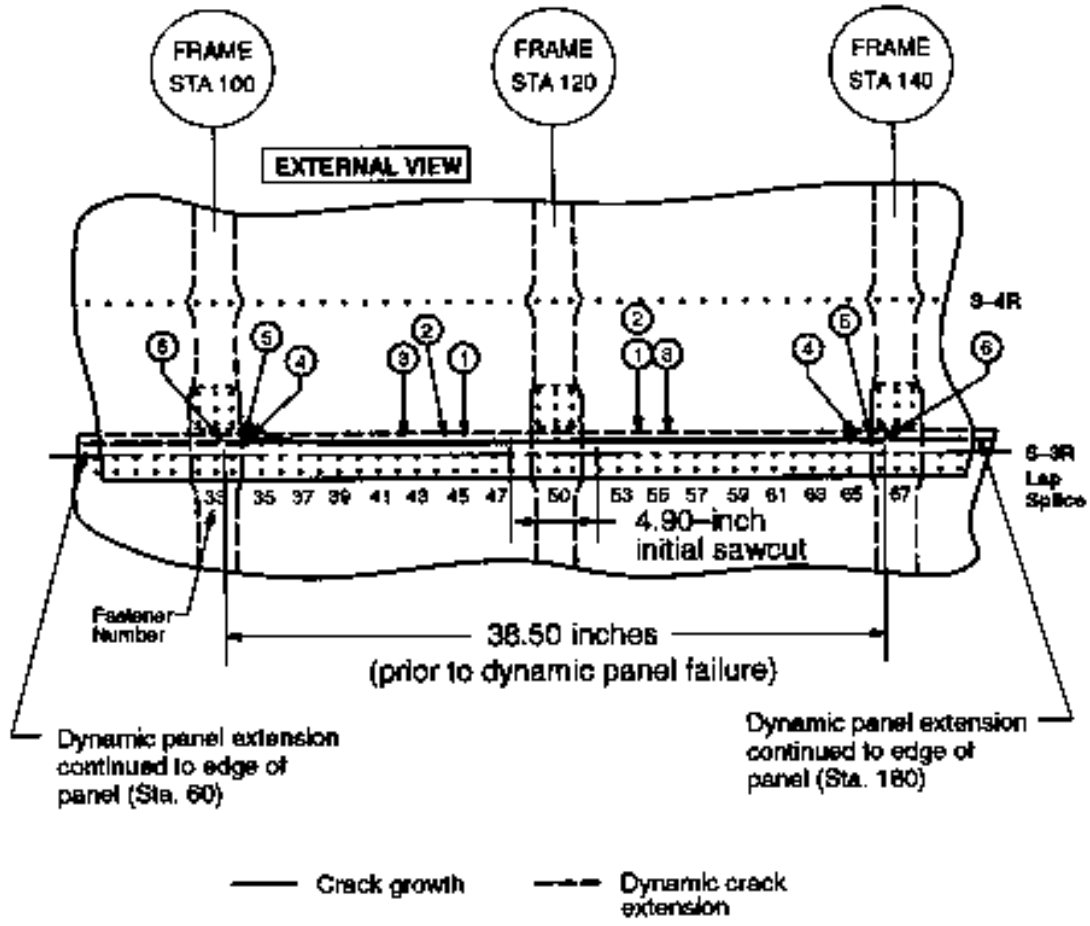

① Cycle 842 – Fwd end of crack grew thru fastener 46. Aft end of crack grew into fastener 54.

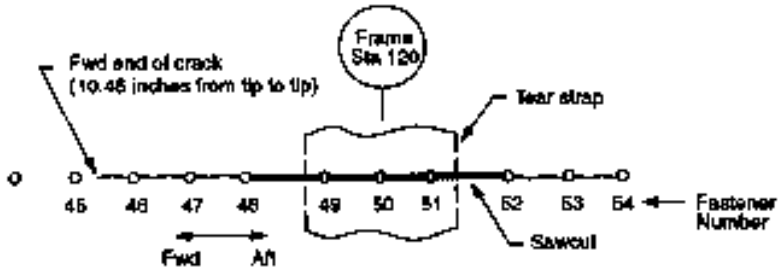

Figure 36. Crack Trajectory of Panel FAA 2, Test 1

② Cycle 858 – MSD crack at fwd side of fastener 55 had grown 0.13 inch beyond fastener head.
– Fwd end of crack grew thru fastener 45 and aft end thru fastener 54.

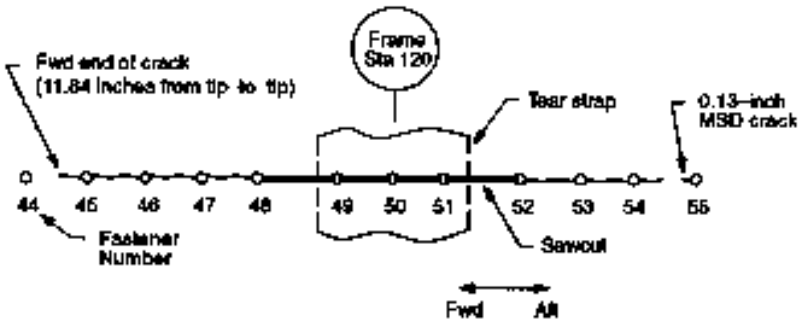

③ Cycle 1278 – MSD crack at aft side of fastener 42 had grown 0.20 inch beyond fastener head.
– Fwd end of crack grew thru fastener 43 and aft end thru fastener 55.

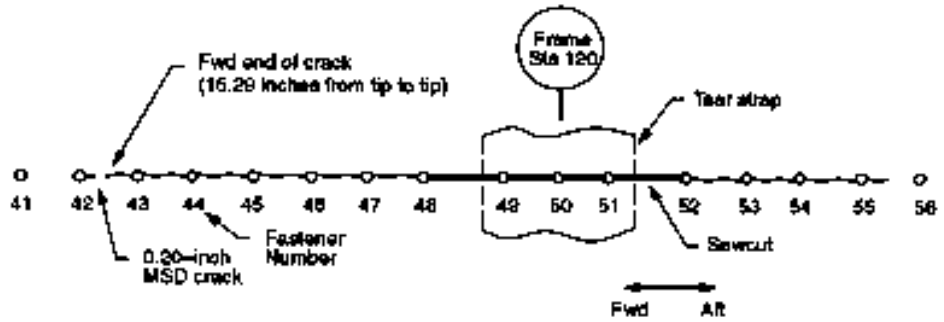

Figure 37. Crack Trajectory of Panel FAA 2, Test 1

④ Cycle 1279 – Crack extended between fastener 35 and 65. 20.43 inches of new growth within one cycle.

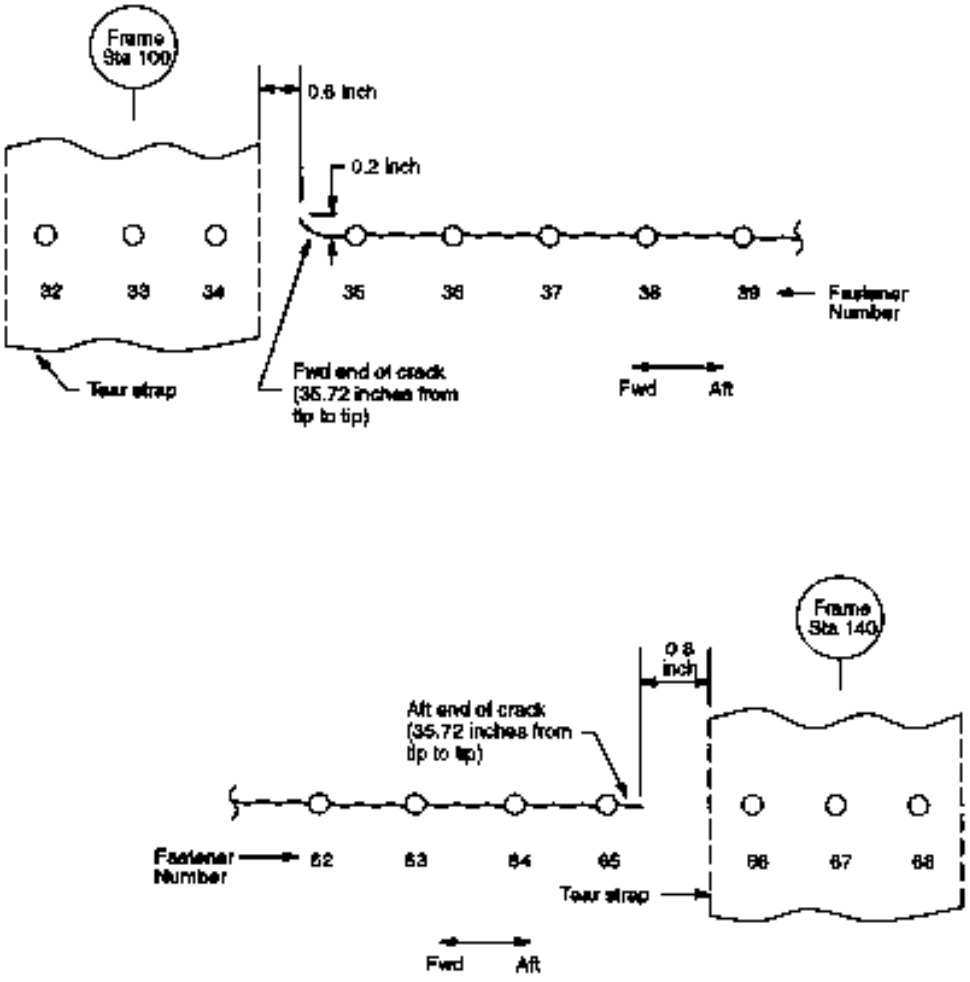

Figure 38. Crack Trajectory of Panel FAA 2, Test 1

⑤ Cycle 1279 – Extension due to sawcut. This was done to simulate FAA 1, Test 2 crack configuration.

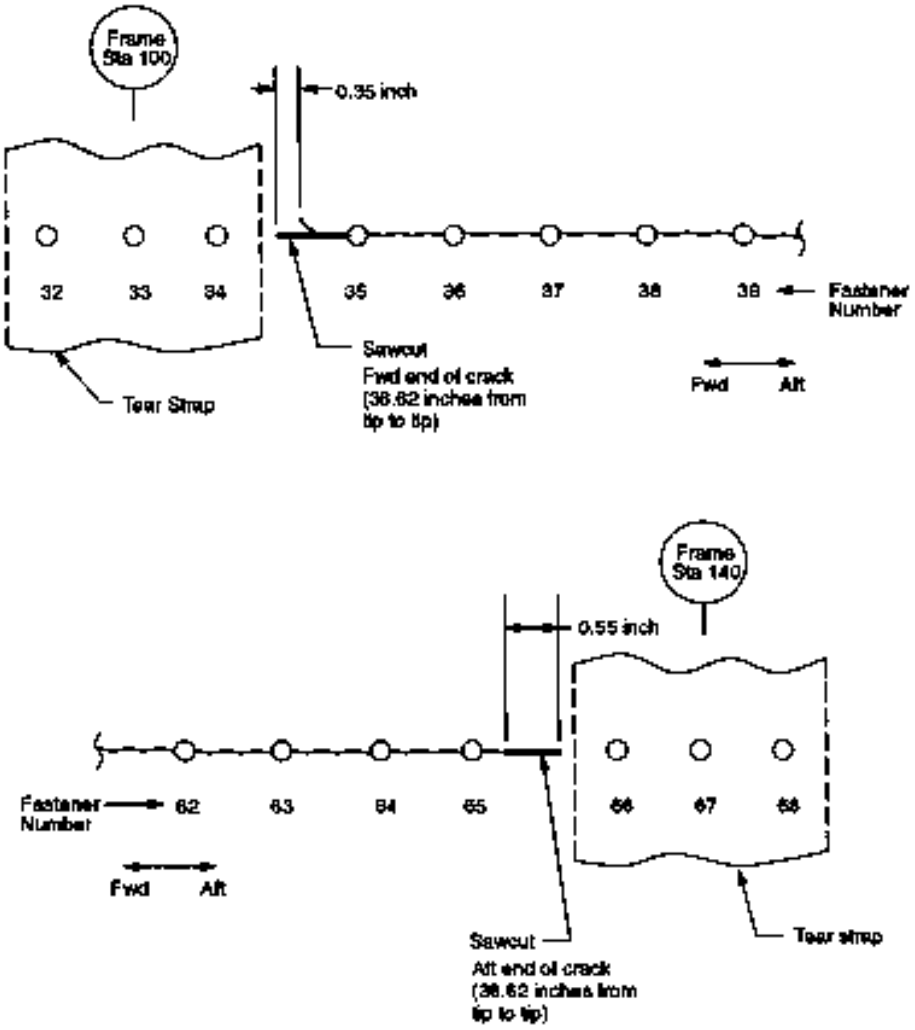

Figure 39. Crack Trajectory of Panel FAA 2, Test 1

⑥ Cycle 1280 – Fwd end of crack grew thru fastener 34 and aft end grew thru fastener 66.
– Sta. 120 frame was cut prior to residual strength test.
– Dynamic panel failure occured at test cycle 1281.

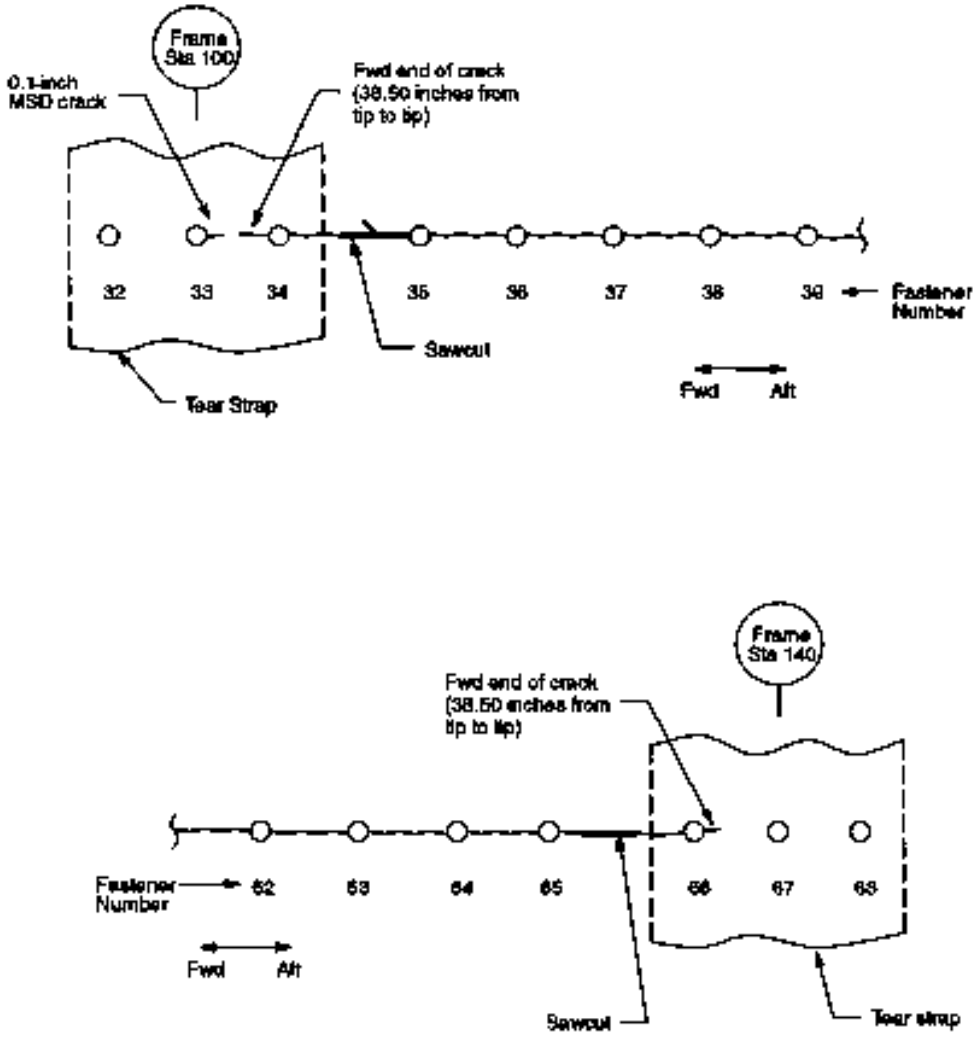

Figure 40. Crack Trajectory of Panel FAA 2, Test 1

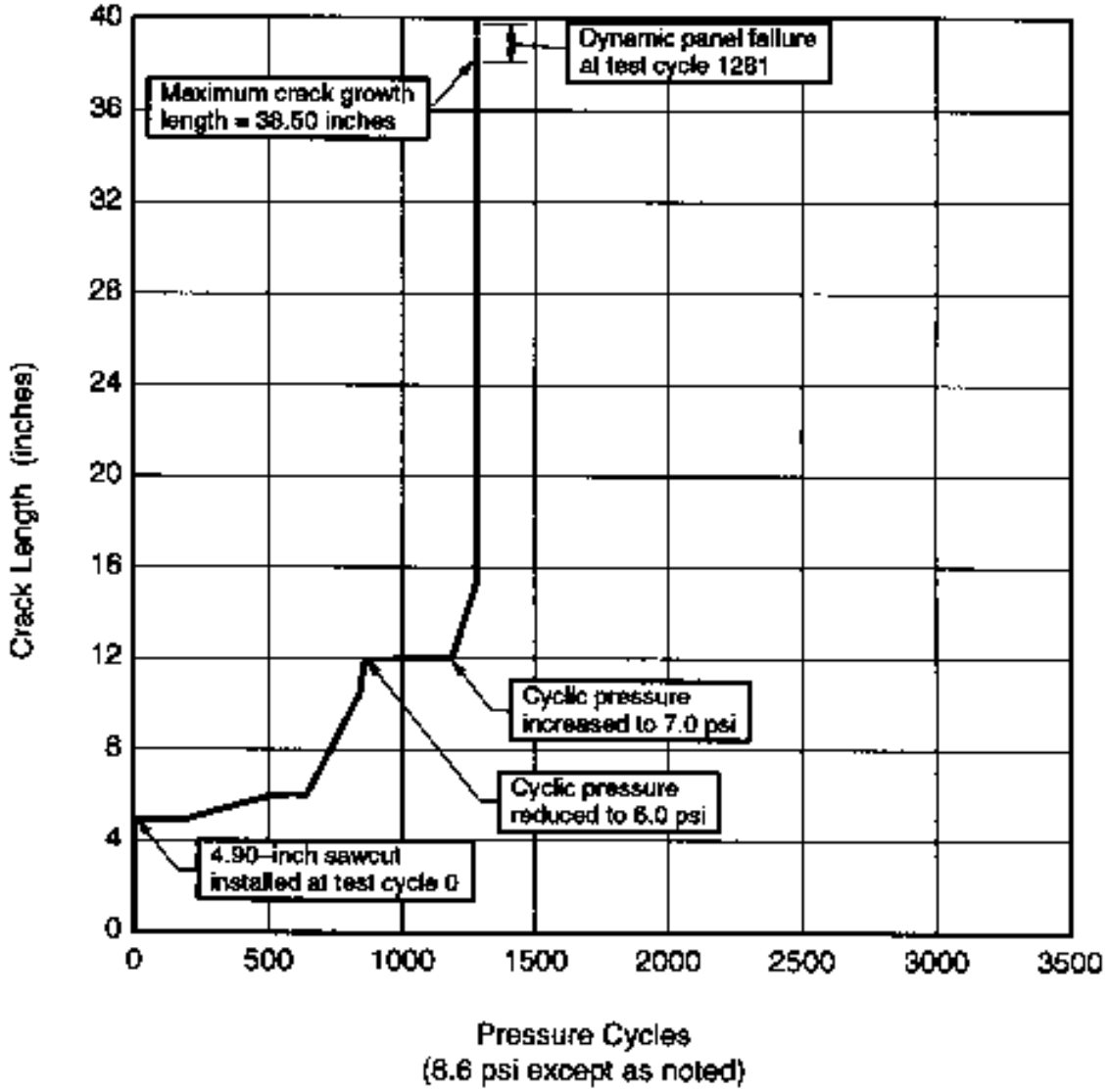

Figure 41. Crack Growth History of Panel FAA 2, Test 1

Table 8. Test Record of Crack Length Measurements From Panel FAA 2, Test 1

Test Cycle Number	Panel Cycle Number	Length of New Growth (inch)	Total (X) Dimension (inch)		Total (Y) Dimension (inch)		Total Crack Length (inch)
			Fwd Tip	Aft Tip	Fwd Tip	Aft Tip	
–	11	Intact	0	0	0	0	0
0	11	Sawcut installed	–	–	–	–	4.90
189	200	0.0	0	0	0	0	4.90
489	500	1.00	0.55	0.45	0	0	6.90
589	600	0.11	0.58	0.53	0	0	6.01
643	654	0	0.58	0.53	0	0	6.01
842	853	4.45 Crack went fwd of fast. 46 and aft into fast. 54	2.83	2.73	0	0	10.46
858	869	1.38 MSD crack grew 0.13 inch fwd of fastener 55 Fwd crack grew thru fastener 45 & thru fastener 54 Operating press. changed from 6.6 psi to 6.0 psi	3.94	3.00	0	0	11.84
878	889	0.11	4.05	3.00	0	0	11.95
928	939	0.0	4.05	3.00	0	0	11.95
1187	1198	0.04	4.05	3.04	0	0	11.99
1205	1216	Operating press. changed from 6.0 psi to 7.0 psi	–	–	–	–	–
1278	1289	3.30 MSD crack grew 0.2 inch aft of fast. 42 Crack grew thru fast. 43 & 55	6.32	4.07	0	0.04	15.29

Table 8. Test Record of Crack Length Measurements From Panel FAA 2, Test 1 (Continued)

Test Cycle Number	Panel Cycle Number	Length of New Growth (inch)	Total (X) Dimension (inch)		Total (Y) Dimension (inch)		Total Crack Length (inch)
			Fwd Tip	Aft Tip	Fwd Tip	Aft Tip	
1279	1290	20.43 Crack extended between fast. 35 and 65	15.50	15.32	0.13	0.06	35.72
1279	1290	0.90 Extension due to sawcut: fwd = 0.35 aft = 0.55 (This was done to simulate FAA 1, test 2)	15.85	15.87	0	0	36.62
1280	1291	1.88 Sta. 120 frame was cut prior to residual strength test Step pressure 1 psi increments from 0 – 8 psi	16.83	16.77	0	0	38.50

Table 8. Test Record of Crack Length Measurements From Panel FAA 2, Test 1

Crack Length, l (inch)	Frame Condition	Internal Pressure (psi)	Correlation Test File
Intact	Intact	8.6	FAA 1, Cycle 10 (Test 1, Intact) FAA 1, Cycle 1259 (Test 2, Intact) FAA 2, Cycle 9 (Test 1, Intact)
5.0			FAA 1, Cycle 21 (Test 1, l = 5.0 inches) FAA 1, Cycle 1796 (Test 2, l = 5.0 inches) FAA 2, Cycle 395 (Test 1, l = 4.9 inches)
30.0			FAA 1, Cycle 4286 (Test 2, l = 32.24 inches)
38.0			FAA 1, Cycle 4351 (Test 2, l = 36.71 inches)
40.0	Broken		FAA 1, Cycle 4355 (Test 2, l = 36.71 inches)

Table 9. Test Record of Crack Length Measurements From Panel FAA 2, Test 1

3.4.3.2 Residual Strength (FAA 2 - Test 1)

The residual strength test consisted of increasing the internal pressure in small intervals until dynamic panel failure occurred. Prior to running the residual strength test the central frame at station 120 was severed.

The crack configuration prior to start was a 2 bay skin crack centered on a severed central frame. The tips of the 38.50-inch crack were through the first fastener common to the tear straps as shown in Figure 40. The pressure was increased at a rate of approximately 0.2 psi. per minute. As the pressure was increased above 6.7 psi. the forward tip grew from fastener hole 34 into the MSD crack aft of fastener 33 (refer to Figure 42 below for fastener numbering). Then at 6.9 psi. approximately 0.1-inch MSD became visible out of the aft side of fastener 32. Then at 7.0 psi. linkup between fasteners 66 and 67 occurred followed by approximately 0.15 inch of visible growth out of the aft side of fastener 67. At 7.2 psi. link up occurred between fastener 32 and 33 with approximately 0.2- inch of MSD was visible out of the forward side of fastener 32. Then as the pressure was increased to 7.51 psi. approximately 0.1-inch of MSD became visible fwd out of fastener 68, then the crack ran dynamically from approximately 41.7 inches to the ends of the panel resulting in catastrophic failure. Figure 43 illustrates the dynamic crack trajectory.

The strain gage stresses are provided prior to failure with the central frame intact and then severed for review in appendix C Figures C-59 through C-62 (intact) and C-63 through C-66 (severed) respectively. Note the pressures at which the stresses are provided for the intact and severed frame conditions do not correspond, 6.0 and 7.51 psi. respectively. This was because no data was available at 7.51 psi. with the frame intact.

The stresses recorded at the highest pressure (7.51 psi.) prior to failure are provided in appendix C Figures C-63 through C-66.

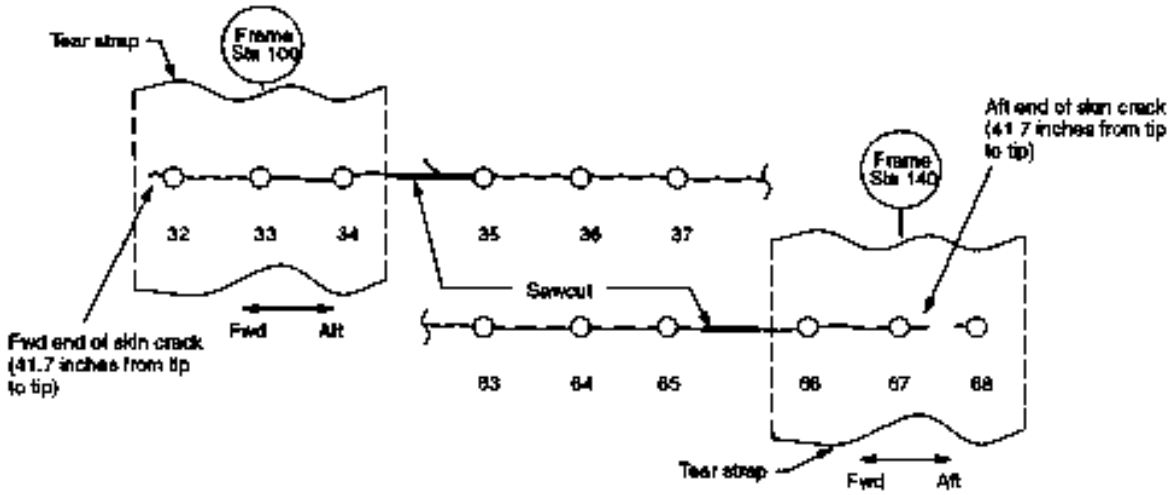

Figure 42. Crack Configuration Prior to Panel Failure

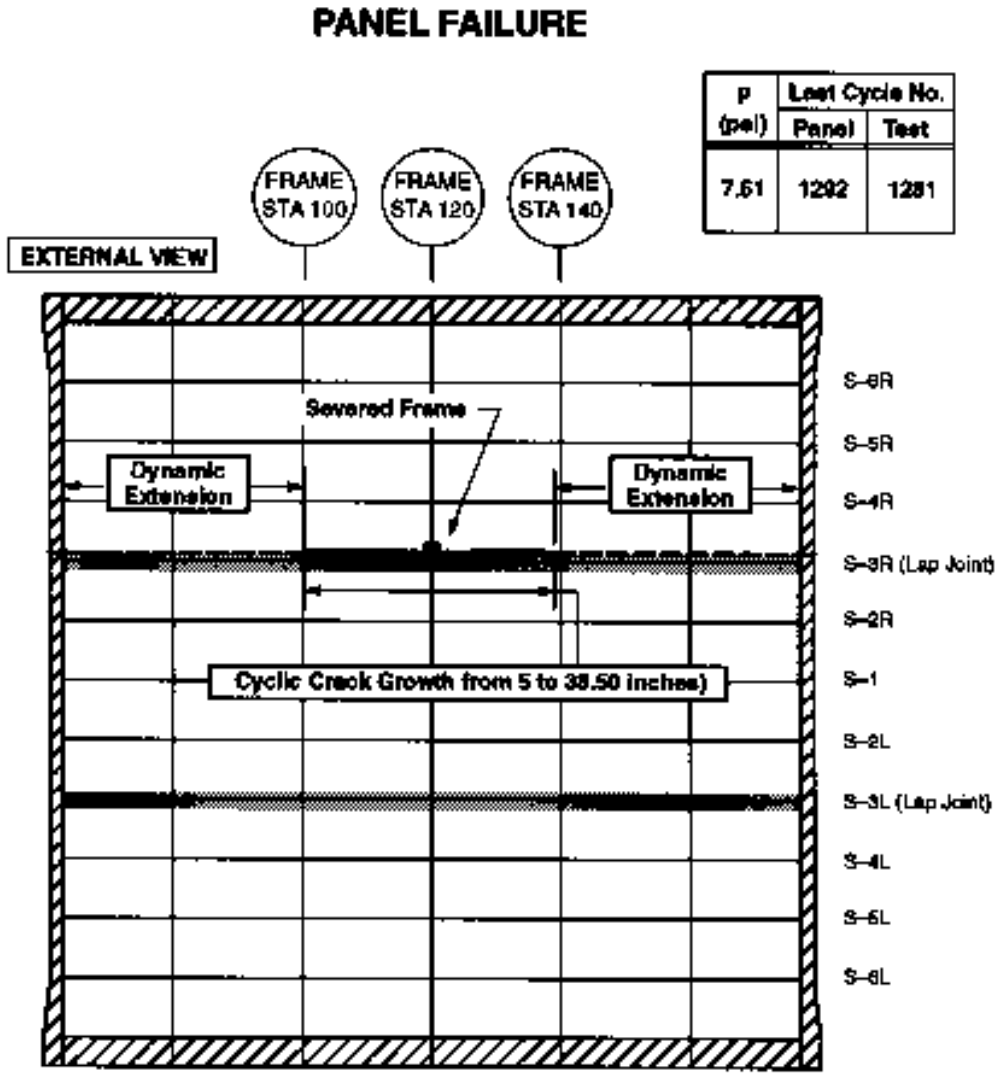

Figure 43. Dynamic Panel Failure, FAA 2, Test 1

3.4.4 Panel FAA 2 - Test 2

This test was not conducted. Boeing and the FAA decided not to perform this test because of program costs.

3.5 Crack Growth and Residual Strength Test Comparison

Figure 44 shows a comparison of crack growth data between panel FAA 1, Test 1 vs. Test 2 (simulated MSD vs. No MSD) normalized to an initial crack length of 5.72 inches.

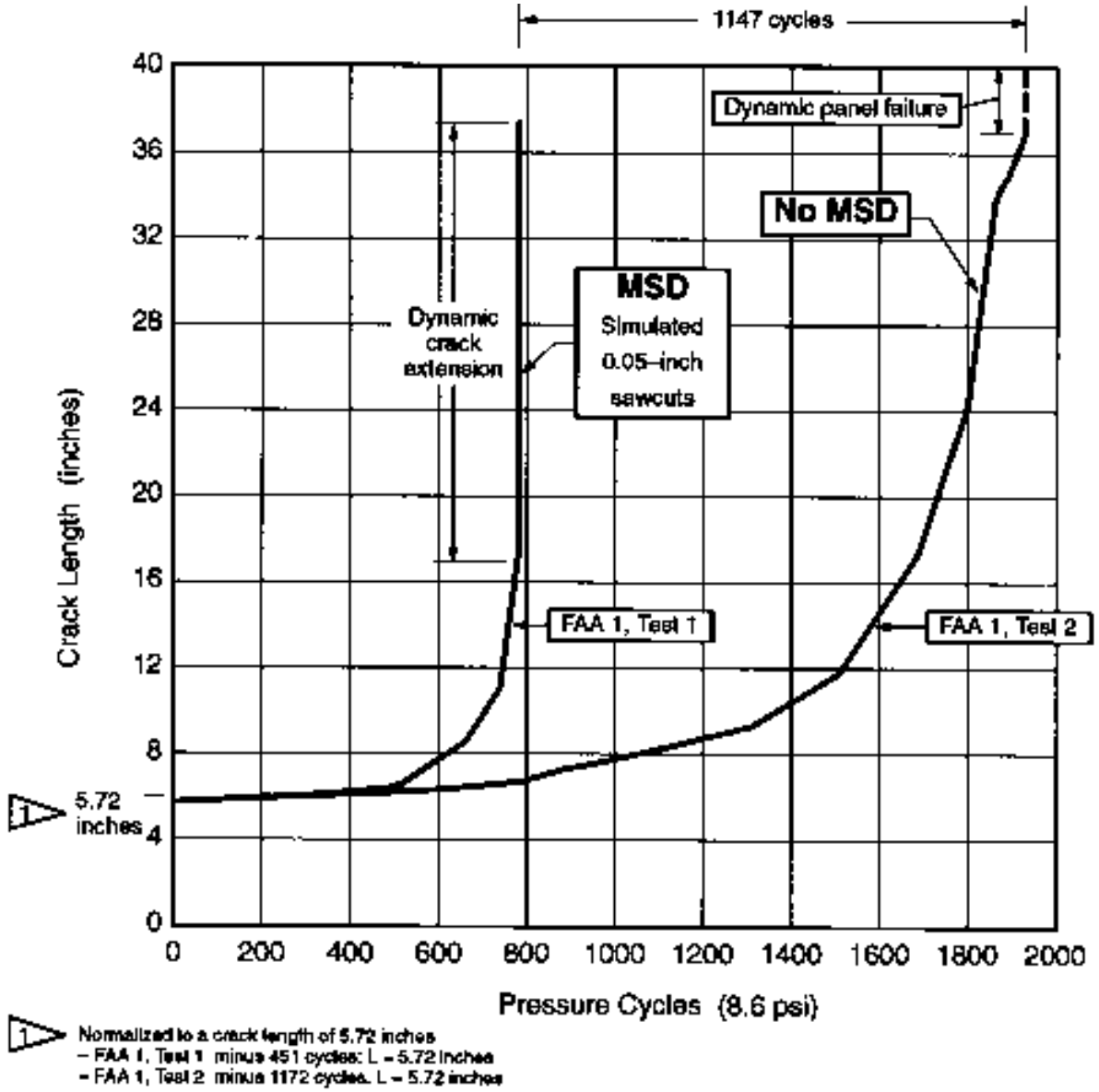

Figure 44. Panel FAA 1, Test 1 and Test 2 Crack Growth Comparison

Figure 45 shows a comparison of the residual strength capabilities between FAA 1, Test 2 and FAA 2, Test 1. Note that the panel with MSD had a 3.5-inch larger crack prior to final failure.

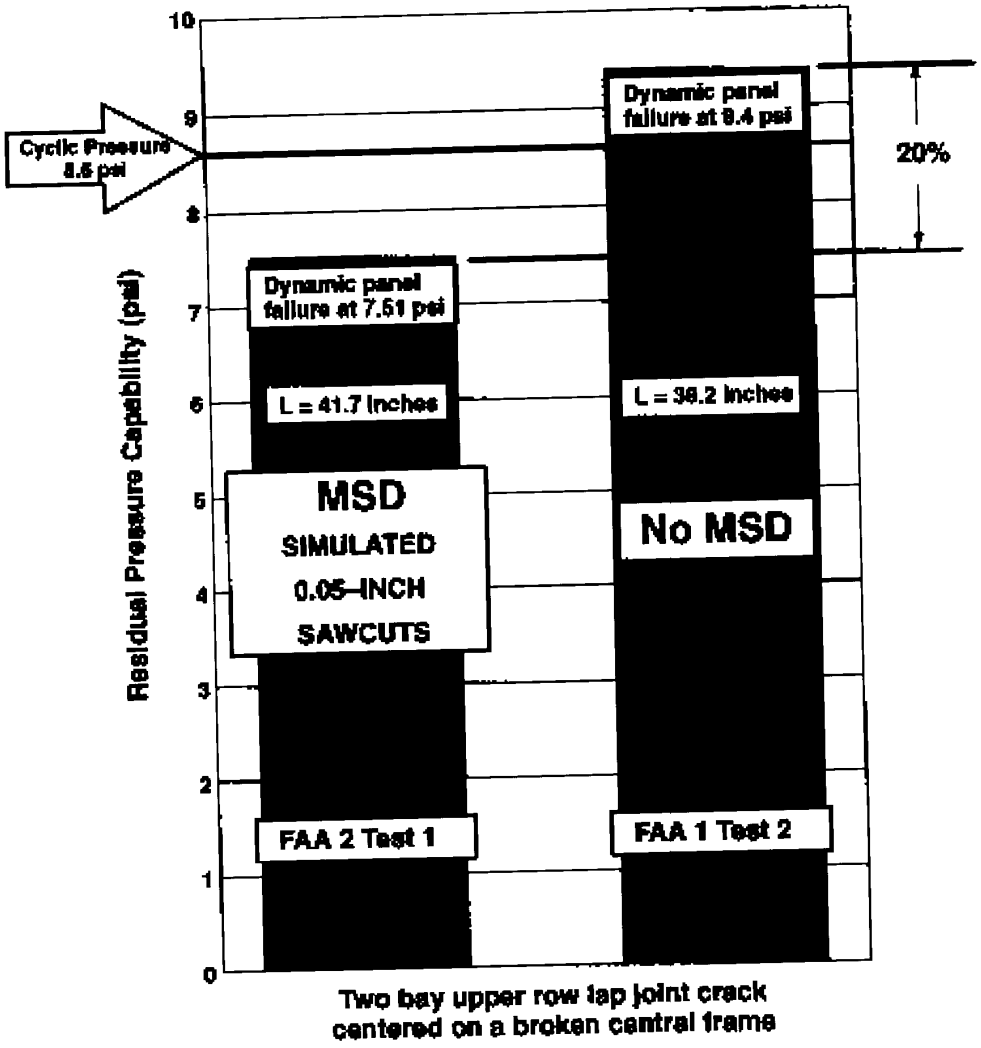

Figure 45. Panel FAA 1, Test 2 vs. FAA 2, Test 1 Residual Strength Comparison

3.6 Curved Panel Testing Discussion

In contrast to the test data presented in this report, past Boeing pressure panel tests, Reference 5, have showed a 10 percent reduction in residual strength capability due to MSD rather than the 20 percent reported here. The referenced Boeing tests were run much the same way as the tests contained in this report: results from one test panel containing simulated MSD in the lap joint were compared with results from a similar panel without MSD. The primary structural difference between the referenced Boeing tests and the tests reported here was the presence of shear ties connecting the skin and tear strap assembly to the frames, essentially increasing the strength and stiffness of the tear straps in the referrenced Boeing tests.

The apparent increased sensitivity of the residual strength capability of structure with floating frames (no shear ties) to MSD suggests that additional tests be conducted to further investigate the significance of varying structural configurations. Specifically, additional testing should be conducted on structure containing an increased tear strap stiffening ratio or on shear tied structure.

4. TASK III: ANALYSIS

This section discusses the development of a finite element model to analyze the FAA test panels. The goal of the analysis was to predict strain gage stresses, crack growth life and residual strength maximum pressure. The scope of the analysis was limited to a general model of the test panel that accounted for major structural effects on the lead crack but did not include the effects of MSD. The output from the finite element analysis was used to predict the stresses at strain gage locations. Stress intensity factors were calculated at different crack lengths and were used to predict crack growth and residual strength. The analysis predictions were then compared with the test results.

4.1 Pressure Panel Finite Element Model Development

Section 3 describes the test fixture and the test panels. The test fixture is a general wide body fuselage structure that has been thickened by approximately 75 percent to achieve a design life goal of one million pressure cycles. The test panels had dimensions of typical fuselage crown structure. Thus, a test fixture/test panel assembly simulated a fuselage crown subjected to cyclic pressure loads. This had implications for the strategy used to model the test panels. For this study, the strategy was to model a section of fuselage crown structure (i.e. the test panel) and apply boundary conditions for cylindrical symmetry. The advantage to this strategy was that a model of the entire test fixture/test panel assembly was avoided allowing a smaller, more detailed model of the test panel to be used. The disadvantage to this strategy was that the effect of the test fixture on the test panel was not modelled. Since this effect has not been quantified, it cannot be dismissed as negligible, although this assumption was implied by the modelling strategy.

The scope of the analysis was limited to modelling the major structure of the test panel, i.e., the skins, tear straps, stringers, and frames. Elements were included to model the load transfer at fasteners and stringer clips, however, local effects such as fastener holes and MSD cracks were not modelled.

Figures 46 through 48 show the different layers of the model of a test panel containing a crack in the upper skin. The model was fifteen stringer bays wide (θ=62.6^o) by three and one-half frame bays long (z=70 inch). Only the six stringer bays nearest the lap joint were modelled in detail. The remainder of the model was a coarse mesh with rigidly connected structural elements. Extending the model beyond six stringer bays was necessary to prevent warping of the frame at station 120 when that frame was severed for residual strength testing. Because the symmetrical boundary conditions imply that all damage is mirrored across the boundaries, there can be significant interactions if the damage is too close to a boundary.

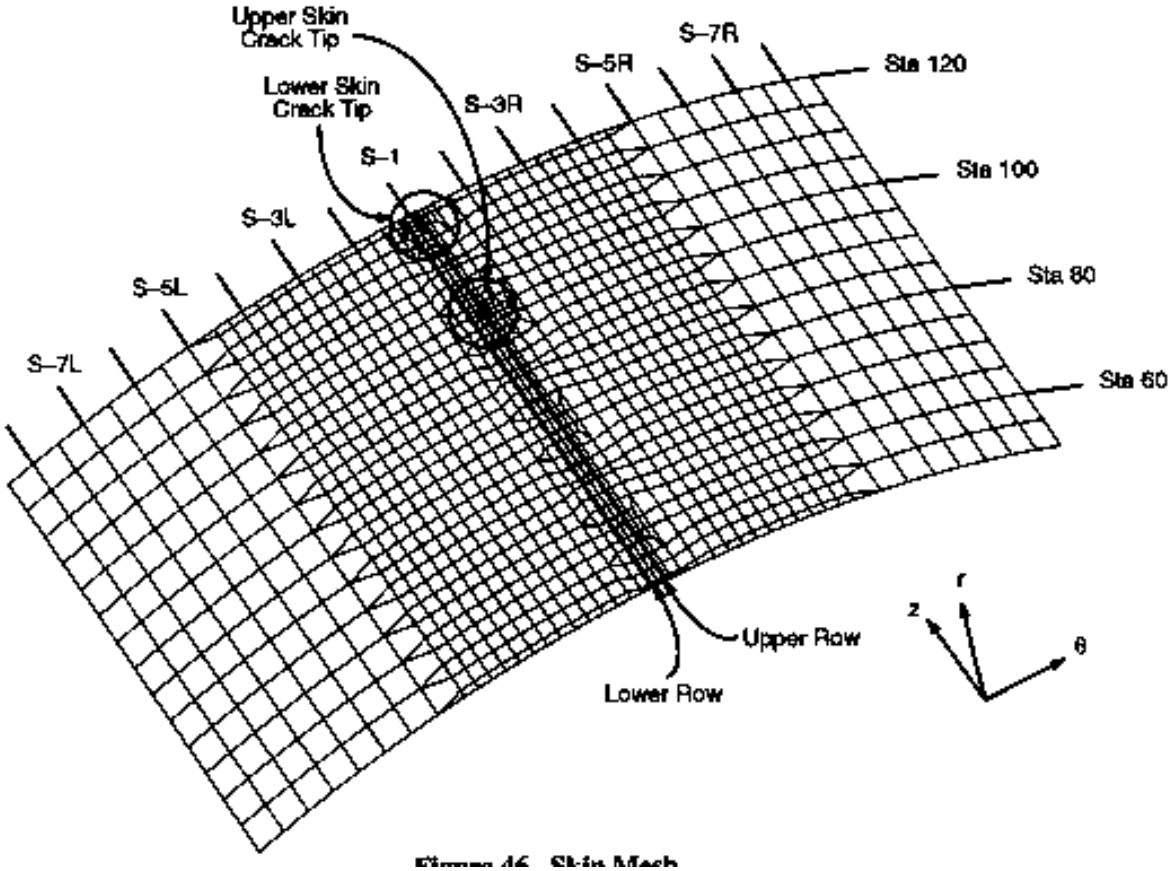

Figure 46. Skin Mesh

Note in Figures 46 through 48 that the lap joint is at stringer S-1. On the test panels there were two lap joints, one at stringer S-3L and the other at stringer S-3R. Only one lap joint was included in the finite element model. However, the directions left and right were consistent between the finite element model and the test panels.

Note as well in Figures 46 that a lower skin crack was included in the finite element model. When the 5-inch sawcut was made in the test panel to initiate the crack in the upper skin, the lower skin was cut as well. However, the lower skin crack did not experience growth as it was near the free edge of the lower skin. In the finite element model, the lower skin crack remained at 5 inches while the upper skin crack varied from 5 to 40 inches.

The sketch in Figure 11 details the structure of the test panels. The skins and tear straps were 0.063 inch thick 2024-T3 clad aluminum. The tear straps were 2.4 inches wide and were bonded to the skin except at the lap joints. The stringers and frames were 0.063 inch thick 7075-T6 clad aluminum. The stringers were riveted to the skin. The frames were free-floating and attached to the stringers via stringer clips. The skins and tear straps were modelled with 0.063 inch thick eight-noded shell elements (ABAQUS element S8R). The stringers and frames were modelled with three-noded beam elements (ABAQUS element B32). The beam cross-sections were input

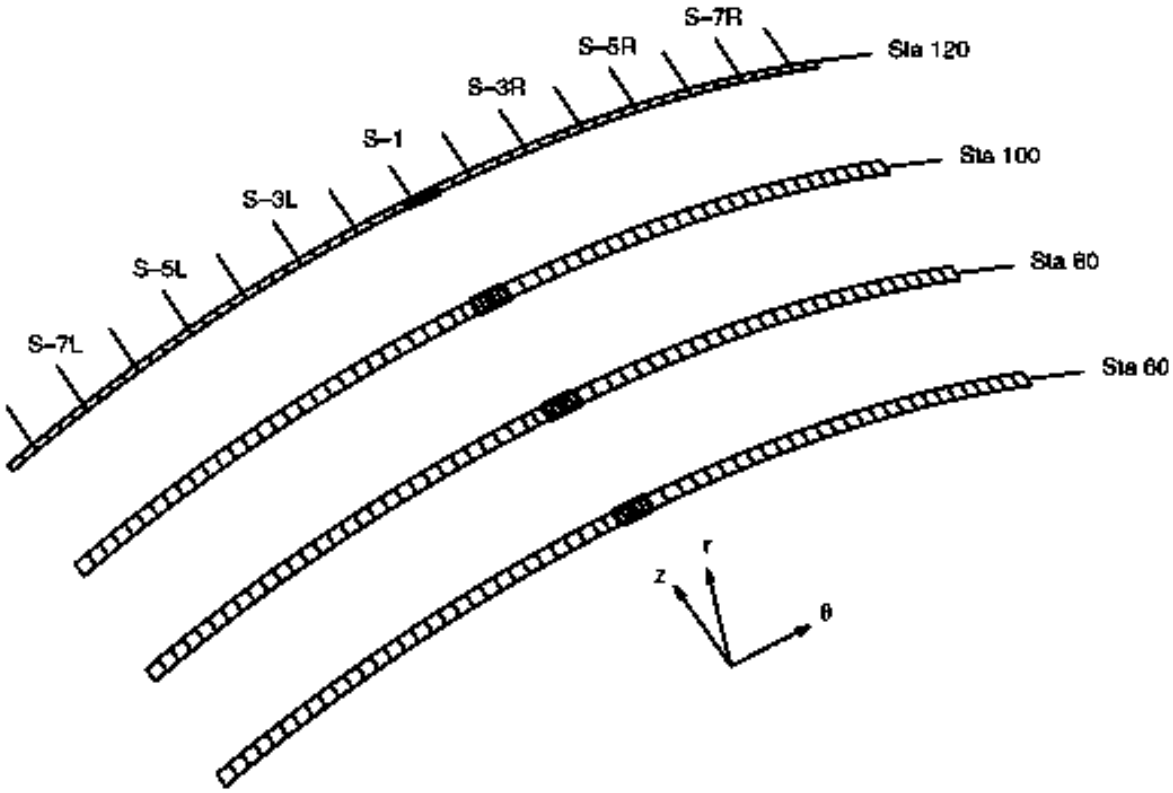

Figure 47. Tear Strap Mesh

explicitly; Figure 49 shows the dimensions and coordinates of the stringers and frames that were used in the model.

Figures 12 and 13 show the details of the rivet patterns in the lap joint and along the stringers. Fastener elements were used at each rivet location to model the effect of load transfer, except along the crack; the fastener elements were removed from the model when the crack grew past them. Fastener elements were circular two-noded beam elements (ABAQUS element B31). The radius of the cross-section was equal to the radius of the shank of the rivet. Similarly, a stringer clip element was used at each stringer clip location. The stringer clip elements were rectangular two-noded beam elements that made a simple connection between a frame node and a stringer node.

Geometric nonlinearity was accounted for in the ABAQUS analysis of the model. As well, material plasticity was accounted for in the residual strength analyses, where the station 120 frame had been severed and significant plastic behavior was expected in the tear straps beneath the crack tips. In the model, the tear strap elements near the lap joint at station 100 were given plastic material properties using the curve shown in Figure 4.

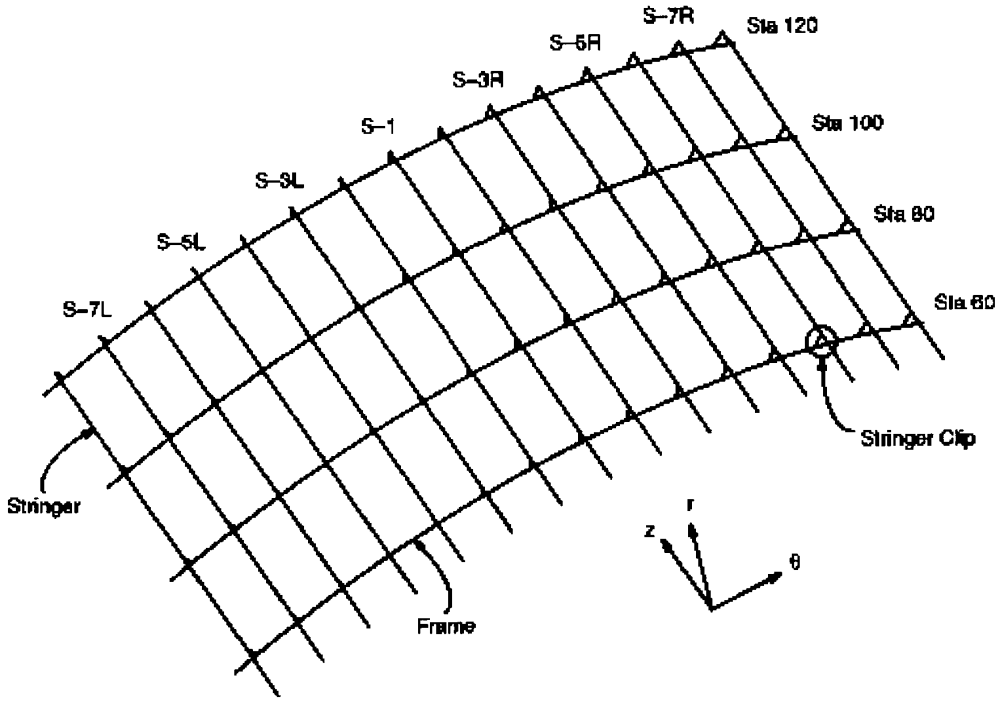

Figure 48. Stiffener Mesh

Symmetrical boundary conditions were applied to all nodes at the edges of the model. If the lap joint is at $\theta=90^{o}$, then displacement u_θ and rotations ϕ_r and ϕ_z were fixed at $\theta=58.7^{o}$ and $\theta=121.3^{o}$. As well, displacement u_z and rotations ϕ_r and ϕ_θ were fixed at station 120. At station 50, rotations ϕ_r and ϕ_θ were fixed. Displacement u_z was constrained to be constant so that a force per unit length of $\frac{pR}{2}$ was applied to the edge of the model. Hence, a load of -15 bays [(9.25 inches) $\frac{pR}{2}$] was applied in the z-direction to the node at station 50 on stringer S-1, and all other nodes at station 50 were fixed in the z-direction with respect to the node on stringer S-1. An outward pressure load, p, was applied to all external skin elements.

Stringer

x-coord	y-coord	thickness
1.2945	-0.9185	0.063
1.2945	-0.9655	0.063
1.26482	-1.07625	0.063
1.18375	-1.15732	0.063
1.073	-1.197	0.063
0.753	-1.187	0.063
0.64225	-1.15732	0.063
0.56118	-1.07625	0.063
0.5315	-0.9655	0.063
0.5315	-0.2215	0.063
0.50182	-0.11075	0.063
0.42075	-0.02968	0.063
0.31	0.0	0.063
-0.31	0.0	0.063
-0.42075	-0.02968	0.063
-0.50182	-0.11075	0.063
-0.5315	-0.2215	0.063
-0.5315	-0.9655	0.063
-0.56118	-1.07625	0.063
-0.64225	-1.15732	0.063
-0.753	-1.187	0.063
-1.073	-1.187	0.063
-1.18375	-1.15732	0.063
-1.26482	-1.07625	0.063
-1.2945	-0.9655	0.063
-1.2945	-0.9185	0.063

Frame

x-coord	y-coord	thickness
1.063	2.015	0.063
1.063	2.192	0.063
1.0427	2.26775	0.063
0.98725	2.3232	0.063
0.9115	2.3435	0.063
0.1515	2.3435	0.063
0.07575	2.3232	0.063
0.0203	2.26775	0.063
0.	2.192	0.063
0.	-2.192	0.063
-0.0203	-2.26775	0.063
-0.07575	-2.3232	0.063
-0.1515	-2.3435	0.063
-0.9115	-2.3435	0.063
-0.98725	-2.3232	0.063
-1.0427	-2.26775	0.063
-1.063	-2.192	0.063
-1.063	-2.015	0.063

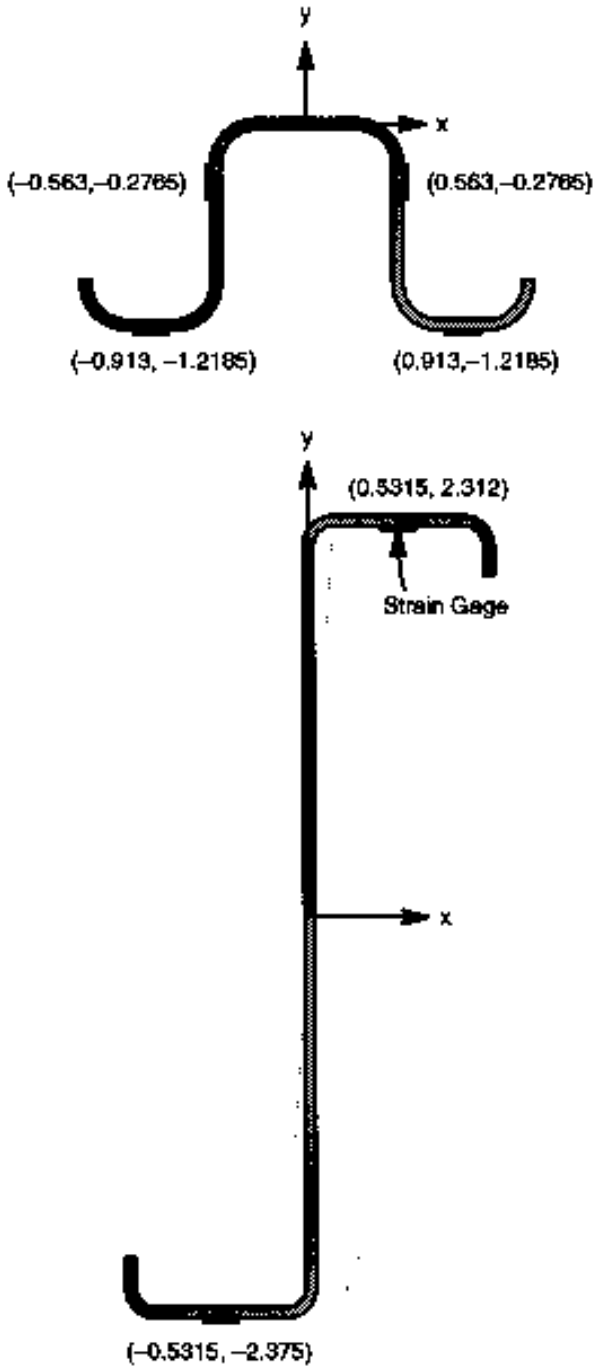

Figure 49. Frame and Stringer Inputs for FAA Test Panel Models

4.2 Results

Figure 50 shows the displaced shape of the skin mesh of the finite model for an intact test panel. Here the magnification factor on the displacements is high enough to see the detail of the skin bulging and the lap joint rotation. Figure 51 shows the displaced shape of the skin mesh

containing a 30-inch crack. Here the bulging of the skin caused by the crack is much more significant than bulging caused by the stiffening structure.

Figures 52 through 55 contain line plots of the stresses predicted by the finite element analyses for different crack lengths. These stresses were used for the strain gage stress comparisons. Note the singular behavior of the stresses near the crack tips.

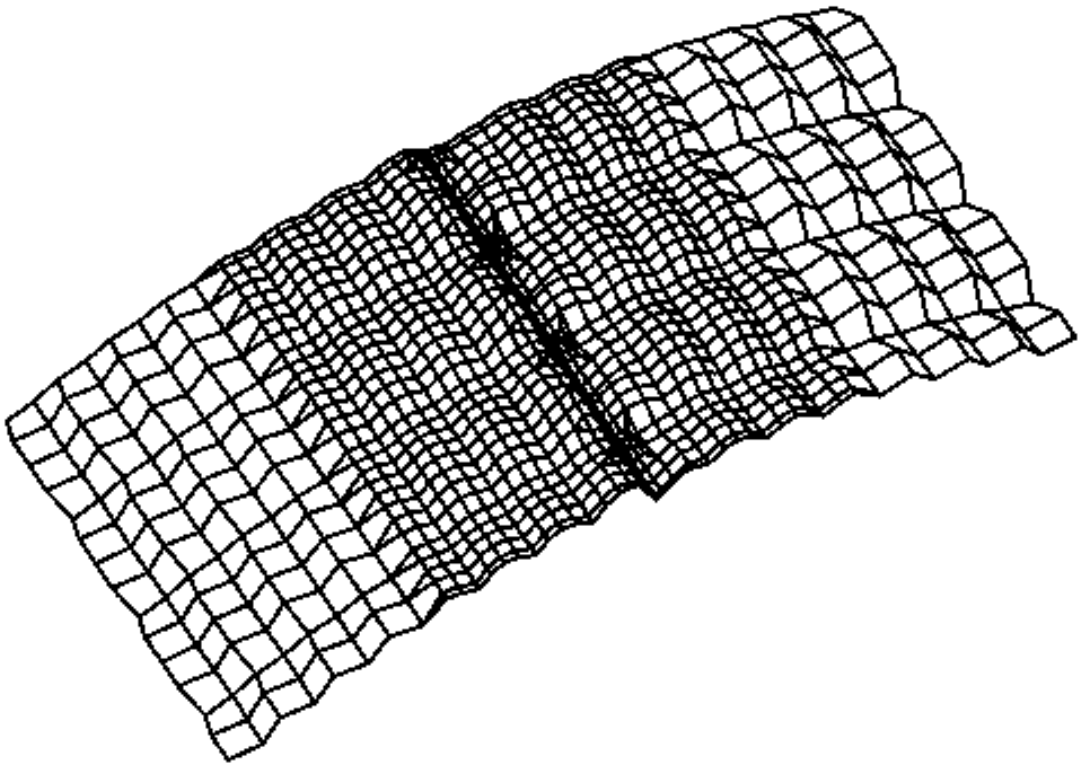

Figure 50. Displaced Intact Skin Mesh, Internal Pressure = 8.6 psi, Magnification Factor - 100x

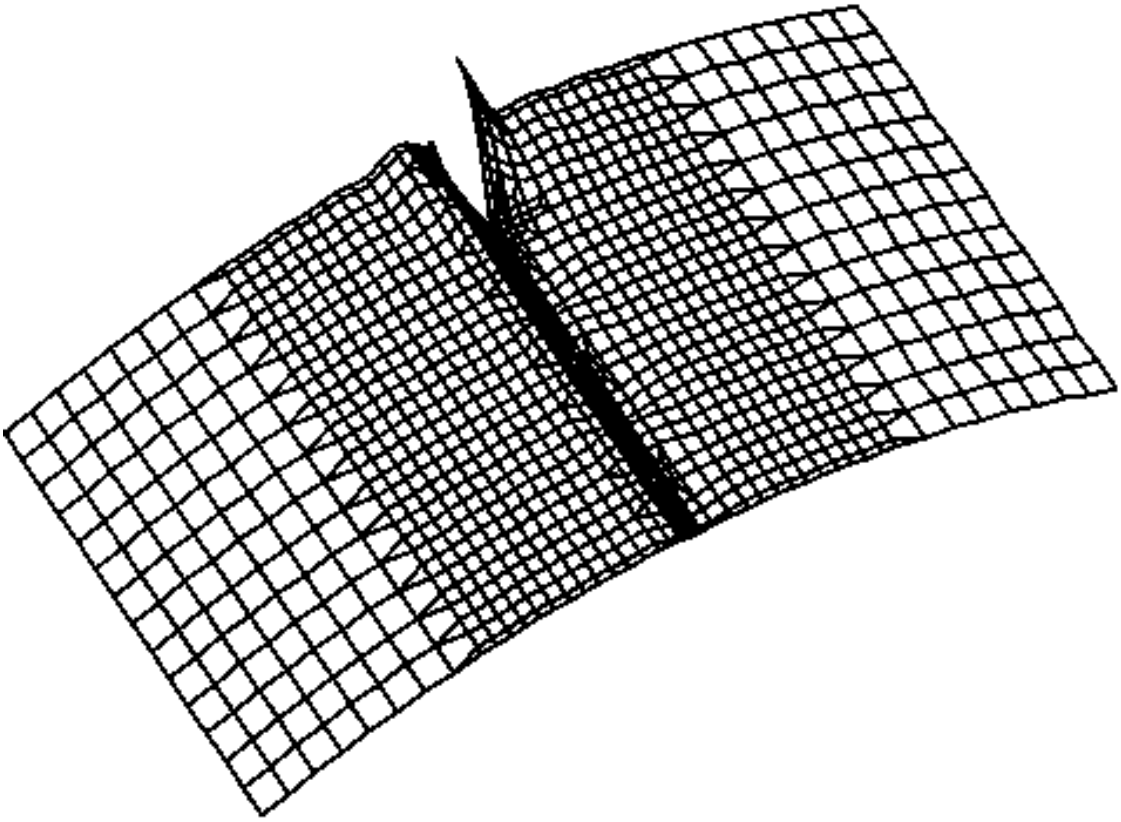

Figure 51. Displaced Skin Mesh Containing a 30-Inch Crack, Internal Pressure = 8.6 psi, Magnification Factor - 10x

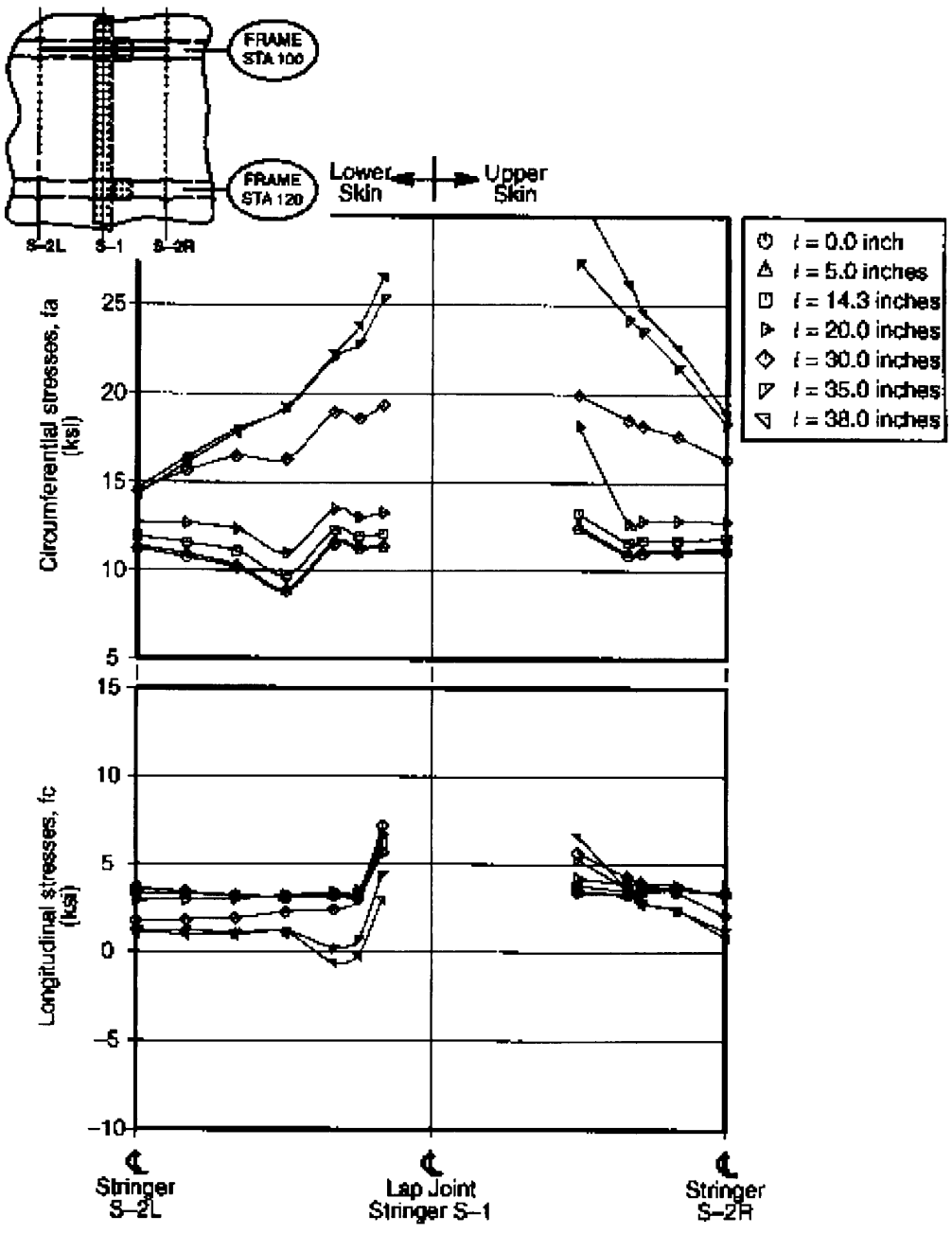

Figure 52. Predicted Midplane Stresses at Station 100

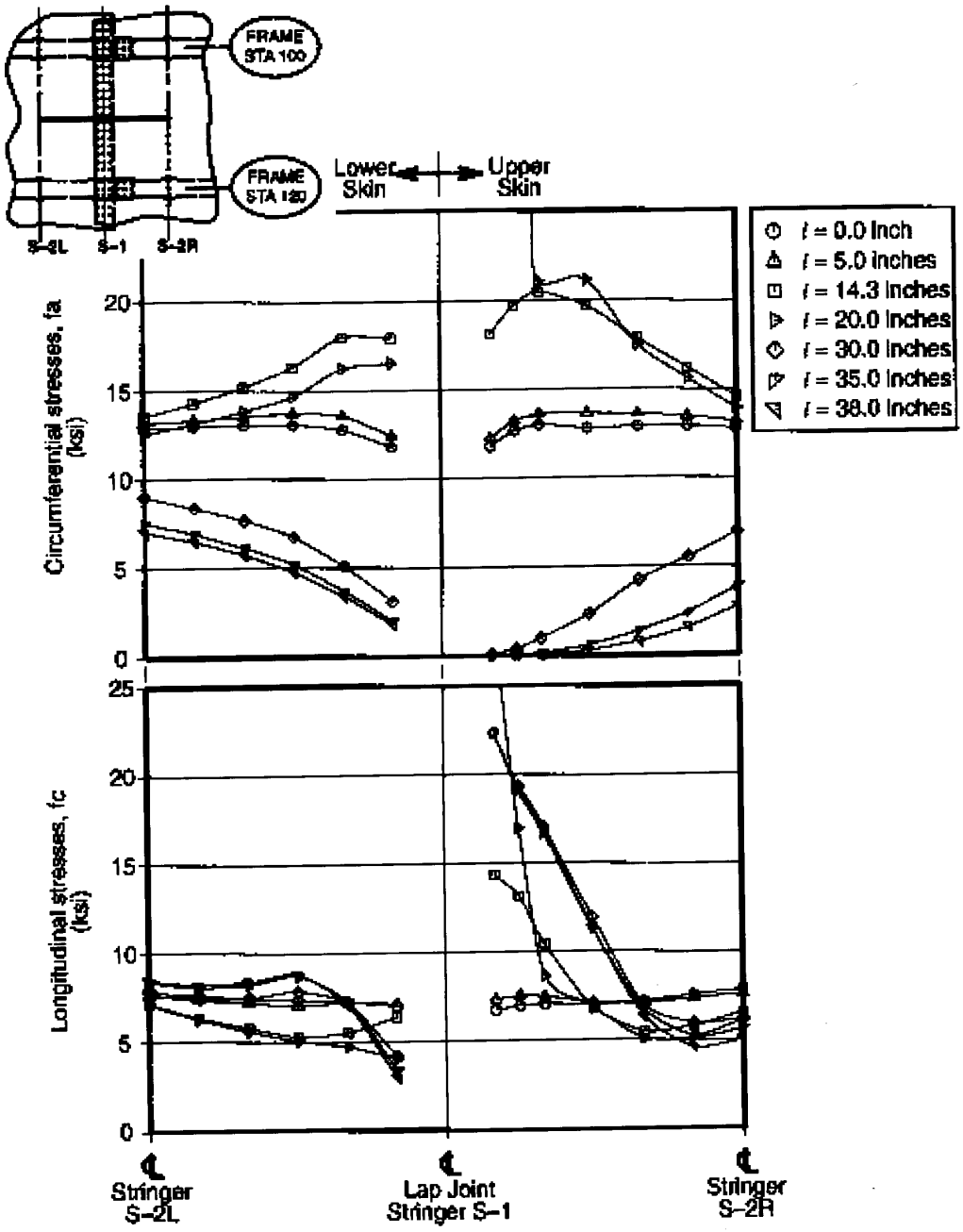

Figure 53. Predicted Midplane Stresses at Station 110

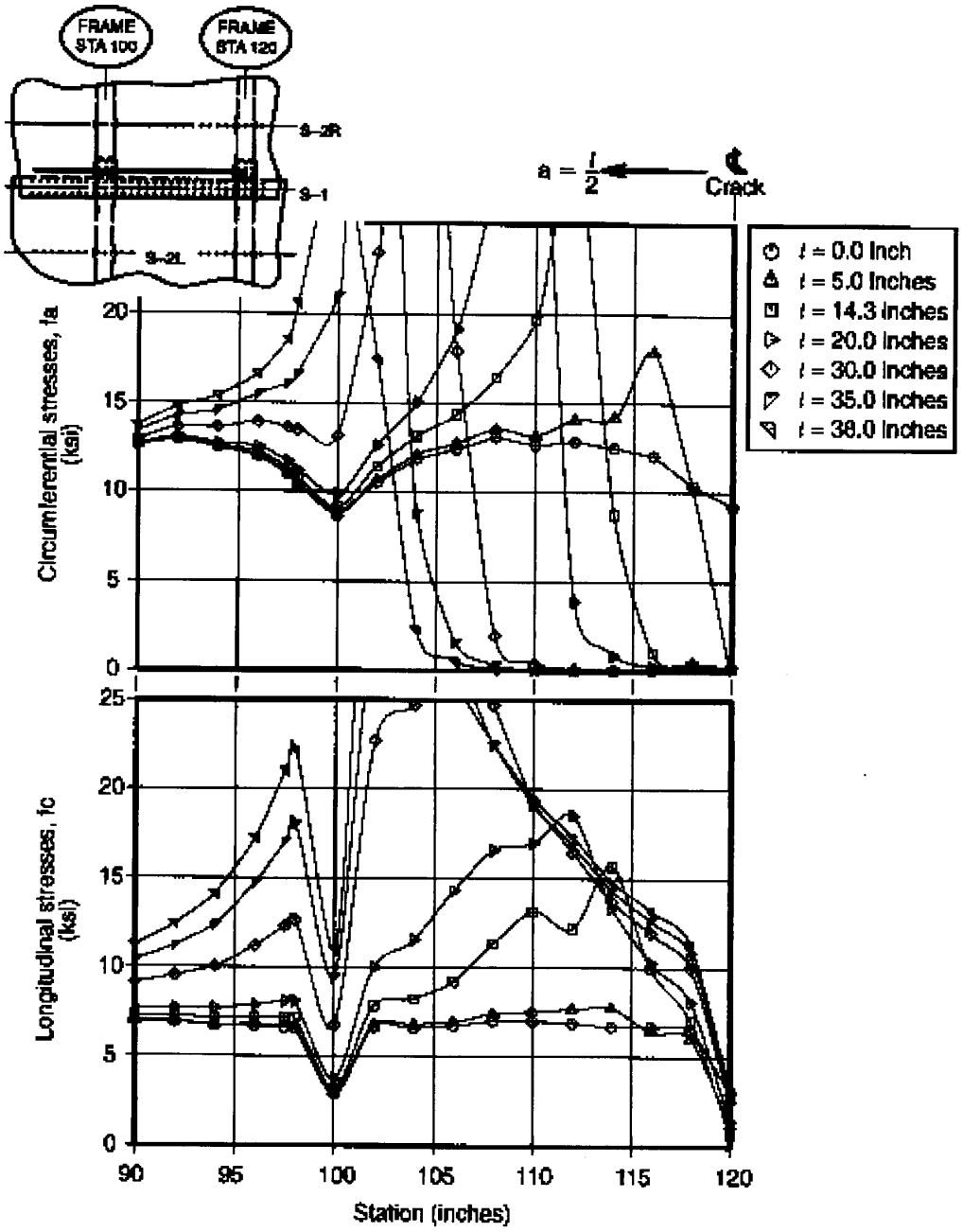

Figure 54. Predicted Midplane Stresses in the Upper Skin 2.3 Inches Right of the Lap Joint Stringer Centerline

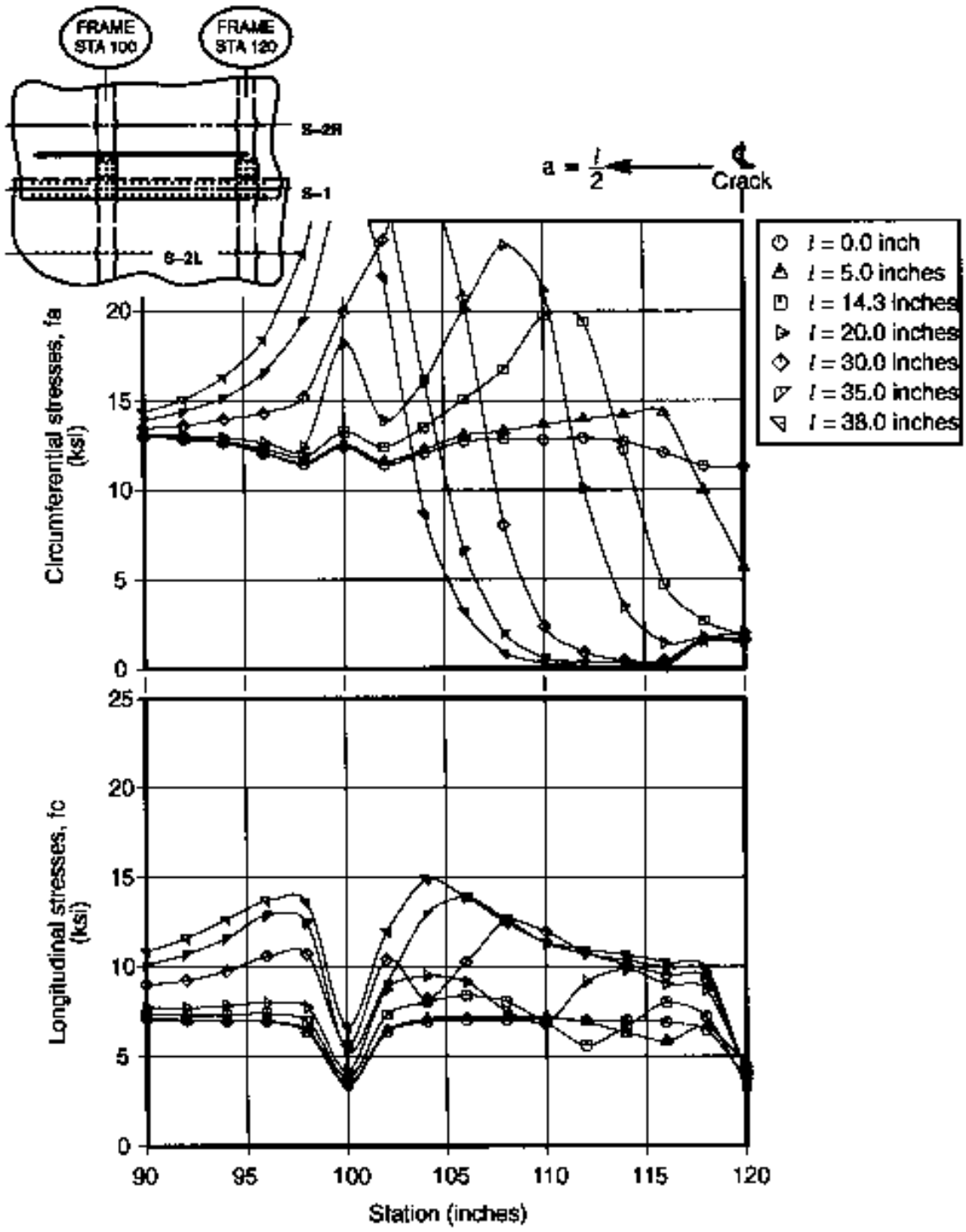

Figure 55. Predicted Midplane Stresses in the Upper Skin 4.6 Inches Right of the Lap Joint Stringer Centerline

A total stress intensity factor that could be related to the strain energy release rate was used to calculate crack growth. Figure 56 contains a plot of the total stress intensity factors vs. crack length. The method for deriving the stress intensity factors from the finite element analysis output is explained in appendix D.

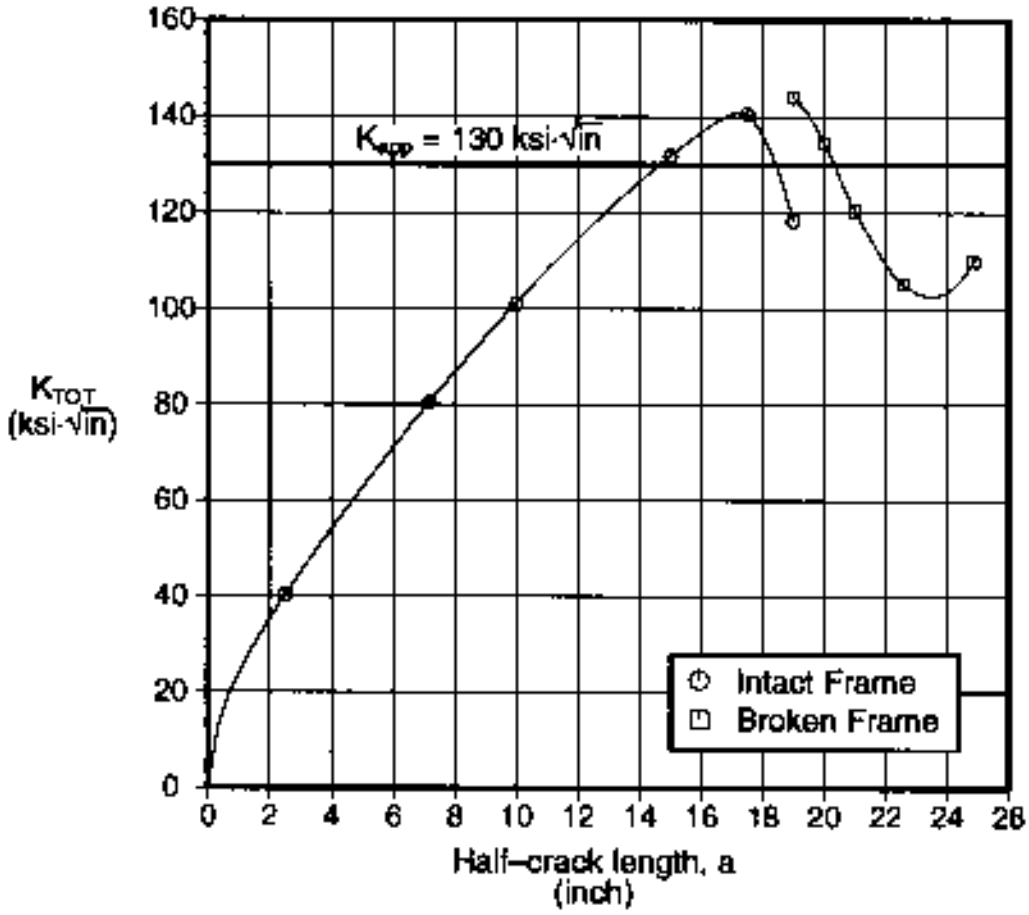

Figure 56. Stress Intensity Factor Predictions at Operating Pressure

4.3 Pressure Panel Test and Analysis Correlation

4.3.1 Strain Gage Stress Comparisons

A stress prediction was calculated for each strain gage. Generally, the location of a strain gage did not coincide with the location of a node on the finite element model. For strain gages on the skins and tear straps of a test panel, the following method was used to calculate a stress prediction. The six nodes closest to the strain gage location were found; these nodes had to lie on the same surface and could not be separated from the strain gage location by a crack front. It was determined if the strain gage was on the inner or outer fiber of the surface containing the six nodes. The inner or outer fiber stresses at the six nodes were then used to make a least squares estimation of the stress at the strain gage location. For strain gages on the stringers and frames, the axial load and beam bending moments were known for all strain gage locations. It was then a simple matter to calculate predicted stresses using standard beam formulae. Table 9 lists the test files that were suitable for correlation purposes; that is, the test crack length was close to an analysis crack length.

Scatter plots for predicted strain gage stresses vs. measured strain gage stresses are shown for the intact test panel in Figure 57 and for the test panel containing a crack in Figures E-1 through E-4 of appendix E. As well, error bands are shown in Figure 57 and Figures E-1 through E-4. These bands are for ±0.5ksi ±10%.

For comparison purposes, membrane and bending stresses were calculated for the skins and tear straps, and axial and bending stresses were calculated for the frames and stringers. These stresses were then compared to test stresses so that trends along a cut of test panel could be observed.

Crack Length, l (inch)	Frame Condition	Internal Pressure (psi)	Correlation Test File
Intact	Intact	8.6	FAA 1, Cycle 10 (Test 1, Intact) FAA 1, Cycle 1259 (Test 2, Intact) FAA 2, Cycle 9 (Test 1, Intact)
5.0			FAA 1, Cycle 21 (Test 1, l = 5.0 inches) FAA 1, Cycle 1796 (Test 2, l = 5.0 inches) FAA 2, Cycle 395 (Test 1, l = 4.9 inches)
30.0			FAA 1, Cycle 4286 (Test 2, l = 32.24 inches)
38.0			FAA 1, Cycle 4351 (Test 2, l = 36.71 inches)
40.0	Broken		FAA 1, Cycle 4355 (Test 2, l = 36.71 inches)

Table 9. Test Files Used for Comparison With Finite Element Analysis

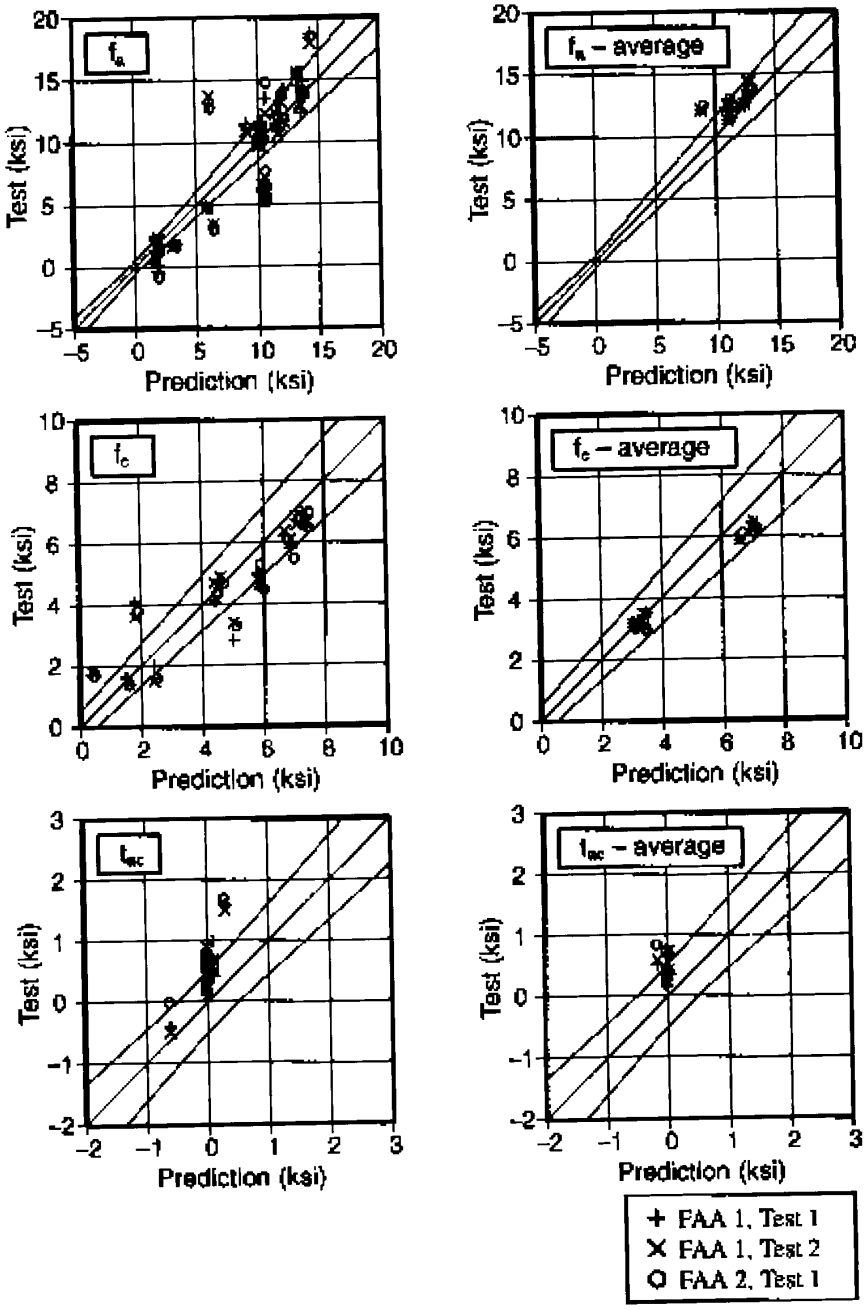

Figure 57. Test / Analysis Strain Gage Correlation for Intact Test Panels

These line plots are shown in Figures 58 through 63 for the intact test panel and in Figures E-5 through E-28 for the test panel containing a crack.

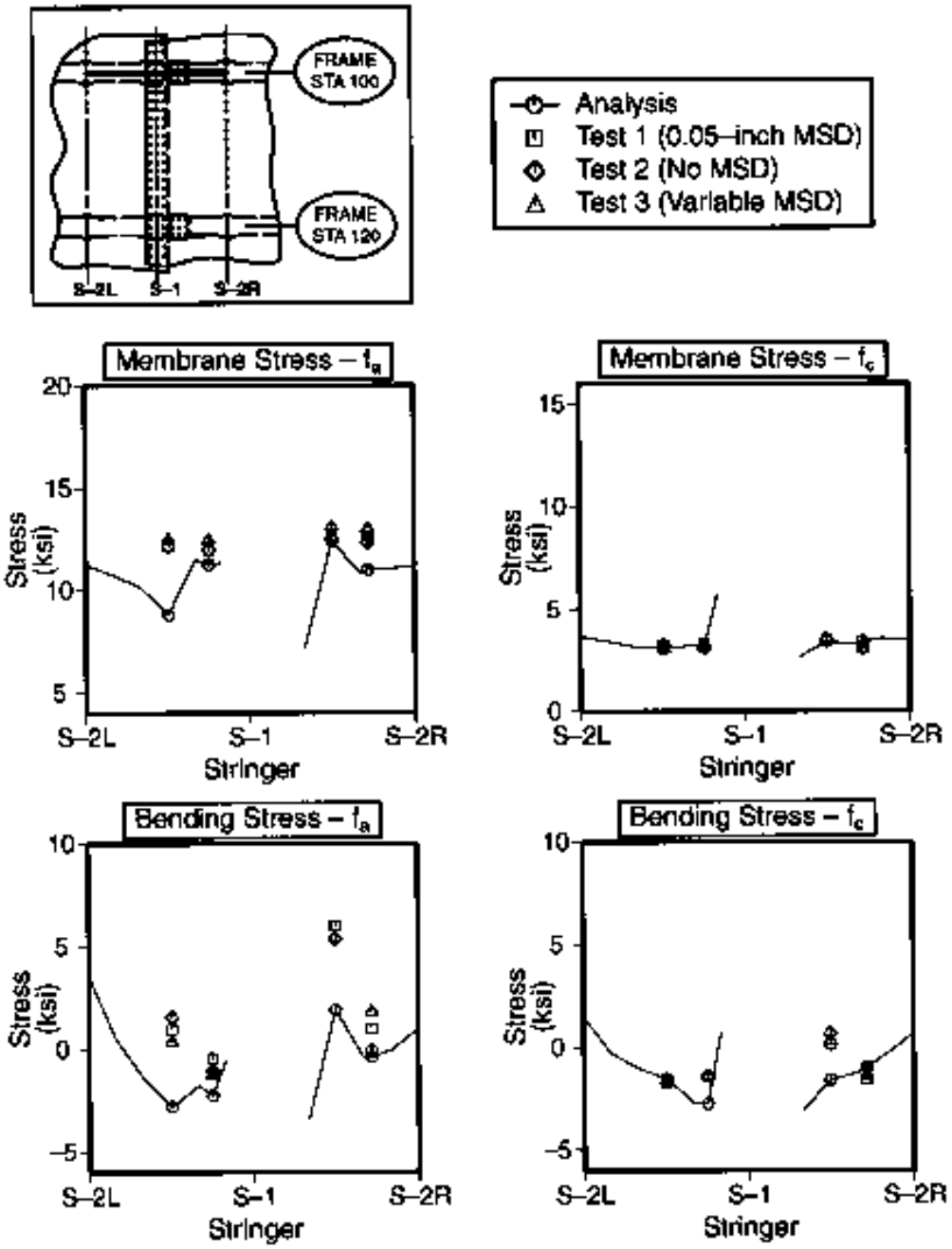

Figure 58. Skin Stress Correlation at Station 100 for an Intact Test Panel

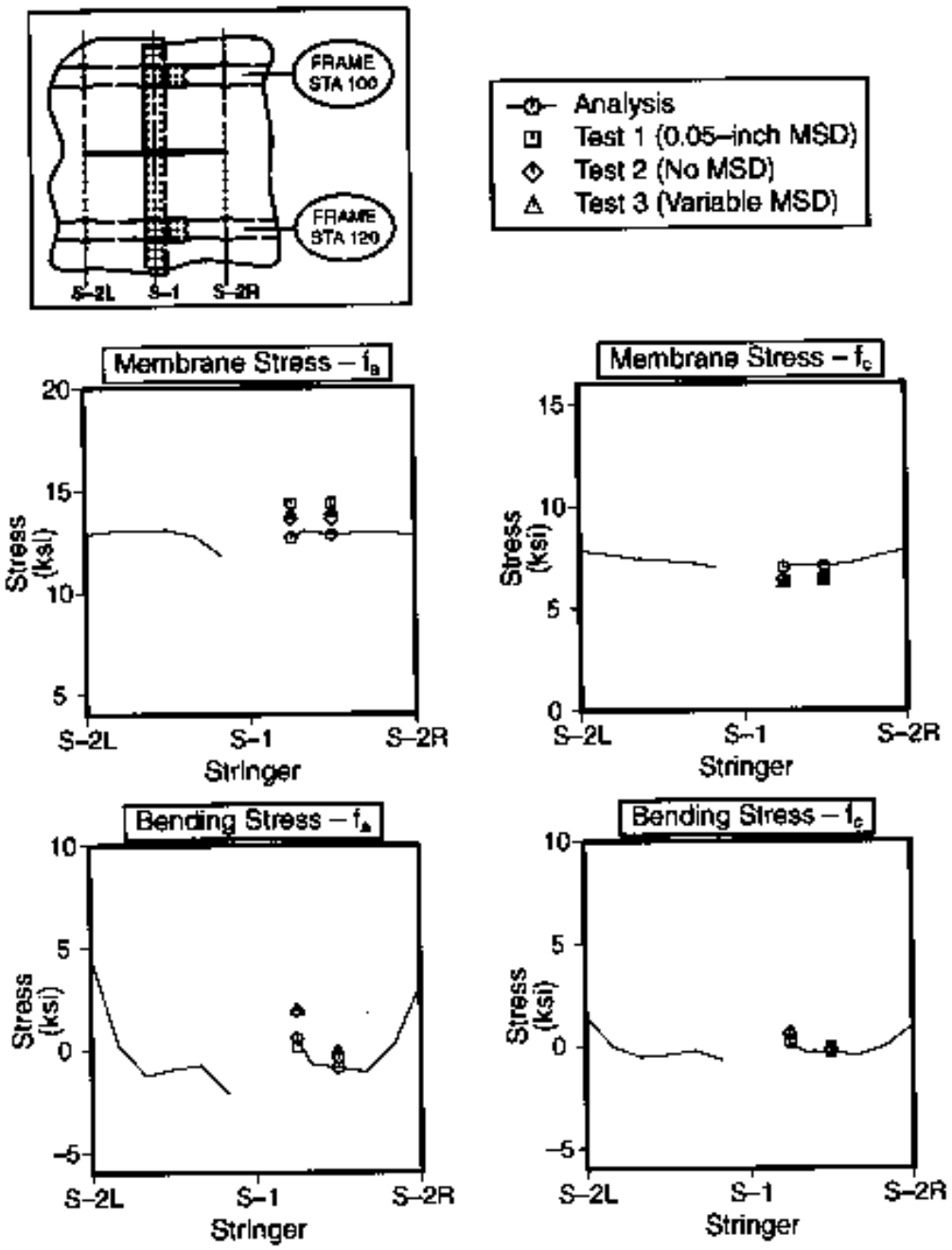

Figure 59. Skin Stress Correlation at Station 110 for an Intact Test Panel

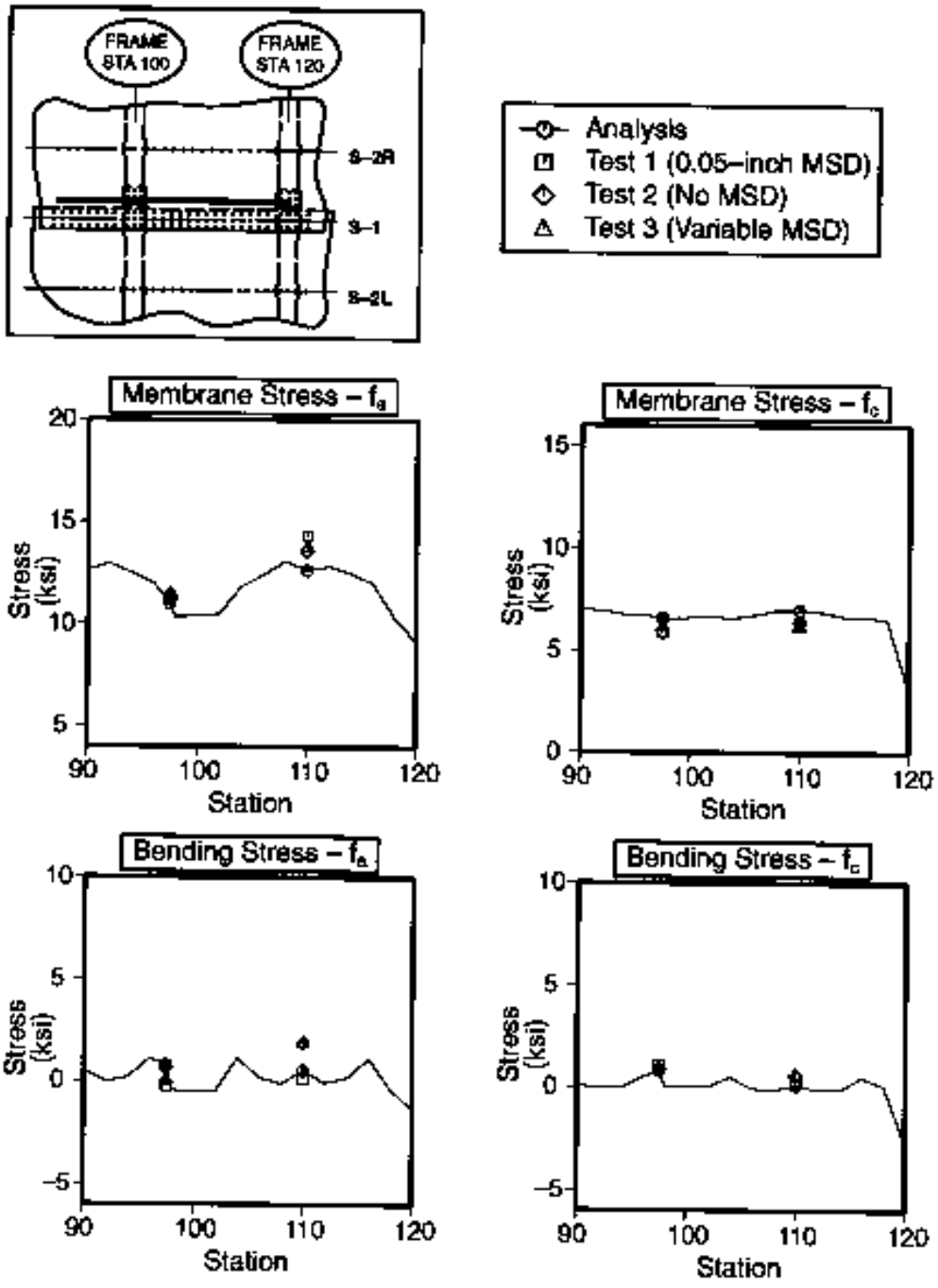

Figure 60. Skin Stress Correlation at Stringer S-1 + 2.3 Inches for an Intact Test Panel

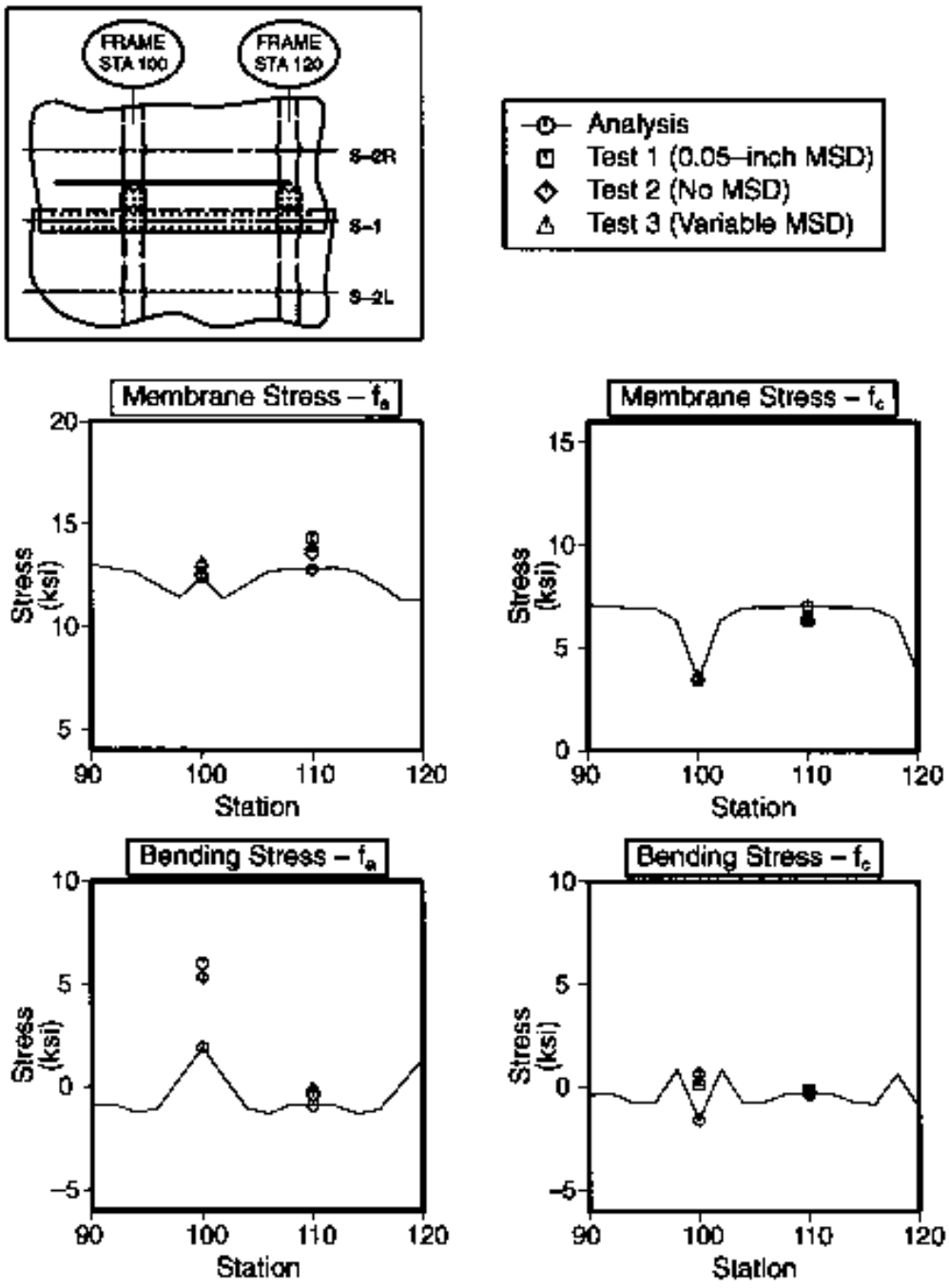

Figure 61. Skin Stress Correlation at Stringer S-1 + 4.6 Inches for an Intact Test Panel

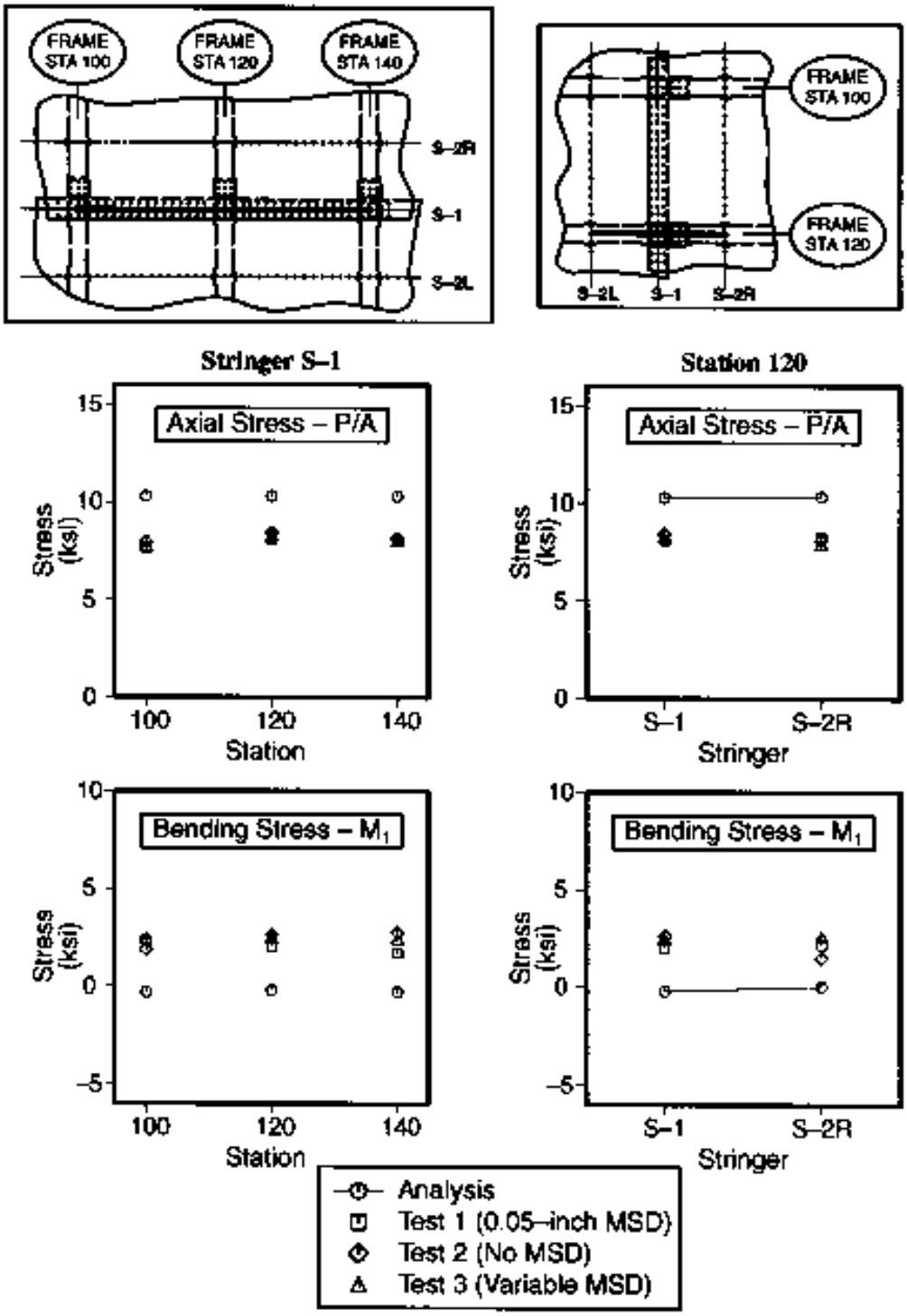

Figure 62. Frame Stress Correlations for an Intact Test Pane

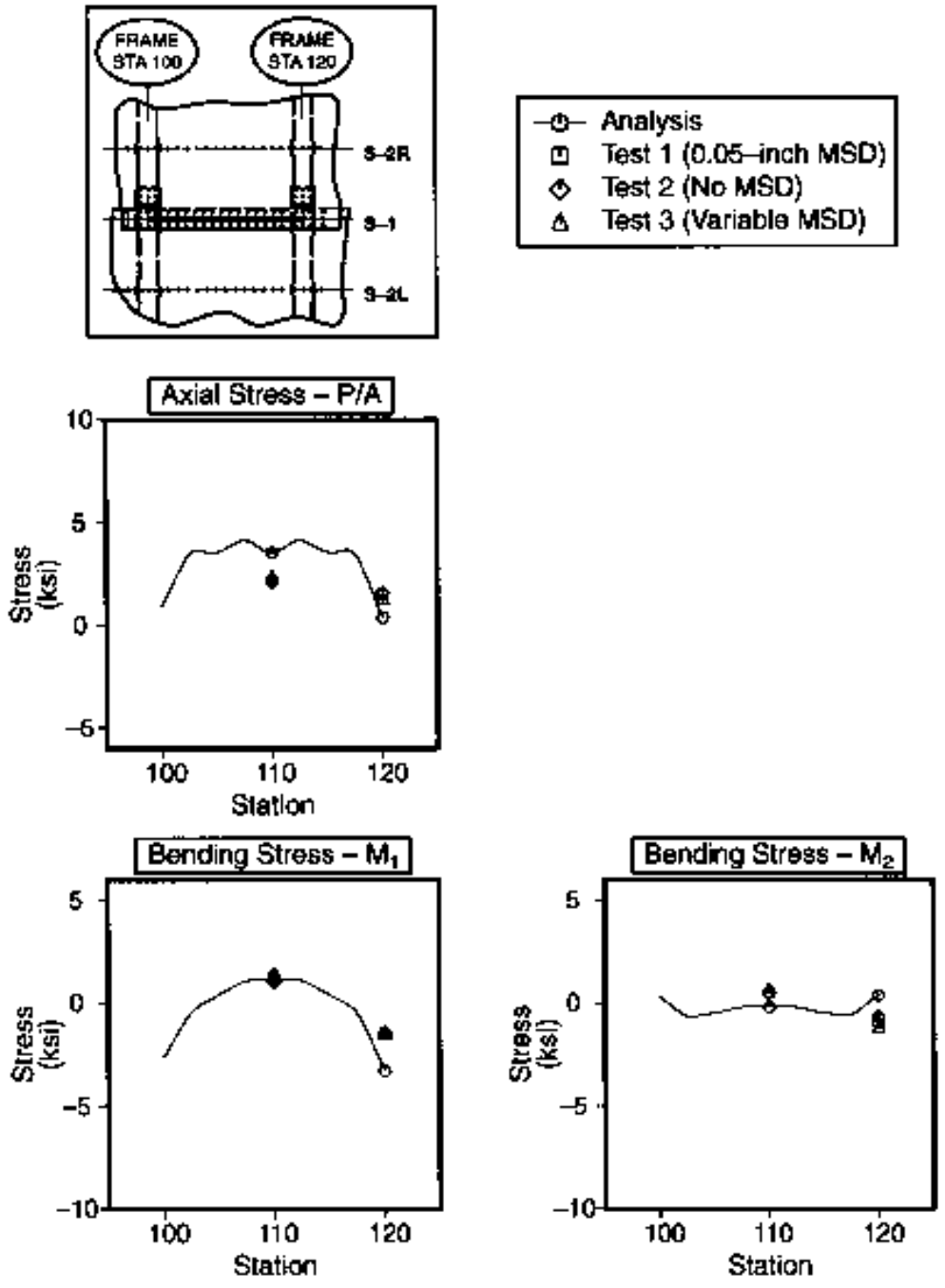

Figure 63. Stringer Stress Correlation at Stringer S-1 for an Intact Test Panel

4.3.2 Crack Growth Comparisons

Crack growth predictions were calculated using the K vs. a curve from the analyses (shown in Figure 56) and the crack growth rate equation derived from the flat panel test results (shown in Figure 6). Figure 64 shows a comparison of prediction vs. test results for crack growth along the lap joint with 0.05-inch MSD emanating from the rivet holes. In this case, the prediction was

calculated so that at each rivet hole, the length of the lead crack was advanced forward the diameter of the rivet shank plus the length of the MSD.

Figure 65 shows the crack growth comparison for the lap joint test without MSD. It was clear from the test that additional pressurization cycles were needed to initiate a new crack tip after the crack grew into a rivet hole. The current Boeing practice is to calculate crack growth without adding fatigue cycles for the crack to re-initiate on the opposite side of the rivet hole. This curve is shown in Figure 65 as a dashed line. A second calculation was made with added pressurization cycles for the lead crack to re-initiate out of the rivet holes.

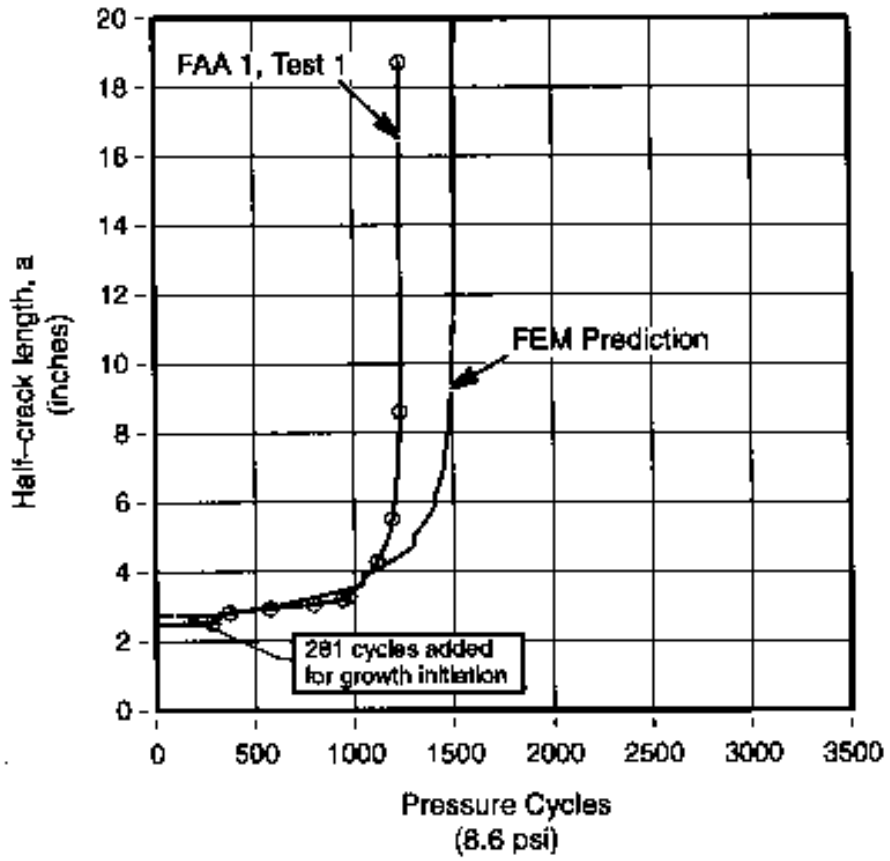

Figure 64. Crack Growth Prediction vs. Test Results for FAA 1, Test 1 (0.05-Inch MSD)

Rivet Location (inch)	Predicted Stress – f_a (ksi)	Additional Fatigue Cycles
3.74	9.3	517
4.88	9.7	109
6.02	9.8	37
7.15	10.0	13
8.29	10.0	6
9.43	10.0	3
10.57	10.0	1
11.71	10.0	1

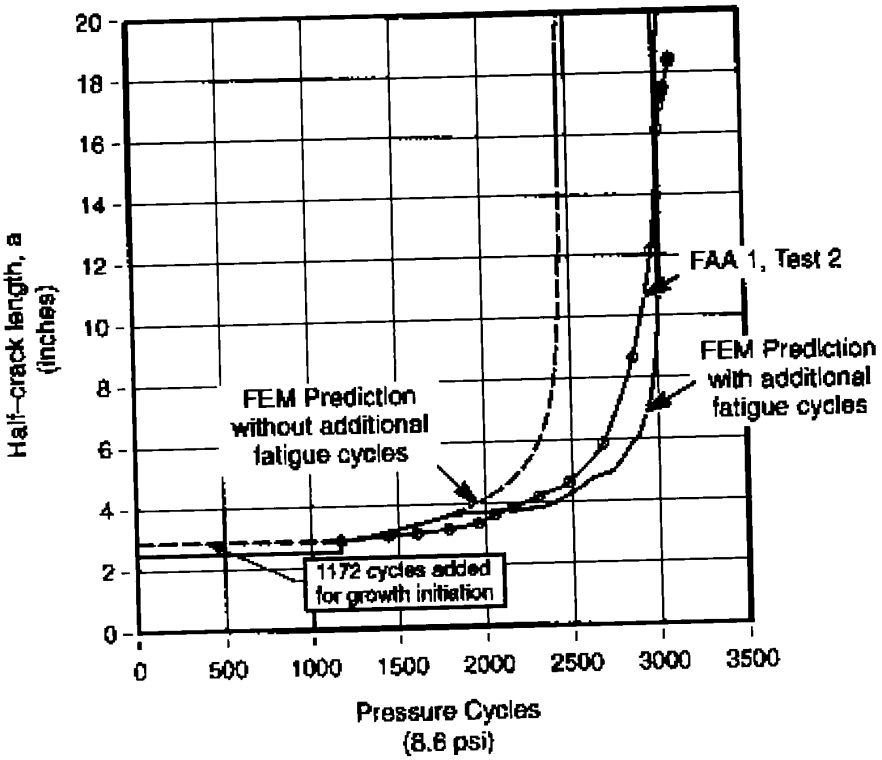

Figure 65. Crack Growth Prediction vs. Test Results for FAA 1, Test 2 (No MSD)

These additional cycles were estimated using the empirical equation below which describes stop drilling test data:

$$N_{add} = [0.61+(f_a/590ksi)\ (1+2\sqrt{a/r_s})]^{-33}$$

where f_a is the membrane hoop stress at the rivet hole predicted by analysis, r_s is the radius of the rivet shank (3/32 inch), and a is the half-length of the crack to the outside edge of the rivet hole. N_{add} is the number of cycles needed for the crack to re-initiate on the outside edge of the rivet hole. The results of the above equation are given in table 10.

Figure 66 contains the crack growth comparison for the lap joint test with variable MSD. The method used here for calculating crack growth was the same as that for the case of 0.05 MSD shown in Figure 64. Here the prediction does not match well with experimental results. Most likely, the larger-sized MSD in this test accelerated the crack growth.

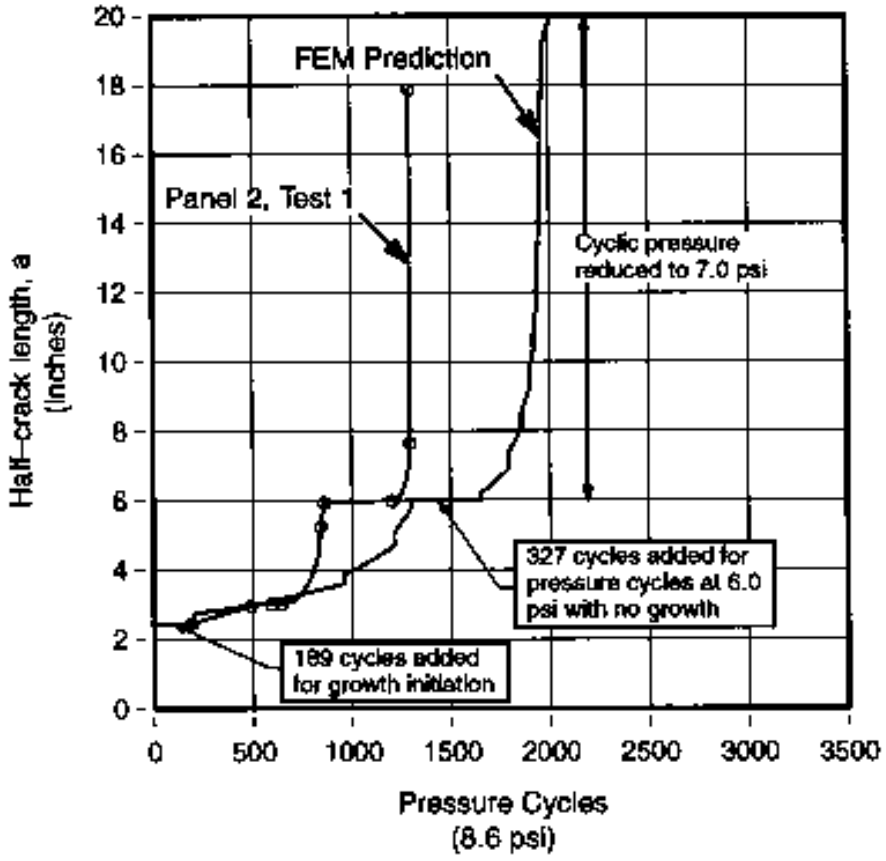

Figure 66. Crack Growth Prediction vs. Test Results for FAA 2, Test 1 (Varied MSD)

4.3.3 Residual Strength Comparisons

The R-curve results from the flat panel tests are shown in Figure 67, along with Kr_{eff} vs. Δa_{eff} calculated from the finite element analysis results using the equations given in Section 2.5.2

and

where $F(a,p)$ is the shape function for the fuselage which is dependent on crack length and pressure load.

The results obtained by using the R-curve to predict panel residual strength assuming an initial half-crack length of a_o = 20 inches are shown in Figure 67. It is obvious that this information alone does not reasonably predict the test panel residual strength. In this case, either the initial total crack length must be significantly greater than 40 inches or the maximum pressure must be significantly greater than 10 psi. In actuality, for the residual strength test without MSD, the initial crack length was 36.7 inches and the maximum pressure was 9.4 psi.

In Figure 68, an apparent fracture toughness of 130 ksi$\sqrt{\text{in}}$ (obtained from the flat panel test results shown in table 5) was used to calculate the maximum pressure vs. half-crack length for the intact frame case and for the case of a severed frame at station 120 and plastic yielding of the tear straps beneath the crack tips. For the severed frame case, a maximum pressure of 10.1 psi was found at a crack length of 46 inches.

The net section failure of the tear strap (shown in Figure 68) was found by calculating the average net stress for the tear strap across the upper rivet row for pressurizations of 7.2 psi, 8.6 psi and 10.0 psi for varying crack lengths. Using a quadratic fit for the three pressurizations, a pressurization that caused the net tear strap average stress to equal the ultimate strength of the material (64 ksi) could be found for varying crack lengths. This curve indicates that as the crack extends, the tear strap is not able to support the additional load and fails, causing total panel failure. Thus, the panel is not able to develop the full 10 psi indicated by the curve for fracture failure of the skin.

The possibility that tear strap failure preceded dynamic skin crack growth was investigated further. Just prior to failure, the test panel without MSD contained a crack of length 38.2 inches and was pressurized to 9.4 psi. The test panel with MSD contained a crack of length 41.7 inches and was pressurized to 7.5 psi (see Figure 44). Figure 69 shows the predicted stresses in the tear strap at station 100 directly below the crack tip for each panel under these conditions. Note that the stresses in the ligament between the outer fastener and the edge of the tear strap are very close in each case. Possibly, this ligament of the tear strap failed, causing complete tear strap failure and dynamic skin crack growth. However, this hypothesis cannot be verified from the test data because of the rapid sequence of events at final failure.

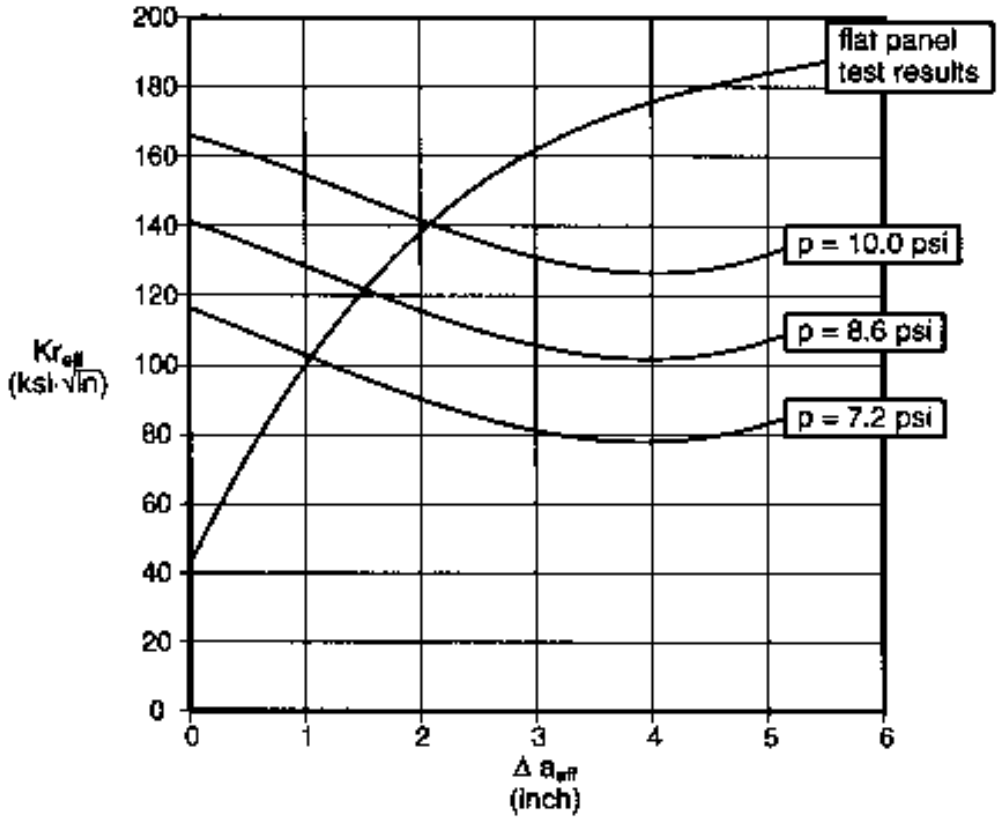

Figure 67. Predicted Kr_{eff} vs. Δa_{eff} for a_o = 20 inches

4.4 Analysis Discussion

The modelling strategy chosen worked well for modelling overall panel behavior. The crack growth predictions for the tests with no MSD and small MSD (0.05 inch) were relatively accurate, although the crack growth prediction for the test with variable MSD (up to 0.15 inch) failed to predict occurrences of fast crack growth. This is reasonable given that the analysis was for the lead crack only. As well, comparison of predicted skin and tear strap stresses with measured strain gage stresses was good. But the model did not reasonably predict stringer and frame stresses. This discrepancy should be investigated further. The stringer and frame strain gages were axial gages which only measured strain parallel to the neutral axis. This strain was transformed into a stress by assuming that the other stress components were zero. It should be determined first if this assumption is valid by comparing predicted strains with measured strains. Given that there is still some discrepancy in results, the model could be further improved. The load transfer to the frame could be investigated to determine the optimal location for nodes along

the frame to be offset from nodes along the stringers, i.e. the optimal location of frame nodes for stringer clip connections. Another improvement to the model would be to change the stringer, frame and stringer clip elements from beams to shell elements. However, this would greatly increase the number of degrees of freedom in the analysis.

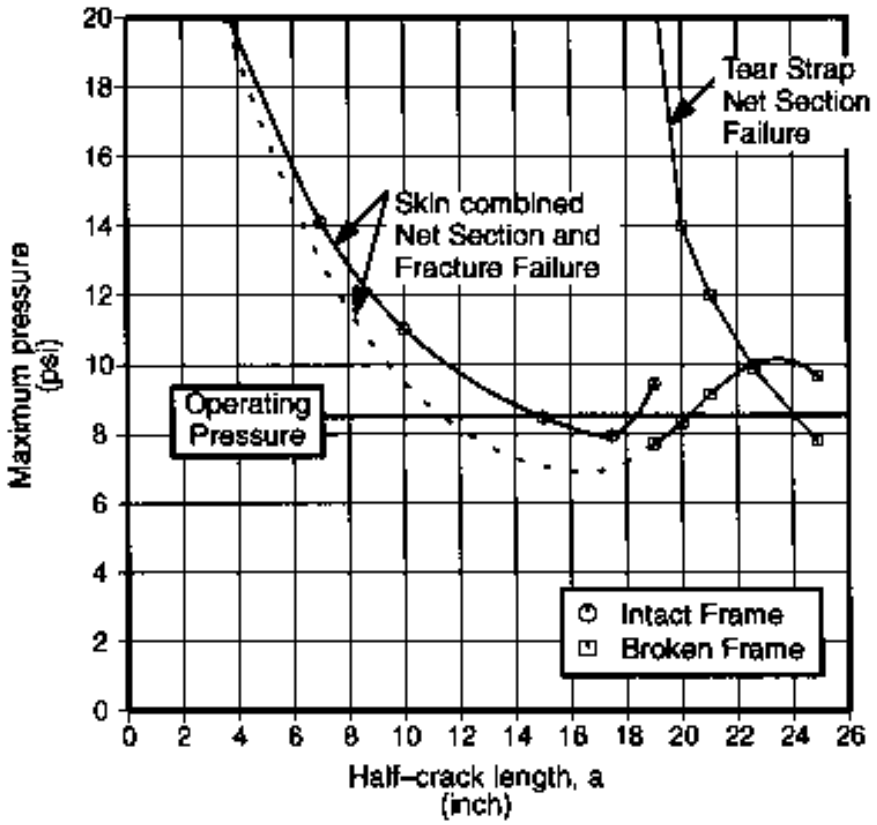

Figure 68. Residual Strength Prediction for a Lap Joint Upper Row Skin Crack

In cases where the effect of the fasteners was important, such as predicting residual strength, the present analysis did not produce good results and a more detailed model is needed. In this case, a global/local modelling strategy would be more effective. The model used for this study could be further refined. Stringers, frames, and stringer clips could be modelled with shell elements. Fastener holes could be modelled as circular cutouts, and the fastener loads distributed as bearing loads on the boundaries. This level of refinement would also allow the explicit modelling of MSD on the fastener holes. As well, a more refined theory could be used to predict residual strength than the apparent stress intensity factor approximation made here, such as plastic collapse of the ligaments between the lead crack tip and the MSD crack tips. Additional refinement of the tear straps would also allow a better prediction of tear strap failure.

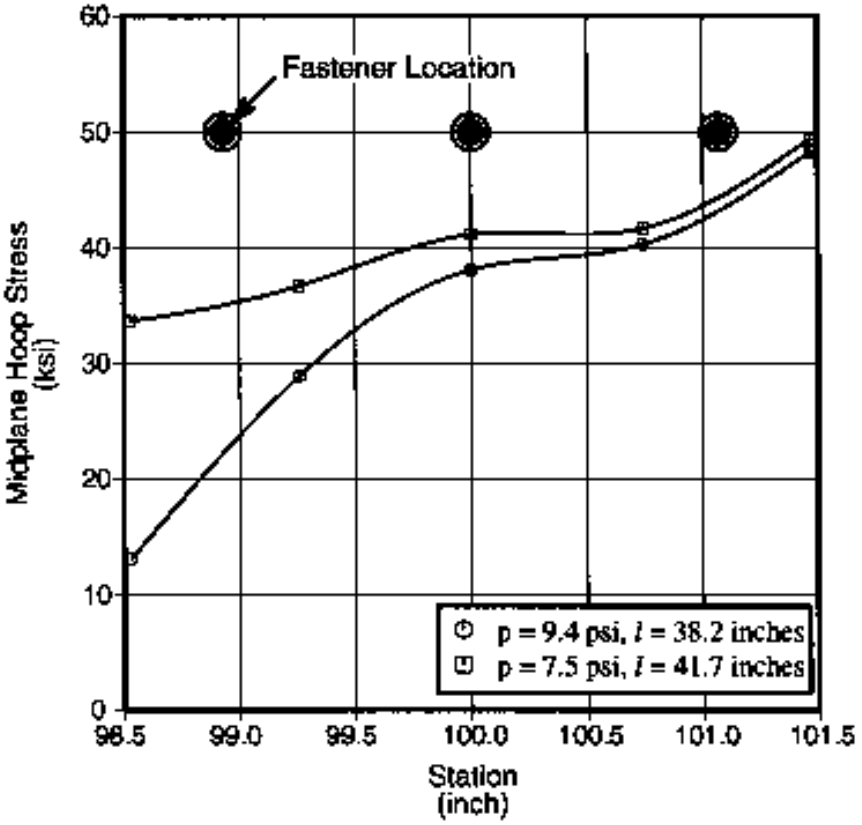

Figure 69. Comparison of the Predicted Midplane Hoop Stresses Along the Upper Row of Fasteners in the Tear Strap at Station 100 for the Residual Strength Tests

5. CONCLUSIONS

5.1 Task I: Flat Panel Testing

- The static, crack growth and toughness properties determined for the 2024-T3 clad aluminum material used in this program were consistent with typical properties used by the Boeing Commercial Airplane Group for damage tolerance analysis of airplane structure.
- The material toughness (K_{app} and R-curve) properties generated from a center-cracked panel were dependent on the buckling restraint effectiveness. A 30 percent reduction in K_{app} was observed when buckling restraints were not used during the toughness tests.

5.2 Task II: Curved Pressure Panel Testing

- The crack growth rate of the lead crack in the lap joint was greater in the presence of simulated MSD. Without MSD the lead crack arrested in each fastener hole and additional cycles were required to extend the crack out of the opposite side.
- For the floating frame panel geometry (no shear ties) and crack lengths tested in this program, the presence of 0.05-inch MSD in the lap joint upper rivet row reduced the residual strength of the panel by 20 percent compared to a panel containing no MSD.
- During the residual strength portion of the tests, the tear straps bridging the crack tips of the two-bay lead crack remained intact until the final failure load was reached. However, the test results are inconclusive as to whether tear strap failure led to dynamic extension of the lead crack.

5.3 Task III:Analysis

- The predictions of skin and tear strap stresses and crack growth history with and without MSD are generally very accurate as shown in the test/analysis correlations. However, frame and stinger stresses could not be reliably predicted.
- The residual strength prediction using an R-curve method and a K_{app} method show that the lap joint lead crack without MSD ahead of the crack tips would not be expected to extend dynamically at the pressures and crack lengths observed in the tests.
- Examination of the stresses in the tear straps bridging the crack tips of the two-bay lead crack indicates that the tear strap probably failed first followed by lead crack instability for both the MSD and non-MSD cases.

6. REFERENCES

1. J. R. Maclin, Performance of Fuselage Pressure Structure," *The Third International Conference on Aging Aircraft and Structural Airworthiness*, Washington D.C., November 1991.

2. U. G. Goranson, 14th Plantema Memorial Lecture: Damage Tolerance Facts and Fiction," *17th Symposium of the International Committee on Aeronautical Fatigue*, Stockholm, Sweden, June 1993.

3. D. Thomson, D. Hoadley, and J. Mchatton, Load tests on Flat and Curved Panels with Multiple Cracks," *Draft Final Report Prepared by Foster-Miller Inc., for the FAA Technical Center*, Atlantic City, New Jersey, September 1993.

4. J. C. Newman Jr., FASTRAN-II A Fatigue Crack Growth Structural Analysis Program," *NASA Technical Memorandum 104159*, February 1992.

5. M. Miller, M. L. Gruber, K. E. Wilkins, and R. E. Worden, Full-Scale Testing and Analysis of Fuselage Structure," *FAA/NASA International Symposium on Advanced Structural Integrity Methods for Airframe Durability and Damage Tolerance*, Hampton, Virginia, May 1994.

6. M. Miller, K. N. Kaelber, and R. E. Worden, Finite Element Analysis of Pressure Vessel Panels," *International Workshop on Structural Integrity of Aging Airplanes*, Atlanta, Georgia, March 1992, pages 337-348.

Note: Appendixes may be obtained upon request.